ANL-6357
Reactor Technology
(TID-4500, 16th Ed.)
AEC Research and
Development Report

ARGONNE NATIONAL LABORATORY
9700 South Cass Avenue
Argonne, Illinois

CRITICAL EXPERIMENTS FOR THE PRELIMINARY DESIGN OF THE ARGONNE HIGH FLUX REACTOR

Edited by J. W. L. de Villiers

Compiled from interim reports and studies by:

Q. L. Baird
J. W. de Villiers
J. O. Juliano
C. N. Kelber
R. Kiyose
K. E. Plumlee

Reactor Engineering Division

June 1961

Operated by The University of Chicago
under
Contract W-31-109-eng-38

DISCLAIMER

TABLE OF CONTENTS

TABLE OF CONTENTS

LIST OF TABLES

LIST OF FIGURES

LIST OF FIGURES

LIST OF FIGURES

CRITICAL EXPERIMENTS FOR THE PRELIMINARY DESIGN OF THE ARGONNE HIGH FLUX REACTOR

Edited by J. W. L. deVilliers

ABSTRACT

Critical experiments were performed with two assemblies simulating a cold clean, and an end-of-cycle, AHFR core. Data were obtained for flux distributions; cadmium ratios; temperature and void coefficients; and control rod, beam hole, and reflector worths. The data obtained furnished confirmation of theoretical predictions. The peak 2200-m/sec flux per unit power was measured as 3×10^7 n/(cm^2)(sec)(watt) for both cores.

The two cores had internal H_2O thermal columns, 12.7 cm x 12.7 cm x 50.8 cm. These were enclosed by 100-liter fuel zones. The radial reflector was 90% beryllium containing 10% H_2O plus Plexiglas by volume. The top and bottom reflectors were H_2O. The critical mass was 3.58 kg U^{235} with a 1.16 metal-to-water ratio in the fuel zone. The critical mass with a 1.60 metal-to-water ratio, taking into account 34.3 kg Type 304 stainless steel, was 7.15 kg U^{235}.

1. SUMMARY

Critical experiments were carried out in support of the preliminary design study for the Argonne High Flux Reactor (AHFR). The major items of interest were: the flux level produced in the internal thermal column per unit of reactor power; the flux and power distributions in the fuel zone; and the effects of variations in compositions and dimensions.

The measured flux peaks for cores of approximately cold clean initial (C-2) and end-of-life (C-1) compositions, were 3.1×10^7 and 2.8×10^7 n/(cm^2)(sec)(watt), respectively. Each core included a 100-liter annular fuel zone, 50.8 cm in height, enclosing a 12.7-cm x 12.7-cm x 50.8-cm internal thermal column (ITC) filled with H_2O. The external radial reflector consisted of beryllium blocks stacked on Plexiglas spacers to yield approximately 90% beryllium and 10% (H_2O and Plexiglas). The top and bottom reflectors were effectively infinitely thick H_2O. The fuel contents of the cores were 7.25 kg (C-2) and 3.64 kg (C-1) U^{235} (highly enriched uranium) contained in 40 fuel clusters. Core C-2 included 34.34 kg of Type 304 stainless steel evenly distributed to simulate burnable poison. The remaining metal was aluminum. The metal-to-water volume ratios were 1.60 (for C-2) and 1.16 (for C-1) in the fuel region.

The ratios of maximum-to-average radial power distributions in the midplane of the fuel region were 2.42 (for C-2) and 2.05 (for C-1); however, variations in these values were noted when liners and thimbles were present in the ITC. The ratios of maximum-to-average power along the axis of individual clusters ranged from 1.25 to 1.46.

The measured effects of physical variations included, among others, the distributed void coefficient (displacement of H_2O) and fuel and poison worths. The temperature coefficient, cadmium ratios of several materials, prompt neutron lifetimes, control rod calibrations, and various other measurements were made. Table 1 gives a summary of the more important results.

Table 1

SUMMARY OF PERTINENT RESULTS

Item	Core	Result	How Obtained
Critical Mass	C-1	3.58 kg	Experimental
	C-1*	2.5 kg	Calculated
	C-2	7.15 kg	Experimental
Prompt Neutron Lifetime	C-1	140 μsec	Calculated
	C-2	71 μsec	Calculated
	C-1	43 $\pm$ 3 μsec	Pile Noise
	C-2	33 $\pm$ 2 μsec	Pile Noise
	C-2	73 $\pm$ 7 μsec	Rossi α
Safety Rod Worth	C-1	1.5% $\Delta k/k$	Calculated
	C-1	1.56% $\Delta k/k$	Measured
	C-2	2.0% $\Delta k/k$	Measured
Fine Rod Worth	C-1	0.8% $\Delta k/k$	Calculated
	C-1	0.7% $\Delta k/k$	Measured
	C-2	1.0% $\Delta k/k$	Measured
Peak 2200-m/sec flux per watt	C-1	2.8×10^7 n/(cm^2)(sec)	Measured
	C-2	3.1×10^7 n/(cm^2)(sec)	Measured
Overall Void Coefficient	C-1	-0.37% $\Delta k/k$ % void	Measured
	C-2	-0.34% $\Delta k/k$ % void	Measured
Temperature Coefficient	C-1	~ -0.024% $\Delta k/k/°C$	Measured
	C-2	~ -0.024% $\Delta k/k/°C$	Measured

*No H_2O in reflector.

2. INTRODUCTION

The proposed Argonne High Flux Research Reactor (AHFR) is described elsewhere.[1,3] It was designed to provide a peak thermal neutron flux of about 4 x 10^{15} n/(cm^2)(sec) at 100 Mw in an Internal Thermal Column (ITC) for the production of transuranium isotopes and the study of fundamental particles. In addition to the ITC, a number of vertical and horizontal experimental facilities are to be provided.

The primary purpose of this report is to record the experimental data obtained in some critical experiments carried out to aid in the preliminary design of AHFR and to serve as a guide to further experimental and theoretical studies.

3. DESCRIPTION OF THE AHFR CRITICAL ASSEMBLIES

The general description applies to the two critical assemblies used, which will be referred to as C-1 and C-2, respectively. They differed only in the fuel loadings, metal and water contents, and sizes of the fine control rods. The assembly C-1 represented a burned-out core, whereas C-2 was a mockup of a new core, loaded with burnable poison. These cores were accommodated in the existing ZPR-VII facility[2] with modifications[3] as shown in Figs. 1, 2, and 3.

A. Fuel

The fuel consisted of a 93.5% U^{235}-aluminum alloy, clad with aluminum and rolled and cut to the dimensions given in Table 2.

Table 2

FUEL PLATE SPECIFICATIONS

	C-1	C-2*
Length, cm	$50.8^{+0.95}_{-0.32}$	50.8 nominal
Width, cm	6.2	6.2
Thickness, cm	0.043	0.094
Weight, gm		
(a) U^{235}	4.1 ± 0.1	7.95
(b) Aluminum	33.9	70.25

*These values are for 206 double-weight plates - see text.

The fuel plates were clamped in aluminum backup plates to form an element, as shown in Fig. 4. Since the fuel was exposed at the ends by a shearing operation, it was sealed with a coating of carnauba wax. Two-hundred-and-six of the plates for the C-2 core were of double thickness, as given in Table 1; the rest of the C-2 elements were made up by clamping two C-1 plates in the same backup plate. The dimensions of the backup plates are given in Table 3.

Table 3

SPECIFICATIONS OF ALUMINUM BACKUP PLATES

Length	56.44 cm
Thickness	0.099 cm
Width	6.985 cm
Volume	37.5 cm^3
Weight	101.3 gm

The fuel clusters shown in Fig. 4 held 22 fuel elements, with the exception of the four clusters adjacent to the flat sides of the fine control rods. These clusters had room for only 20 elements, the remaining space being taken up by the aluminum rod guides.

The C-2 clusters each contained an additional 17 stainless steel strips, of dimensions given in Table 4, to simulate burnable poison. A third loading, containing the same amount of U^{235} as in C-2, but with only 12 stainless steel strips per cluster, will be referred to as C-2'. A few runs, to determine the worth of the beryllium reflector, were also made with no stainless steel.

Table 4

DIMENSIONS OF STAINLESS STEEL POISON STRIPS

Length	56.44 cm
Width	6.985 cm
Thickness	0.0184 cm
Volume	6.53 cm^3
Weight	50.6 gm
Density	7.75 gm/cm^3

B. Core Configuration

Forty fuel clusters were assembled within a 0.16-cm-thick aluminum shroud in an annular configuration, as shown in Fig. 2, with dimensions given in Fig. 3. The core compositions are given in Table 5. The internal thermal column, 13.97 cm x 13.97 cm, contained light water; the moderator also was light water. The axial light water reflectors were essentially infinite.

Table 5

CORE COMPOSITIONS

Item	C-1	C-2
Volume of Fuel Zone, liters	100.862	100.862
Volume of ITC, liters	8.193	8.193
Weight of U^{235}, kg	3.641	7.251
Weight of Stainless Steel, kg	-	C-2:34.335 C-2':24.236
U^{235} Density, gm/cc*	0.0316	0.0719
Stainless Steel Density, gm/cc	-	C-2:0.341 C-2':0.240
Aluminum Density, gm/cc	1.44	1.495
H_2O Density, gm/cc	0.45	0.384
Metal/Water Volume Ratio	1.16	1.60
H/U^{235} Atomic Ratio	323	138.3
Excess Reactivity, % $\Delta k/k$	~1.2%	C-2:~0.4 C-2':2.6

*Numbers following this pertain only to fueled region and do not include the ITC.

The radial reflector was beryllium of dimensions shown in Fig. 3. It consisted of about 3500 pieces of beryllium, none larger than 5 cm x 5 cm x 10 cm, stacked on Plexiglas spacers as shown in Fig. 1. The Plexiglas and water volume in the beryllium reflector amounted to about 10% of its volume. The reflector was confined by an aluminum shroud as in Fig. 2.

C. Control

Control was achieved by means of four cross-shaped control rods and two blade-type, aluminum-clad, cadmium rods of dimensions given below. The locations of these rods are evident from Fig. 2 and Fig. 3.

Safety Rods

Square cross	24.5 cm across
Length	152 cm
Thickness	0.0508-cm cadmium clad in 0.159-cm thick aluminum

Fine Rods

Length of Cadmium Portion	61 cm for C-2 and 30 cm for C-1
Width	5.08 cm
Thickness	0.0508-cm cadmium sandwiched between aluminum plates, 0.127 cm thick

D. Beam Tubes

Two beam tubes were provided in C-1. One, the west beam tube, was situated at the midplane of the core and butted up against the aluminum shroud around the core (see Fig. 2). The south beam tube, which was dispensed with in C-2, was located with its centerline 5.1 cm below the top of the fuel clusters, and extended to within 5 cm of the fuel-beryllium interface. The tubes were of 10.16-cm-ID aluminum tubing, 0.295-cm wall thickness, and were closed off with 0.3-cm aluminum discs.

E. Startup Source

The startup source consisted of an activated antimony pellet which could be inserted by means of a pneumatic drive into the beryllium reflector to provide photoneutrons. The location is shown in Figs. 1 and 2.

4. CORE LOADINGS AND EXCESS REACTIVITY MEASUREMENTS

The first AHFR Critical Experiment, C-1, attained criticality on February 1, 1960. Criticality was achieved by progressively loading fuel into the core described in Section 3. Inverse multiplication measurements (see Fig. 6) indicated a clean critical mass of approximately 3.6 kg of U^{235}. As the core was designed to hold only 872 fuel elements (3575 g U^{235}), it was necessary to reduce the ITC to 12.7 cm x 12.7 cm by adding 16 extra

fuel plates. This brought the total number of plates to 888, or 3640.8 g of U^{235}. Criticality was achieved with safety rod No. 5 withdrawn 15.2 cm, corresponding to an excess reactivity of about 1.2% $\Delta k/k$ (see Section 6, "Control Rod Calibrations").

The second core loading, C-2, achieved criticality on June 24, 1960, by loading the C-2 fuel as described in Section 3 in the same manner as described above. The critical mass was approximately 7.15 kg U^{235}. Corrosion effects, discussed in the following subsection, caused a gradual loss of reactivity. It was therefore again necessary to reduce the size of the ITC to 12.7 cm by 12.7 cm by adding 16 thick plates (containing 7.95 gm U^{235} each), giving a total of 206 thick and 1338 thin plates, or 7.251 kg U^{235}. This yielded an excess reactivity of 1.54 $\Delta k/k$. This excess reactivity was reduced by further corrosion. By adding about 5 ppm of potassium and sodium dichromates the corrosion was nearly completely prohibited and the excess reactivity during most of the operation of C-2 remained at approximately 0.4% $\Delta k/k$.

The available excess reactivity in the C-2' loading was about 2.6% $\Delta k/k$.

Table 5 (see Section 3) lists the component densities of the two AHFR critical assembly cores. The quoted numbers pertain to the 50.8-cm fuel zone only, and do not include the end fittings of the clusters.

A. Corrosion Effects

The reactivity drift in C-2 mentioned in the preceding paragraphs was attributed to the formation of hydrogen bubbles caused by the corrosion of the aluminum in the core. This corrosion rate was enhanced by the "couple" or galvanic cell effect formed by the H_2O, stainless steel, and aluminum components.(4)

Two corrosion-resistant lacquers were tried on the stainless steel. One was a phenolic "200" lacquer used by Continental Can Company. The lacquer was rolled on to a thickness of 0.0025 cm (1 mil) and then baked in a 200°C oven for 10 to 12 min. The other lacquer was Paladin (vinyl lacquer - Interchemical Corporation). The stainless steel strips were hand dipped in the Paladin and air dried for 72 hr. The phenolic coating withstood 8-hr immersion in boiling water, whereas the Paladin peeled badly after a one-day test period in 24°C water.

The corrosion rate was measured with the water in a highly purified state, and also with an oxidizing agent added to it. When an oxidizing agent like dichromate ($Na_2Cr_2O_7$ or $K_2Cr_2O_7$) is added to the corroding solution, it helps to repair breaks in the protective oxide film, thereby stopping further reaction at the local anode on the metal surface.

The corrosion rates were measured as follows: one fuel cluster was immersed in reactor water in a plastic box. An M-S-A Explosimeter was used to measure the amount of hydrogen evolved, a full-scale reading of 100% corresponding to an explosive air mixture containing 4.1% hydrogen.

The corrosion rates listed in Table 6 were calculated by means of the data presented in accordance with reaction: $2\ Al + 6\ H_2O \rightarrow 2\ Al(OH)_3 + 3\ H_2$. The exposed area of aluminum per cluster was 15,710 cm^2.

Table 6

CORROSION RATES

Stainless Steel Sample	H_2O Purity, megohm	Test Time, hr	Reading, %/hr	Corrosion Rate, $mg/(cm^2)(day)$ $(x\ 10^{-3})$
I. Uncoated				
Trial 1	0.8	5	0.8	11.2
Trial 2	0.4	27	1.296	18.1
Trial 3	1% dichromate	42	0.357	4.9
II. Coated (Paladin)	<0.1	16	2.5	35
III. Coated (Phenolic "200")				
Trial 1	0.8	8	~0.0	~0.0
Trial 2	0.4	24	0.417	5.8
Trial 3	5 ppm dichromate	9	0.444	6.2
Trial 4	5 ppm dichromate	24	0.875	12.3

The corrosion rates given in Table 6 are of the same magnitude as could be inferred from published data.(4) Using the corrosion rate of the Paladin test as the worst condition, it is noted that gas evolution was reduced to one-third to one-sixth of the uninhibited value using either dichromate in the moderator or applying phenolic lacquer to the stainless steel strips. As there were about 700 stainless steel strips in C-2, it was more convenient to add dichromate to the water. Previously, the hydrogen evolution for a full core was about 1 liter/hr, with approximately one-fourth of this amount retained in the core, producing a steady reactivity loss of 1/3% $\Delta k/k/hr$. Upon adding dichromate, the steady negative drift was nearly eliminated.

5. MEASUREMENT OF THE PROMPT NEUTRON LIFETIME, DELAYED AND PHOTONEUTRON EFFECTIVENESS

A. Prompt Neutron Lifetime

Two methods were employed in the measurement of ℓ, the prompt neutron lifetime, viz., the Pile Noise[5] method and the Rossi-α[6] method. The Rossi-α is the ratio of the effective delayed neutron fraction to the prompt neutron lifetime, i.e., β_{eff}/ℓ at delayed critical. The results are given in Table 7. The prompt neutron lifetime was calculated by the $1/v$ poison method,[7] using the PDQ code.[8]

Table 7

PROMPT, DELAYED AND PHOTONEUTRON PARAMETERS

Item	Method	C-1	C-2
$\alpha = \beta_{eff}/\ell$	Pile noise: Run 1 Run 2	182.5 ± 21 sec^{-1} 180.9 ± 7 sec^{-1}	250.5 ± 25 sec^{-1} 228.9 ± 13 sec^{-1}
$\alpha = (\beta_{eff} - \rho)/\ell$	Rossi-α experiment	-	308 ± 30 sec^{-1}
$\epsilon = \epsilon_p/\epsilon_D$	Cohn[9] (experimental)	0.12	0.159 ± 0.005
ϵ_D	Calculated	1.19	1.19
$\beta_D(U^{235})$	ANL-5800[10]	0.0065	0.0065
$\beta_p(D_2O)$	Bernstein et al.[11]	0.001	0.001
β_{eff} (total)	$\beta_{eff} = \epsilon_D(\epsilon\beta_p + \beta_D)$	0.0079	0.0079
ℓ (neutron lifetime)	Pile noise	43 ± 10^{-6} sec	$33 \pm 2 \times 10^{-6}$ sec
ℓ	Rossi-α		$73 \pm 7 \times 10^{-6}$ sec
ℓ	Calculated	140×10^{-6} sec	71×10^{-6} sec

B. Delayed Neutron and Photoneutron Effectiveness

The relative photoneutron effectiveness was measured in both cores by a method devised by Cohn.[9] If ϵ_p and ϵ_D are the photoneutron- and delayed-neutron effectivenesses (as compared to fission neutrons), the relative photoneutron effectiveness is defined as $\epsilon = \epsilon_p/\epsilon_D$. The value for the delayed neutron fraction β_D was taken as 0.0065[10] and the photoneutron fraction was taken from the D_2O data of Bernstein et al.[11] as $\beta_p = 0.001$. The D_2O data was assumed to be applicable to the

AHFR system without introducing any significant errors.[12] The results of these measurements are presented in Table 7. The delayed neutron effectiveness ϵ_D was calculated by using age theory and distinguishing the prompt and delayed neutrons by means of their different ages.[13]

The Rossi-α determination was done with safety rod No. 1 fully inserted from a critical position of 36.06 cm, i.e., 1.48% ρ ($\rho = \Delta k/k$) subcritical. There was also an observed loss of reactivity during this and a subsequent Rossi-α experiment which puts this measurement somewhat in doubt. It should be noted, however, that a loss of reactivity during the experiment, which is not considered in the calculation of ℓ from α, would yield a minimum value for ℓ. The discrepancy between the calculated ℓ-values and the pile-noise results is as yet not fully understood. Although a one-group bare reactor model was used in analyzing the experimental data, it was thought[14,15] that this assumption would not introduce any significant errors in the range of the experiments. Work at other installations,[16,17] however, indicate that this may not be the case.

6. CONTROL ROD CALIBRATIONS

Apart from the necessity to know how much excess reactivity could be held down by the control rods, a calibrated rod was needed as a reference to determine the reactivity worths of various core components and samples introduced in the experimental thimbles.

Safety rods No. 5 and No. 1 (also referred to as coarse control rods) as well as the (fine) control rods No. 1 and No. 2 were calibrated for C-1, C-2, and C-2' by observing the rising periods resulting from an incremental withdrawal (in approximately 3.5-cm steps) of the respective rods from a critical position. After each withdrawal, criticality was restored by inserting a compensating rod. The reactivity worth of each step was obtained from period versus reactivity curves computed from the in-hour equation, using the data given in Table 8. These reactivity increments were then summed to give the integral worth of the rod, or used to find the differential worth as a function of rod position (see Figs. 7, 9, 13, and 14).

Table 8

DATA FOR C-1 AND C-2 INHOUR CURVES

Core	$\Sigma\beta_i$	ϵ_D	ϵ_p/ϵ_D	ℓ
C-1	0.0065	1.19	0.12	140×10^{-6} sec
C-2	0.0065	1.19	0.16	60×10^{-6} sec

In the computation of the period versus reactivity curves for C-2, the value of 60 μsec was used for ℓ, because the calculated value was not yet available. This does not influence the rod calibrations, as it is only at very short periods that the lifetime term in the inhour equation becomes significant. The delayed neutron data are those of Keepin and Wimett,[18] whereas the photoneutron data was obtained from Bernstein et al.[11] as explained in Section 5.

In the C-2 core, control rod calibrations were also made by the "Ramp Insertion" method, where the decrease in neutron flux is noted while a rod is inserted at a steady rate. The reactivity as a function of rod position was then computed by means of the IBM-704 Code RE-138.[19] Comparable results were obtained as can be seen in Figs. 11, 12, and 13.

The effect of temperature on rod worth was also determined for safety rod No. 1. This is presented in Fig. 12.

The data obtained by these various methods are presented in Figs. 7, 8, 9, and 10 for C-1; and in Figs. 11, 12, 13, and 14 for C-2 and C-2'. The "four extra plates" loading referred to in Figs. 7 and 8 consisted of the normal loading of 888 fuel plates with four extra plates inserted at Positions 32, 33, 34, and 35 (see Fig. 5). This loading change did not seem to affect the differential worth of safety rod No. 5, but an apparent increase in total worth from 1.56% $\Delta k/k$ to 1.66% $\Delta k/k$ can be noted, as shown in Fig. 8.

From the slopes of the worth curve (Fig. 12) at different temperatures, it can be estimated that the No. 1 safety rod worth in C-2' decreased by 0.5 to 1.0% of its worth at 27°C per degree rise in temperature.

A small increase in total worth of the safety (or coarse) control rods from 1.97% $\Delta k/k$ to 2.03% $\Delta k/k$ could be noted in comparing the C-2 worths with C-2' worths.

As no effort was made to do a least-squares fit for the data on the rod worths, the errors involved cannot be accurately stated. It is believed, however, that the data presented in Table 9, for comparison with calculated data, is reproducible to within 3%.

The agreement between the theoretical and experimental data is satisfactory.

Table 9

COMPARISON OF MEASURED AND CALCULATED CONTROL ROD WORTHS

Core	Total Worth per Safety Rod, % Δk/k	Total Worth per Fine Rod, % Δk/k	Total Rod Worth in Core, % Δk/k
C-1 measured	1.56	0.7	7.64
C-1 calculated[3]	1.5	0.8	7.6
C-2 measured	1.97	~1 (not measured)	~10
C-2' measured	2.03	1.1	10.32

7. ABSOLUTE FLUX AND POWER MEASUREMENTS

One of the main purposes of the AHFR design is to provide fluxes of magnitude not previously available for experimental purposes. It was therefore important to know the maximum available flux as a function of reactor power. This was measured as described below.

A. Relative Fission Rate Measurements

A flux map, with and without a 3.81-cm-OD, 0.056-cm-wall, Type 304 stainless steel thimble in the ITC, was obtained over a quadrant of both cores C-1 and C-2 by irradiating uranium-aluminum foils in a horizontal plane at the position of the axial flux maximum. The locations of the foils are given in Fig. 15 for C-1 and in Figs. 16 and 17 for C-2. Axial plots, from measurements with manganese foils for C-1 and uranium-aluminum foils for C-2, were also obtained at point 32, Fig. 5.

The foils were counted in an automatic counting setup,[20] with corrections applied for decay by using a reference foil. The usual background and resolving time corrections were automatically applied.

During the foil irradiations, the control rods were completely withdrawn, and criticality was maintained by adjusting the water (top reflector) height. The virtual absence of the top reflector does not influence the relative flux values significantly, but the peak flux-to-power ratio is increased since the effect of a reflector is generally to lower the peak-to-average flux.

The corrected and normalized foil activations are presented in Figs. 15, 16, and 17. The subcadmium flux map (Fig. 17) for C-2 was obtained from Fig. 16 with the aid of the cadmium ratios as given in Fig. 17. These were obtained from radial cadmium ratio measurements (see Section 8). These data were integrated numerically, using a five-point quadrature formula[21] for each cluster to yield the "average activation" to the "activation at point 32" ratios as presented in Table 10.

Table 10

"AVERAGE ACTIVATION" TO "ACTIVATION AT POINT 32" RATIOS WITH AND WITHOUT STAINLESS STEEL THIMBLES

Item	Total Activation Ratio				Subcadmium Activation Ratio for C-2	
	With SS Thimble		Without SS Thimble			
	C-1	C-2	C-1	C-2	With SS Thimble	Without SS Thimble
Inner ring of fuel plates	1.708	2.126	1.780	2.203	2.486	2.569
Outer ring of fuel plates	1.628	1.838	1.530	1.905	2.112	2.184
Fuel clusters	1.067	0.951	1.030	0.954	1.009	1.012

The errors involved in this method of integration cannot be computed without fitting a two-variable polynomial to the data. However, the errors computed[21] for a surface of greater curvature than presented by the foil activations were less than 1% for the same relative mesh spacing.

The axial plots, presented in Fig. 48 for C-1 and Fig. 36 for C-2, yielded maximum-to-average values of 1.238 for C-1 and 1.158 for C-2. The counting statistics for all these foils had a standard deviation of less than 1%.

B. Determination of Absolute Flux and Fission Rates

Absolute flux and fission rate measurements by means of gold and U^{235} foils were made at reference points along a radial traverse through the cores. The gold foils were counted in standard counters and corrected for decay, background, counter efficiency, and dead time. The U^{235} foils were analyzed radiochemically for the Mo^{99} fission product activity, from which the total number of fissions could be determined.

The data thus obtained are presented in Table 11. The absolute flux and fission rates were computed from this data, using cross sections and applying corrections as described in the following paragraphs. The foils in the fuel zone were located at position 32 in Fig. 5 (at midplane of the core), whereas the foils in the ITC were located in the center of the reactor. Channel V is a "log-power" recorder.

Table 11

ABSOLUTE FLUX AND FISSION RATES IN CORES C-1 AND C-2

Foil Dimensions, cm	Core	Location	Conditions	Reading on $\overline{V}$/Time (min)	Bare Saturated Activity or Fission Rate per gm
Gold	C-1	Fuel	with SS Thimble	55 8/10	1.2283×10^9 dis/(gm)(min)
0.00254 x 1 x 1		Fuel	with SS Thimble	55.8/10	$1\ 2384 \times 10^9$
		ITC	with SS Thimble	55.8/10	2.9752×10^9
		ITC	with SS Thimble	55.8/10	$3\ 0363 \times 10^9$
		Fuel	without SS Thimble	76/20	2.809×10^{10}
		ITC	without SS Thimble	76/20	$6\ 9628 \times 10^{10}$
U^{235}	C-1				
2.223 x 1 27 x 0.00254		ITC	with SS Thimble	55.8/10	$1\ 353 \times 10^8$ fiss/(gm)(sec)
3.175 x 1.27 x 0 00254		Fuel	with SS Thimble	55.8/10	4.01×10^7
2.54 x 2 54 x 0.00254		ITC	without SS Thimble	76/25	2.64×10^9
2.54 x 2.54 x 0.00254		Fuel	without SS Thimble	76/25	7.57×10^8
Gold	C-2	Fuel	without SS Thimble	57/8 5	$2\ 216 \times 10^9$ dis/(gm)(min)
0.00254 x 1 x 1		ITC	without SS Thimble	57/8 5	$9\ 607 \times 10^9$
U^{235}	C-2	Fuel	without SS Thimble	57/8 5	4.186×10^7 fiss/(gm)(sec)
0.0127 x 1 27 x 1.27		ITC	without SS Thimble	57/8.5	2.882×10^8

C. Cross Sections Used in Computing Absolute Flux and Correction Factors

Assuming a cadmium cutoff of 0.4 ev, the thermal cross sections for the fuel zone and the ITC were computed by means of the Sofocate code.(22) The foil cross sections were also averaged over the fuel and ITC spectra by the same code.

The 2200-m/sec cross sections were computed by means of Westcott's prescription,(23) in which

$$\hat{\sigma} = \sigma_{2200}\,(g + rs) \quad ,$$

and r is obtained from:

$$\text{Cadmium ratio for a thin } 1/v \text{ absorber} = \frac{g + rs}{r}\left[s + \frac{1}{K}\sqrt{\frac{T}{T_0}}\right]^{-1} \quad .$$

The cadmium ratios were determined for gold foils, with 0.0508-cm cadmium covers, assuming gold to be $1/v$ below 0.4 ev, g and s as given by Westcott, and K = 2.0728 for a 0.0508-cm cadmium cover.(24) The neutron temperature T was found approximately from the cross section of a unit $1/v$ absorber in the Sofocate computed spectrum for the relevant region. The neutron temperatures were approximately 87°C and 340°C for the C-1 and C-2 fuel regions, respectively, and $T = T_0 = 20$°C in the ITC in both cores.

The values of the "epithermal index" r thus computed are presented in Table 12.

Table 12

EPITHERMAL INDEX r

Region	Average Gold-Cadmium Ratio		r	
	C-1	C-2	C-1	C-2
Fuel Zone	2.112	1.764	0.0494	0.0696
ITC	9.837	9.531	0.0064	0.0066

The computed cross sections are given in Table 13. The gold thermal cross sections were found by multiplying the 0.0253-ev value of 98.8 b by the cross section for a unit 1/v absorber as found by the Sofocate computations.

Table 13

THERMAL AND 2200-m/sec CROSS SECTIONS FOR C-1 AND C-2

Item	C-1		C-2	
	Fuel Zone	ITC	Fuel Zone	ITC
Σ_a [cm^{-1}] thermal	0.04839	0.01902	0.08567	0.01859
λ_{tr} [cm] thermal	0.7136	0.4361	1.4199	0.4956
Σ_a^{235} [cm^{-1}] thermal			16.179	23.807
Σ_f^{235} [cm^{-1}] thermal			13.60	20.07
Σ_a^{Au} [cm^{-1}] thermal			3.377	4.878
Σ_a^{235} [cm^{-1}] Westcott	32.03	32.50	27.861	28.614
Σ_f^{235} [cm^{-1}] Westcott	27.17	27.23	23.151	24.043
Σ_a^{Au} [cm^{-1}] Westcott	10.86	6.51	12.896	6.534
σ_a(unit 1/v) [barns] thermal	0.7785	0.8862	0.5783	0.8354

The U^{235} foil cross sections given in Table 13 were also corrected for spectral hardening in the foils.(25)

D. Corrections to Foil Data

The U^{235} foil data were corrected for self-shielding and flux depression by means of Tittle's procedure.[26] The corrections for the gold and uranium-aluminum foils were found to be of the order of 1% but were not applied.

The correction factors for the U^{235} foils are listed in Table 14.

Table 14

FOILS USED AND CORRECTION FACTORS APPLIED

Foil Size, cm	Location	Core	Cross Sections Used	Unperturbed Flux / Activation Flux
2.223 x 1.27 x 0.00254	ITC	C-1	Westcott	1.25
3.175 x 1.27 x 0.00254	Fuel zone	C-1	Westcott	1.17
2.54 x 2.54 x 0.00254	ITC	C-1	Westcott	1.29
2.54 x 2.54 x 0.00254	Fuel zone	C-1	Westcott	1.18
1.27 x 1.27 x 0.0127	ITC	C-2	Westcott	1.89
1.27 x 1.27 x 0.0127	Fuel zone	C-2	Westcott	1.65
1.27 x 1.27 x 0.0127	ITC	C-2	Thermal	1.75
1.27 x 1.27 x 0.0127	Fuel zone	C-2	Thermal	1.40

Applying the above correction factors to the observed fission rates, the total fission rates for the respective measurements were computed and from this the flux-to-power ratios were found as given in Table 15.

Considering the magnitude of the corrections applied to the U^{235} data, the agreement between the gold and U^{235} foil measurements in C-2 is satisfactory.

The predicted peak flux at 100 Mw is 3.5×10^{15} n/(cm)(sec) for C-1 as computed by the PDQ code,[8] in fair agreement with the measurements. The flux per unit power for C-2 was not calculated.

Table 15

MEASURED PEAK FLUX PER UNIT POWER

Foils Used and Flux Specified	Core	Axial Maximum Flux at 32 (Fig. 5), $n/(cm^2)(sec)$	Central Peak Flux, $n/(cm^2)(sec)$	Central Flux / Flux at 32 (Fig. 5)	Power, watts	Central Peak Flux per Watt, $n/(cm^2)(sec)(watt)$
Gold, 2200 m/sec (with)*	C-1	3.66×10^7	1.49×10^8	4.07	5.41	2.8×10^7
U^{235}, 2200 m/sec (with)	C-1	3.22×10^7	1.16×10^8	3.60	4.6	2.5×10^7
Gold, 2200 m/sec (without)	C-1	8.35×10^8	3.45×10^9	4.13	115	3.0×10^7
U^{235}, 2200 m/sec (without)	C-1	6.17×10^8	2.33×10^9	3.80	87	2.7×10^7
Gold, thermal (without)	C-2	0.855×10^8	5.68×10^8	6.64	15	3.8×10^7
U^{235}, thermal (without)	C-2	0.582×10^8	4.55×10^8	7.82	12.2	3.7×10^7
Gold, 2200 m/sec (without)	C-2	0.565×10^8	4.74×10^8	8.39	15.2	3.1×10^7
U^{235}, 2200 m/sec (without)	C-2	0.557×10^8	4.23×10^8	7.59	13.47	3.1×10^7
U^{235}, thermal (with)	C-2	0.582×10^8	4.23×10^8	7.27	12.15	3.5×10^7
U^{235}, 2200 m/sec (with)	C-2	0.557×10^8	3.93×10^8	7.06	13.47	2.9×10^7

*(with) or (without) refers to stainless steel thimble.

8. FLUX DISTRIBUTIONS AND CADMIUM RATIOS

In order to anticipate cooling requirements and also to place the experimental facilities in the most advantageous positions regarding maximum available flux, detailed knowledge of the flux and power distributions in the reactor is necessary. The flux distributions were measured experimentally. Cadmium ratio measurements were also made to provide an estimate of the ratio of the thermal to the fast neutron flux.

Bare and cadmium-covered foils (0.0508-cm cadmium) of dysprosium, manganese, gold, and uranium-aluminum were used in radial and axial flux traverses in both cores at positions indicated in Fig. 5. The foil dimensions and compositions are given in Table 16. The foils were counted and the data processed as described in Section 7.

Table 16

FOIL DIMENSIONS AND COMPOSITIONS

Foil	Thickness, cm	Diameter, cm	Composition
Mn	0.0102	0.559	Mn with 20 wt-% Cu
In	0.0127	0.559	Pure In
Dy	0.0203	0.559	Dy with 95 wt-% Al
U-Al	0.0660	0.559	U(93.5% U^{235}) with 82 wt-% Al
Au	0.00254	1 cm x 1 cm sq	Pure Au

During the irradiation of the foils, except in the study of the effects of the fine control rods on the flux distribution, all the control rods were withdrawn and the reactor controlled by adjusting the water (top reflector) height. The water height in most cases was between 56.6 cm and 57.8 cm above the bottom of the fuel clusters. This meant that there was virtually no top reflector during these measurements. The radial flux measurements were made at 28 cm above the base plate (i.e., the bottom of the fuel clusters), at the maximum of the axial flux distribution. Several axial and radial traverses were made with a Type 304 stainless steel tube (length 61 cm, OD 3.81 cm, and wall thickness 0.056 cm) in the center of the ITC in order to determine its effect on the flux distribution. This stainless steel tube simulates a centrally located irradiation thimble in the reactor proper. Two radial traverses were also made in C-2 with a 0.635-cm aluminum liner in the ITC.

A. Axial Flux Distributions

The relative bare and cadmium-covered foil activities, corrected for background and decay, are presented for C-1 in Figs. 18, 19, 20, 21, and 22 for gold, dysprosium, indium, manganese, and U^{235}, respectively.

The stainless steel thimble caused an overall reduction of the axial flux, but did not change the shape of the flux distribution. This is shown in Figs. 19, 21, and 22.

Due to the reduced thickness of the top reflector, in most cases only 3.5 cm, the axial maximum does not occur at the center of the fuel region, i.e., at 28.9 cm as shown in Fig. 18, but at about 28 cm above the base plate. This shift in central maximum is less marked for C-2. All the above measurements were made at the center of the ITC. Figure 36 is an axial-direction plot obtained with U^{235}-aluminum foils at point 32 (Fig. 5) in the fuel region. The maximum-to-average ratios for the U^{235} foil traverses, considered to be proportional to the power, were computed and are presented in Table 17.

B. Radial Flux Measurements

The radial foil activations are presented in Figs. 23, 24, 25, 26, 27, and 28 for C-1 and in Figs. 37, 38, 39, 40, 41, 42, and 43 for C-2.

The effect of the stainless steel thimble can be noted in Figs. 24, 26, and 27 for C-1 and in Fig. 41 for C-2. The maximum in the ITC is reduced by approximately 11% in C-1 and 7% in C-2. The flux in the fuel region is not affected by the presence of the thimble in the ITC.

The dotted line in Fig. 27 is the calculated U^{235} activation in C-1. Although the experimental values in the fuel region agree quite well with the calculated values, some discrepancy may be noted in the ITC. This might be due to the fact that the neutron temperature was considered constant in each region for calculation purposes. This is not the case, as can be noted from the cadmium ratios discussed in a following section.

In Fig. 28 the subcadmium activations for the various foils in C-1 are presented. The solid curve is the calculated activation for a $1/v$ detector below 0.4 ev. The foil data have not been corrected for flux depression and self-shielding. The cadmium cutoff energy for a 0.0508-cm cadmium cover will also be somewhat higher than 0.4 ev. The experimental points agree with the calculated curve as far as the general shape is concerned.

The maximum-to-average ratios for the uranium-aluminum foils under various conditions are given in Table 17.

Table 17

MAXIMUM-TO-AVERAGE POWER RATIOS IN C-1 AND C-2 USING URANIUM-ALUMINUM FOILS

A. Axial Direction - Maximum-to-average Power

Position	Core	Maximum/Average
In center of ITC	C-1	1.27
In center of ITC	C-2	1.25
At position 1 (Fig. 5)	C-1	1.24
At position 2 (Fig. 5)	C-1	1.34
At position 3 (Fig. 5)	C-1	1.46
At position 32 (Fig. 5)	C-2	1.16

B. Radial Maximum-to-average Power Ratios

Conditions	Core	Maximum/ Average Fuel Zone	Maximum in ITC* / Average in Fuel
Clean, no liner, no thimble	C-1	2.05	3.32
Clean, no liner, no thimble	C-2	2.42	6.19
With central stainless steel thimble	C-1	1.94	3.07
With central stainless steel thimble	C-2	2.18	5.77
With aluminum liner, no thimble	C-2	2.18	6.87

*Fission rate ratio with sample of U^{235} in ITC.

1. Effect of a 0.635-cm Aluminum Liner around the ITC

The effect of placing a 0.635-cm aluminum liner around the ITC in C-2 was studied. The curve in Fig. 41 was obtained with the liner around a 12.7-cm x 12.7-cm ITC. As can be noted, the maximum in the ITC is considerably increased (11%) by the liner, whereas the peak in the fuel next to the ITC is somewhat reduced. The same effect is noted in Fig. 42 for the C-2' core (12 stainless steel plates per cluster, 13.97 x 13.97-cm^2 ITC). In this case the increase in the central maximum flux was only about 7%, whereas the reduction in the fuel peak flux was accentuated. All this indicates that the ITC was larger than the optimum size for maximum peak flux. The aluminum has a smaller slowing down

power than water and thus allows the fast neutrons to penetrate deeper into the ITC before being thermalized. This reduces the neutron capture rate in the water and yields an increase in the thermal flux.

2. Effect of a Simulated Void in the ITC

The effect of placing evenly distributed Teflon sheets (38% Teflon, 62% H_2O) in the ITC, simulating a void, is shown in Fig. 43. No large difference in flux distribution was achieved.

These measurements seem to indicate that the ITC is somewhat oversized as far as optimum peak flux per unit power is concerned.

C. Beam Tube Flux Distributions

Radial activation measurements were made through the beam tubes in both C-1 and C-2. Indium and dysprosium foils were used in C-1 and indium and uranium-aluminum foils were used in C-2. The data are presented in Figs. 46a and 47, respectively, for C-1 and C-2.

In Fig. 46a the indium curve was obtained in the south beam tube of C-1. This tube centerline was 5.1 cm below the top of the fuel clusters, while the other traverses were taken along the axis of the west beam port in both cores, 28 cm above the baseplate. The 10.16-cm-ID west beam tube extended up to the fuel face and was plugged with 10.1-cm-diameter beryllium discs for a distance of 15.24 cm from the fuel boundary, i.e., to a distance of 43 cm from the center of the reactor. The rest of the way the tubes were empty, but surrounded by beryllium to a radial distance of 58.5 cm and from there on by water. The approximate cadmium ratios for indium are presented in the same figures. The continued increase in the indium-cadmium ratio can be attributed to further thermalization and "diffusion cooling."

1. Neutron Energy Spectrum in West Beam Hole of C-1

The neutron energy spectrum between 1.1 Mev and 2.9 Mev was measured for C-1 by placing nuclear emulsions (Ilford L2) at five positions in the west beam tube. The emulsions were processed and scanned by J. H. Roberts of Northwestern University.[27] The emulsion plates were stacked in the following order, starting from the fuel face:

0.0508-cm Cd,	plate 2-316,	0.0254-cm Cd,	2.286-cm Be,
0.0254-cm Cd,	plate 4-316,	0.0254-cm Cd,	2.43 -cm Be,
0.0254-cm Cd,	plate 6-316,	0.0254-cm Cd,	4.712-cm Be,
0.0254-cm Cd,	plate 8-316,	0.0254-cm Cd,	4.826-cm Be,
0.0254-cm Cd,	plate 10-316,	0.0254-cm Cd,	

The diameters of the cadmium discs and the beryllium plugs were the same as the inside diameter of the beam tube.

Plates 2-316, 4-316, 6-316, 8-316, and 10-316 were 0.3, 3.0, 6.1, 11.5, and 16.9 cm respectively from the fuel boundary. Between 2000 and 3500 tracks were measured for each of the first four positions, and about 700 tracks for the fifth. Proton tracks in all directions were measured in the 400-micron emulsions. The volume of emulsion scanned was recorded so that the track density could be calculated. No tracks were measured which did not have at least one end 80 microns from either emulsion surface, so that no correction for escape of tracks through the emulsion surface was required. The neutron spectra were calculated from

$$F(E) = \frac{E}{n_p \sigma(E)} \frac{dM(E)}{dE} \quad ,$$

where $F(E)$ is the neutron spectrum in neutrons/(cm^2)(Mev) at energy E, n_p is the hydrogen density in the emulsion in atoms/cm^3, $\sigma(E)$ is the neutron-proton scattering cross section at energy E in cm^2, and $M(E)$ is the number of proton tracks per Mev/cm^3 of emulsion at energy E.

The results for the neutron spectra are shown in Fig. 46b. The results are in terms of the absolute fluxes. The values for position 10-316 were estimated by assuming the same shape as for position 8-316 and by taking the ratio of the track density for positions 8-316 and 10-316. The bars in Fig. 46b give the standard deviation for $dM(E)/dE$ over a broad range in energy. For example, the bars at 1.55 Mev for positions 2-316 and 4-316 give the standard deviation for the energy range from 1.1 Mev to 2 Mev. Similarly, the bars at 2.05 Mev give the corresponding quantity for the energy range 1.6 to 2.5 Mev.

Perhaps the most significant quantities that can be expressed for the results are $\int F(E)dE$ for the various energy ranges. Table 18 gives these values for four spectra. The values for position 10-316 were obtained from the corresponding values for 8-316 by multiplying the latter by 0.484, the ratio of the track densities for the two positions. These values have not been calculated for 6-316, which appears to have inconsistent results.

Table 18

$$\int_{1.1}^{2.0} F(E)dE \text{ and } \int_{2.0}^{2.9} F(E)dE$$

FOR NEUTRON SPECTRUM IN WEST BEAM TUBE OF C-1

Position	Energy Range, Mev	$\int F(E)dE \times 10^{-6}$ [n/cm^2]
2-316	1.1 to 2.0	32.0 ± 2.4
2-316	2.0 to 2.9	17.9 ± 2.8
4-316	1.1 to 2.0	25.3 ± 2.0
4-316	2.0 to 2.9	11.0 ± 2.4
8-316	1.1 to 2.0	7.4 ± 0.6
8-316	2.0 to 2.9	1.97 ± 0.39
10-316	1.1 to 2.0	3.6
10-316	2.0 to 2.9	0.95

D. Cadmium Ratios

The cadmium ratios for the various foils used were obtained from the ratio of the bare saturated activities to the cadmium-covered saturated activities. This is represented in Figs. 29 and 30 for C-1 and in Figs. 44 and 45 for C-2. These curves were obtained from the smoothed plots of the bare and cadmium-covered activities and are therefore also fairly smooth. In the radial cadmium-ratio curves, Figs. 30 and 45, the ratios in the center of the ITC were obtained from the axial measurements. The values of the cadmium ratios for the various foils in the center of the ITC and the center of the fuel zone (17 cm from the center of the ITC), along with the calculated[28] values, are given in Table 19.

As can be seen from the values listed, dysprosium is primarily a thermal neutron detector. The change in the uranium-aluminum foil cadmium ratio from 72 in the ITC for C-1 to 31 for C-2 is not understood. There is very little change in the average neutron temperature in the ITC due to the heavier loading of C-2, borne out by the cadmium ratios for the other foils, so that this change in the U^{235}-cadmium ratio is difficult to explain. The errors listed in Table 19 are the standard deviations computed from the foil-counting data only. Good correlation between the axial determinations and the radial determinations were found, so that the experimental errors cannot account for the discrepancy in the uranium-aluminum cadmium ratios.

Table 19

AVERAGE CADMIUM RATIOS IN THE FUEL REGION AND ITC

Foils	ITC		Fuel	
	Calculated	Experimental	Calculated	Experimental
Cadmium Ratio for C-1				
Au	3.6	10.5 ± 0.2	1.6	2.15 ± 0.05
Dy	-	312 ± 80	-	64 ± 4
In	7.24	14.7 ± 0.6	2.44	3.5 ± 0.1
Mn	45.6	55 ± 2	11.6	9.1 ± 0.2
U-Al	82 ± 4	72 ± 14	19.0 ± 0.7	16.1 ± 2
Cadmium Ratio for C-2				
Au	3.6	9.4 ± 0.1	Not Calculated	1.65 ± 0.02
Dy	-	290 ± 30		~17 ± 2
In	7.24	13.5 ± 0.2		2.05 ± 0.02
Mn	45.6	55 ± 2		4.8 ± 0.05
U-Al	82 ± 4	31 ± 1		3.6 ± 0.04

E. Effect of the Control Rods on the Flux Distribution

Since it is important in burnup calculations to know the flux distribution in the fuel clusters at different control rod positions, two such measurements were made with manganese foils. The results for C-1 are depicted in Fig. 48. The curve numbers refer to positions given in Fig. 5. The results from symmetrically located clusters were combined in the construction of these curves. In Fig. 48(2), safety rods No. 1 and No. 5 were inserted 5.41 cm below the top of the fuel clusters, i.e., they extended 1.92 cm into the fuel region. Control rods No. 1 and No. 2 were fully inserted, i.e., the cadmium portion extended to the center of the core in the axial direction. This difference in rod positions explains the shift in the central maxima.

In Fig. 48(3), the safety rods No. 1 and No. 5 were inserted to 24.5 cm below the top of the fuel clusters while control rods No. 1 and No. 2 were fully withdrawn.

The flux distribution at position 1, Fig. 48(1), was not affected significantly by these two rod positions, and it was obtained by combining the measurements obtained at each of the rod configurations. The

maximum-to-average ratio of the flux distributions for positions 2 and 3 are given in the figure. The central maximum is shifted away from the rod position and flattened on the control rod side of the maximum.

Detailed determinations of the flux distribution around control rods No. 1 and No. 2 were made with uranium-aluminum foils for C-1 in two perpendicular directions a-b and c-d in Fig. 5. Two conditions were compared in the same run, assuming symmetry of control rods No. 1 and No. 2 and neglecting the effect of rod No. 1 on the flux shape at rod No. 2. Control rod No. 1 was inserted with foils attached to its surface and located axially at various distances from rod No. 1. At the same time a plastic rule with attached foils was inserted into the rod No. 2 guide.

The results are shown in Figs. 49 and 50. Marked peaking in the control rod slot is evident from Fig. 49-A. The flux is considerably distorted by the presence of the control rod in the upper part of the core, as shown in Figs. 49-B and 50-B. The peaking in the control rod slot is masked by the high peak in the ITC, as is evident from Fig. 50-A.

In C-2, horizontal flux plots were obtained with uranium-aluminum foils at the midplane of the reactor along the same two directions as for C-1. These results are presented in Figs. 51-A and 52. Although there is considerable scatter in the foil data, the same effects can be noted in C-2 as in C-1.

9. GAMMA DOSE RATE IN C-2

The gamma dose rates listed in Table 20 have been measured for C-2 using duPont's film packet Type 544, completely surrounded by waterproof tape, 0.476-cm Lucite plates (one on each side but none along the edges), 0.127-mm cadmium sheet, and 0.318-cm boral plates, in that order. The dimensions of the constructed packs were: length 6.7 cm, width 5.7 cm, and thickness 2.3 cm. The purposes of the Lucite, cadmium, and boral were to achieve electronic equilibrium, gamma-ray energy independent response, and neutron filtration without intense gamma production, respectively.[29]

Control films were exposed to a standard radium-gamma source. These films were developed with the experimental films. The film densities were determined with an extended range densitometer in order to obtain a calibration curve for reading the experimental films. The coordinate system was chosen so that the origin was at the center of the reactor. The x-axis was along the E-W direction, the y-axis along the N-S, and the z-axis along the vertical.

Table 20

GAMMA DOSE RATES IN C-2

Location (x,y,z),cm	Dose Rate, r/(hr)(watt)	Remarks
0, 0, 0	89,77	
4.1, 5.8, 0	82	
-5.8, -4.1, 0	80	
-3.0, -5.8, 3.5	68	
3.0, -5.8, 3.5	63	
0, 0, 25.4	28	
4.1, -14.0, 30.1	29	
9.9, -14.0, 30.1	31	
14.6, 3.5, 30.1	31	
20.4, 3.5, 30.1	28	
29.1, 0, -0.9	44	
9.9, 24.1, 17.8	41	
29.1, 2.9, 17.8	34	
29.1, -2.9, 17.8	35	
-29.1, 2.9, 28.5	18	
-29.1, -2.9, 28.5	20	
-41.8, 0, -0.9	8.3	
59.6, 2.9, 0	3.1	
59.6, -2.9, 0	2.9	
3.9, -82.2, 0	0.76	
-3.9, -82.2, 0	0.79	
2.9, -101.7, 0	0.3	
-2.9, 101.7, 0	0.3	
69.6, -75.8, 0	0.27	
75.8, -69.6, 0	0.26	
-102.9, 0, -0.9	0.68	In west beam hole preceded by 15.2 cm of beryllium.
-, -, 50.8	4.9	Staggered around a Lucite rod, 4.1 cm from center of core.
-, -, 76.2	2.5	
-, -, 101.6	1.4	
-66.7, 2.9, 101.6	0.93	
-66.7, -2.9, 101.6	0.83	

These experiments were repeated at three different power levels. A gold foil at reference point 32 was exposed at the same time in order to compute the power for each run. The computed power levels for the three runs were 0.774 watt, 0.873 watt, and 34.14 watts.

The dose rates were multiplied by correction factors in order to satisfy the condition of equilibrium fission product activity.[30,31] The

correction factor is defined as the ratio of the theoretical equilibrium fission product power integrated over the core operating time during the run to the theoretical fission product power integrated over the film exposure time including core shutdown time. Such a correction factor does not account for the difference in the fission product gamma energy spectrum (upon which spatial dose depends) of the relatively short experimental operating time as compared with long operating times where equilibrium fission product concentrations effectively exist.

10. REACTIVITY EFFECTS

A. Sample Reactivity Worths in the Core

1. U^{235} Worths

The increase in reactivity associated with the introduction of a 1.7-gm sample of U^{235} (5.71 cm x 1.77 cm x 0.0127 cm) at various heights in the center of the ITC was measured in both C-1 and C-2. The sample was attached to one of the fine rod drives and the position of either of the two equivalent safety rods No. 1 and No. 2 noted for steady operation at each of the sample positions. The worth of the sample at the center of the reactor was also determined for C-2 by observing the rising period on introduction of the sample. The results of these measurements are presented in Fig. 53.

The increase in worth of C-2 was due to the higher fission rate in the ITC compared to the average fission rate in the fuel, as can be noted from results with the radial uranium-aluminum foil reported in Section 9. The shift in the maximum towards the bottom of the core can be explained by the difference in the average position of safety rods No. 1 or No. 5 during these measurements, as noted in Fig. 53. The greatest shift in the maximum could be expected for the rod position nearest the midplane of the reactor, which was the case for the C-2 measurements. No correction to the U^{235} worths was made for flux depression.

The average worth found by integration of the curve in Fig. 53 for C-1 was 2.28×10^{-4} $\Delta k/k/gm\ U^{235}$. A determination of the U^{235} worth was also made in C-1 by inserting a 54.6-cm x 0.033-cm x 2.24-cm strip of polyethylene in which 3.25 gm of U^{235} were dispersed. The U^{235} density in this strip was 0.806 gm/cc and the disadvantage factor close to unity. This measurement should be compared with the average U^{235} worth, and yielded a value of 6.07×10^{-4} $\Delta k/k/gm$ as compared with 2.28×10^{-4} $\Delta k/k/gm$.

The reactivity worths associated with the insertion of extra fuel plates in various locations in the core for C-1 and C-2, as shown in Fig. 5, are given in Table 21. These values should also be compared with

the average values in the ITC given above. The values for C-2 were obtained by successively withdrawing the fuel strips while the reactor was still in operation, as contrasted with shutting down the reactor for addition or removal of the plates in C-1. This procedure was necessary due to the drift observed after successive shutdowns in C-2.

Table 21

U^{235} WORTHS IN C-1 AND C-2

Location (see Fig. 5)	Reactivity Worth/gm 93.5% Enriched U^{235}, 10^{-4} $\Delta k/k$	
	C-1	C-2
Center of ITC	2.28	3.32
34	1.18	0.26
	1.35	
35	0.92	0.13
36	0.99	0.19
37	0.96	
38	0.89	
39	0.81	
40	0.78	
41	1.28	
42	0.77	
43	0.96	
44	0.31	
Around ITC periphery 16 fuel plates, 8.2 gm U^{235} each	-	1.34

2. Cadmium Worths

The decrease in reactivity caused by placing a cadmium sample at various locations in the core was determined in the same way as were the U^{235} reactivity worths. The reactivity worth in the axial direction in the No. 2 control rod position in C-1 and in the center of the ITC in C-2 was measured by attaching a 0.053-cm x 2.54-cm x 5-cm cadmium sheet to the control rod No. 2 drive, as for the U^{235} worth. The results are given in Fig. 54. The average reactivity worth for cadmium in the control rod slot of C-1 was found to be $-1.3 \times 10^{-3}\%$ $\Delta k/k/cm^2$ for the center 45-cm portion, and $-1.7 \times 10^{-3}\%$ $\Delta k/k/cm^2$ for C-2 in the center of the ITC over the same vertical distance. These values have not been corrected for flux depression.

The reactivity worth of cadmium at other locations in the core was found by inserting either a cadmium strip P (53.34 cm x 1.27 cm x 0.053 cm), or a cadmium tube T (50.8 cm long x 0.343 cm OD x 0.241 cm ID) in C-1 at these locations. In C-2, a cadmium tube R (57.79 cm long x 0.0889 cm ID x 0.1905 cm OD) was used. These tubes were considered as black rods of geometric area of $2\pi r\ell$, i.e., 54.75 cm^2 for C-1 and 34.6 cm^2 for C-2. The results are presented in Table 22. The locations are noted in Fig. 5.

Table 22

CADMIUM WORTHS IN C-1 AND C-2

Location (Fig. 4)	Cadmium Used	Remarks	$(-10^{-5}\ \Delta k/k)/cm^2$ Cadmium*	
			C-1	C-2
Center	T	Inside SS thimble	1.3	
Center	P	Without thimble	1.4	
B	P	Without thimble	3.6	
C	P	Without thimble	3.1	
1	P	Without thimble	2.7	
E	P	Without thimble	2.2	
F	P	Without thimble	3.0	
G	P	Without thimble	2.6	
H	P	Without thimble	2.4	
I	P	Without thimble	1.8	
J	P	Without thimble	2.2	
34	R	Period measurement		2.5
35	R	Period measurement		2.0
36	R	Period measurement		1.0

*The areas considered were the geometrical areas only, i.e., 2 x length x width for flat plates, and π x diameter x length for the rods.

The values found with the 53.34-cm long strip in C-1 were consistently higher than those found with the 2.54 x 5-cm^2 sheet. This may be attributed to the difference in flux depression due to the different geometrical sizes. The neutron-absorbing areas per unit height were about 5 cm^2/cm, 2.5 cm^2/cm, and 1.1 cm^2/cm for the sheet, strip, and tube, respectively.

3. Stainless Steel Central Thimble Worth

The reactivity worth of the central stainless steel thimble (Type 304 stainless steel, 3.81 cm OD, 61 cm long, 0.056-cm wall thickness) was measured when voided and when filled with water. The results are as follows:

	C-1	C-2
Voided	-	+0.2 % $\Delta k/k$
H_2O filled	-0.1% $\Delta k/k$	-0.14% $\Delta k/k$

4. Worths of the Stainless Steel Poison Strips in C-2

In measuring the reactivity worths of the stainless steel strips, simulating burnable poison, in the fuel zone, it was necessary to reduce the excess reactivity in the core before removing the steel. This was accomplished by removing the 16 extra fuel plates along the periphery of the ITC. Their average worth was 0.1×10^{-2} $\Delta k/k$/plate, or 1.34×10^{-4} $\Delta k/k$ gm, as reported in Table 21.

The 680 stainless steel strips were removed in three increments, one of 24, one of 174, and the last of 480. In removing plates, the remainder was relocated in order to keep a uniform distribution.

For the first measurement, two plates were removed from each of the twelve boxes forming the outer ring of fuel. This provided a means of estimating the total amount to remove in order to obtain the required excess reactivity for temperature-coefficient measurements. In the second increment a total of 198 plates was removed to leave 12 plates per cluster evenly distributed. This constitutes the C-2' loading. After some experiments (control rod calibrations, temperature coefficient measurements, etc.) were performed with this loading, the rest (480) of the stainless steel was removed. These three determinations yielded an average worth of -0.38×10^{-5} $\Delta k/k$/gm of Type 304 stainless steel. This is a reactivity worth of -13.3% $\Delta k/k$, which also would be approximately equal to the reactivity worth of the C-2 minus C-1 U^{235} content, viz., 3480 gm of U^{235}.

According to the above, C-2 unpoisoned had 13.3% more excess reactivity than C-1, yielding a worth of 0.38×10^{-4} $(\Delta k/k)$/gm U^{235}. This compares favorably with the values listed in Table 21, if it is kept in mind that the worth per gram decreases as the total mass of U^{235} increases, starting from about 0.9×10^{-4} $\Delta k/k$ as for C-1 and ending at about 0.2×10^{-4} $\Delta k/k$ as for C-2.

B. Reactivity Effects Associated with Fuel Displacement

As it might be necessary to assemble a new core for an operating reactor under water, the reactivity effects associated with cluster displacement were investigated.

1. Comparison of Fuel Box Reactivities in C-1

Since some question existed about the variations in fuel and water contents of fuel boxes, an arbitrarily selected box was interchanged systematically with twelve others. The differences appeared to be too small to determine accurately within the reproducibility of the measurements. The standard deviation from the average for twelve boxes was $2 \times 10^{-2}\%\ \Delta k/k$. Comparison of reference runs gave a standard deviation $3 \times 10^{-2}\%\ \Delta k/k$, so that no conclusions can be drawn from these measurements.

2. Vertical Displacement of a Fuel Cluster in C-2

The reactivity effect of raising a fuel cluster vertically out of the core is shown in Fig. 55. Except for the four clusters next to the ITC, where the axial flux peaking in the top reflector is less marked, a small increase in reactivity (not over 0.05% ρ) was found for the first 14 cm to 20 cm of displacement, although a decrease is observed for each cluster entirely removed from the core.

3. Tilting a Fuel Cluster into the ITC in C-2

Figure 56 shows the effect on reactivity obtained by tilting one of the surrounding fuel clusters into the ITC as measured by compensation with a calibrated control rod.

According to this graph, about 1 dollar of reactivity is gained by tilting the cluster fully over into the ITC (at about 13.6° as shown). This could conceivably occur with two clusters moving simultaneously; consequently the effect might be quite large if permitted in the design of a reactor.

4. Reactivity Effects of Moving Four of the Eight Peripheral Clusters into the ITC

The reactivity gained by moving a cluster from the peripheral zone (e.g., clusters 18 and 24, Fig. 5) into the ITC of the C-2 core with all the stainless steel removed was measured by rod substitution.

Moving a cluster into the corner of the ITC ($13.97 \times 13.97\ cm^2$) adds 4.8% $\Delta k/k$. Moving another cluster to a position adjacent to the first adds another 3.7% $\Delta k/k$. Placing it into the ITC diagonally opposite to the first results in an increase of 4.4% $\Delta k/k$. Closing up the ITC completely by adding two more peripheral clusters diagonally results in a further reactivity increase of 1.2% $\Delta k/k$.

This means that the clean unpoisoned C-2 core, with the four east-west peripheral clusters moved into the ITC has approximately 10.8% Δk more reactivity than the regular unpoisoned C-2 core.

C. Reactivity Worths of Various Materials in the Beam Tubes

Measurements were made of the reactivity effects of Lucite, beryllium, and cadmium in the west horizontal beam port of the reactor (see Section 2 and Fig. 4). This 10.14-cm-ID tube faces against the aluminum separator between the fuel and the beryllium reflector. The worths of the various samples were determined in the second core, C-2, by inserting them in the beam tube while the reactor was critical and compensating with coarse control rod No. 1. In C-1, criticality was obtained without the sample, the rod position noted, the reactor scrammed, and after insertion of the sample the reactor was again made critical and the new rod position noted. The worths of the samples obtained for the second core, C-2, although they cannot be compared with the values for C-1 because of different loadings, are therefore more reliable, as these measurements were influenced by the reactivity drift encountered between runs in both cores.

The beryllium sample consisted of four cylindrical plugs (each of 10.13-cm diameter) stacked to a total length of 14.27 cm. The Lucite plug was 31.24 cm long and about 10.13 cm in diameter. The Lucite-cadmium collimator consisted of a similar cylinder bored to a 2.54-cm ID and lined with a 0.058-cm-thick cadmium sleeve. The cadmium disc was 0.053 cm thick and 10.109 cm in diameter. This disc was inserted into the beam tube by placing it ahead of the Lucite plug. The reactivity worths of each configuration for both cores C-1 and C-2 are given in Table 23.

Table 23

REACTIVITY WORTHS OF SAMPLES IN THE HORIZONTAL BEAM TUBE

Sample	Change in Reactivity, %	
	C-1	C-2
Beryllium	+0.274	+0.316
Lucite	+0.099	+0.078
Lucite-Cadmium Collimator	+0.013	~0.0005
Cadmium Disc	-0.013	-0.170

D. Reflector Worths

The reactivity worth of the top reflector (H_2O) has been determined for both cores of the AHFR critical assembly. This was done by two techniques, by the ramp input reactivity method,[8] and by rod substitution. In the rod substitution method, safety rod No. 1 was used in C-2 and safety rod No. 5 in C-1. These results are plotted in Figs. 57 and 58. In the ramp input

method (see Fig. 58), the detector used for observing the flux decline was located below the reactor vessel on the core centerline. The reflector was allowed to drop slowly at a fairly constant rate from 134 cm to 53 cm. In studying the curves in Figs. 57 and 58, it should be kept in mind that the fuel zone extends to 54.3 cm, and that the aluminum tops of the clusters extend another 3.5 cm to 57.8 cm.

Several details should be noted. For the second core, the total worth by the ramp input technique differs from the rod substitution value by a factor of 3. The ramp input curve is also not monotonic, but is characterized by a hump at 64 cm. Tests in a transparent container showed that if water was allowed to stand at a height of about 130 cm above the bottom of the fuel clusters for some time, and then let out slowly, fairly large bubbles escape from the clusters between about a water height of 60-70 cm. This might explain the shape of the "ramp input" curve.

For the first core, C-1, the total worth curve levels off at a water level of about 64 cm, i.e., 10.7 cm above the fuel. For C-2 there is only a change in slope at this point. This result is attributed to compression of bubbles in the fuel zone.

E. Beryllium Reflector Worth and the Reactivity of the Unpoisoned C-2 Core in Water

The beryllium reflector consisted of small assorted blocks in 10.2-cm-thick layers, separated by 0.64-cm-thick Lucite plates. There were five layers of each, Lucite being the bottom layer.

The comparative worth of this reflector versus water as reflector was determined by successively removing the top layers of beryllium. After the first layer was removed, it was necessary to remove all the stainless steel to maintain criticality. The first layer yielded a worth of 2.13×10^{-2} $\Delta k/k$ when replaced by water. The second layer was worth 3.63×10^{-2} $\Delta k/k$, and the third 3.94×10^{-2} $\Delta k/k$. From the symmetry of the core, the last two of the five layers were considered of equal worth to the first two. From this the total worth of the beryllium as reflector rather than water as reflector was found to be of the order of 15.5% $\Delta k/k$.

It was further found that a 6-by-6 array of clean C-2 fuel clusters (no ITC, no stainless steel) yielded an excess reactivity of approximately 3.6% when totally water reflected. Table 24 lists these data for comparison. The numbers give the order of magnitude only.

It would thus seem that the poisoned core may safely be assembled and stored under water, as filling the ITC accidentally with fuel would not yield a critical configuration. The 180-gm U^{235} per cluster unpoisoned fuel could, however, not be handled in this manner, as the presence of only one cluster in the ITC would make it critical.

Table 24

EXCESS REACTIVITIES AND REACTIVITY WORTHS ASSOCIATED WITH VARIOUS CORE CONFIGURATIONS

Description	Reactivity, % Δk/k
Clean C-1 core, 12.7 x 12.7 cm^2 ITC, 3.64 kg U^{235}, beryllium reflector.	~1.2 (excess)*
Clean C-2 core, 17 stainless steel plates per cluster, 12.7x12.7 cm^2 ITC, 7.25 kg U^{235}, beryllium reflector.	~0.4 (excess)*
C-2 core, 13.97x13.97 cm^2 ITC, 7.12 kg U^{235}, 17 stainless steel plates per cluster, beryllium reflector.	1.2 (subcritical)
C-2' core, 13.97x13.97 cm^2 ITC, 7.12 kg U^{235}, 12 stainless steel plates per cluster, beryllium reflector.	2.6 (excess)*
C-2 core, 13.97x13.97 cm^2 ITC, no stainless steel, 7.12 kg U^{235}, beryllium reflector.	12.1 (excess)
Worth of 34.34 kg of stainless steel ≡ 3.48 kg U^{235}. (This is the difference between C-1 and C-2.)	13.3% Δk/k
C-2 core, no stainless steel, 7.12 kg U^{235} with east and west peripheral clusters moved into ITC, beryllium reflector.	22.5% (excess)
C-2 regular core, totally water reflected, 7.25 kg U^{235}, 12.7x12.7 cm^2 ITC, 17 stainless steel plates per cluster.	15.1 (subcritical)
C-2 core, 7.12 kg U^{235}, 13.97 x 13.97 cm^2 ITC, 17 stainless steel plates per cluster, water reflected.	16.7 (subcritical)
C-2' core, 7.12 kg U^{235}, 13.97 x 13.97 cm^2 ITC, 12 stainless steel plates per cluster, water reflected.	12.9 (subcritical)
C-2 core, 7.12 kg U^{235}, 13.97 x 13.97 cm^2 ITC, no stainless steel, water reflected.	3.4 (subcritical)
C-2 core, 7.12 kg U^{235}, four east-west peripheral clusters into ITC, no stainless steel, water reflected.	~7 (excess)
6 x 6 array of clean C-2 fuel clusters in water, no stainless steel.	~3.6 (excess)
Worth of beryllium reflector rather than water reflector in C-2.	15 5% Δk/k

*These numbers were found by calibrated control rod substitution.

The water-reflected C-1 core, containing 90 gm of U^{235} per cluster and no stainless steel, was slightly subcritical after the ITC was filled by moving peripheral clusters into the ITC. The subcriticality was less than 1% $\Delta k/k$, as indicated by multiplication measurements. Core C-1 would thus be subcritical by approximately 15% if totally water reflected, and even the addition of unpoisoned C-2 clusters in the ITC would not make it critical in water without the beryllium reflector.

11. REACTIVITY COEFFICIENTS

A. Void Coefficients

Measurements of void coefficients were made in various locations of both C-1 and C-2. These data are presented in Figs. 59 to 64 and in Table 25.

Table 25

VOID COEFFICIENTS AT VARIOUS POSITIONS IN CORE C-1

Strip Positions (Fig. 5)	Teflon Volume Used, cm^3	Distance from Center, cm	Void Coefficient,* % ρ/% Void
Centerline	27.1	0.0	+0.46
55	-	3.5	+0.58
50	1022	4.9	+0.73
53	150.6	6.4	+0.18
53	76.7	6.4	+0.47
60	75.3	6.6	+0.73
60	99.1	6.6	+0.54
54	75.51	6.8	+0.62
53	75.51	6.9	+0.47
51	75.51	7.1	+0.64
52 and 75	75.3	7.2	+0.19
46 and 34	113	11.9	-0.90
46	75.3	12.6	-1.02
46 and 58	150.6	13.6	-0.65
47 and 57	150.6	18.1	-0.61
48, 56, and 59	150.6	23.4	-0.06
61	113	23.57	+0.36**
45 and 49	212.6	28.0	+0.24**

*Calculated as % void of total fuel zone and ITC volume, excluding beryllium and top and bottom reflectors (108.3 liters).

**Between fuel zone and beryllium reflector.

Teflon was used in most of these measurements because of its near equivalence to air in small volumes. The small spaces available for void insertion in the fuel region required thin devices, which were readily made from Teflon. It is readily seen from Fig. 63 that up to about 10% of the ITC volume, i.e., 800 cm^3 evenly distributed, Teflon and air are nearly equivalent. Tests for small strips of Teflon showed no measurable difference between air and Teflon. Figure 60 depicts the data obtained by traversing with an 800-cm^3 Teflon plug inside a voided tube in the ITC of C-2. It acts mostly as an absorber in the center of the reactor, but has some scattering properties when used as an upper reflector. The data in Figs. 61 to 64 were obtained by inserting strips of Teflon of less than 80-cm^3 volume, extending all the way through the core. In this manner, the worth as presented in Fig. 60 was averaged out. The change in reactivity due to the "void" was observed either by rod substitution or by observing the rising period due to void removal (fuel region in C-2). The shift in the maxima in Fig. 59 may be due to the different control rod positions during the measurements.

From Table 25 and Fig. 61, it is evident that the void coefficient is positive in the ITC. This positive region extends about 1 cm further into the fuel region. The scatter in the data at the boundary is due to the difficulty in locating the strips in the core accurately and the fact that the gradient is fairly steep in that region. There is an approximate 2-cm annulus around the fuel region in C-1, extending into the beryllium reflector, where the void coefficient is also positive. The overall void coefficient however is negative.

The data in Table 25 and Fig. 61 are presented as %-reactivity/void-% of the total core volume excluding the beryllium and top and bottom H_2O reflectors. This was done in order to obtain continuity going from the ITC to the fuel region. All the other void coefficient data are expressed as %-void of the ITC only. The volumes were as follows:

Volume of the ITC = 8.19 liters (12.7 x 12.7 x 50.8 cm^3)

Volume of the fuel region = 100.1 liters (6.985 x 6.985 x 50.8 x 40 cm^3)

Total Volume = 108.29 liters

The average void coefficients, expressed as %-reactivity/%-void of total core volume (108.3 liters), are given in Table 26.

Table 26

AVERAGE VOID COEFFICIENTS FOR C-1 AND C-2

Region	Void Coefficient % Δk/% Void	
	C-1	C-2
ITC	+0 68	+1 1
Fuel Region	-0 45	-0 45
Core and ITC	-0 37	-0 34

These values were obtained by numerical integration of Fig 61, where

$$\text{Average void coefficient} = \frac{\int_{r_1}^{r_2} (\text{void coefficient})\, r\,dr}{\int_{r_1}^{r_2} r\,dr}$$

Although the void coefficient is positive in the ITC, the overall coefficient is still negative As it was thought possible to make the central vertical thimble large enough so that the void coefficient, with the thimble in place, would be negative, measurements of the void coefficients were made with different fixed void volumes in the ITC Teflon strips were used in all these measurements

Figure 62 presents the data obtained for various fixed volumes of air (Lucite boxes), Teflon (thin distributed strips) and aluminum (thin distributed plates) The volume of the fixed "void" is presented as per cent of the ITC volume (8 2 liters) It is evident that the void coefficient turns negative at about 70% total volume of air or aluminum This is also born out by the integral worths as presented in Fig 63 A 40% fixed void in the ITC might be considered as a "safe" condition, as increasing the void fraction from this to 70% void would add less than one dollar in reactivity

The effect of removing the central sample or thimble while the reactor is operating was also studied The curves shown in Fig 64 were obtained by withdrawing the "void" (aluminum or Teflon strips, or a Lucite box) from the ITC while compensating with a calibrated control rod Because the void coefficient turns negative at approximately 70% total void, the total worth of 81% void in the ITC is nearly equal to the reactivity worth of the 56 25% void

B. Temperature Coefficient of Reactivity

The temperature coefficients for C-1 and C-2 were measured by heating the water moderator in the storage tank and then circulating it through the reactor. The reactivity drift with temperature was then measured by allowing the reactor to cool off while compensating with a calibrated control rod.

In C-1, only two thermocouples were used, one between the control rod channel and the beryllium, and the other about 5 cm away from the tank wall in the water. In C-2, eleven thermocouples were installed at various locations in the core and reflector. Readings were only recorded after equilibrium temperatures were reached. A stirrer was also added in the reactor tank to ensure thorough mixing of the water and to facilitate the reaching of equilibrium conditions.

The data obtained are presented in Fig. 65 for C-1 and in Fig. 66 for C-2. The reactivity temperature coefficient measurements for C-1 were fitted to the empirical equation

$$\rho = 0.013\,[1 - \exp(-0.00742\,T_1^* - 0.04306\,T_2^*)] \quad ,$$

where $T^* = (61.0 - T)°C$ and covers the range from 16 to 58°C. The temperature T_1 is that of the H_2O, whereas T_2 is assumed to represent the mean beryllium temperature. It should be noted that the beryllium reflector contained about 10 vol-% H_2O and Lucite.

The selection of the form of the equation was governed by the problem at hand. This equation was fitted for least-squared errors by multiple correlation of reactivity with two variables, T_1 and T_2. The equation does not provide for changes in sign of a coefficient in the range of the data fitted, but provides for variations in magnitude in both coefficients.

The derivative with respect to temperature ($T_1 = T_2$) indicates an increasing magnitude of the temperature coefficient as the temperature increases. The slope of the fitted curve (Fig. 65) yields a value of $-0.055\%\ (\Delta k/k)/°C$ at 59°C and $-0.01\%\ (\Delta k/k)/°C$ at 20°C. Efforts to fit for linear coefficients over short segments of the data consistently gave positive coefficients for the beryllium (containing 10% H_2O and Lucite) reflector near room temperatures. It should also be kept in mind that for C-1, positive void coefficients were found at the fuel-beryllium interface. Thus, a change in sign of the beryllium temperature coefficient seems to be indicated at higher temperatures.

The fitted curve discussed above is presented also in Fig. 66 for comparison. The data for C-2 between 55°C and 62°C were obtained for a single continuous run, following the temperature over a seven-hour

period. The dotted line through these points (see Fig. 66) yields a temperature coefficient of -0.01 $\Delta k/°C$. The data near room temperature, taken as linear with temperature, indicate a temperature coefficient in this range of -0.008% $(\Delta k/k)/°C$. The points marked with an asterisk (*) in Fig. 66 were obtained during a run in which some instabilities were induced by the stirrer in the core tank, and no significance can be attached to the apparent positive coefficient as measured.

The following should be noted regarding the temperature coefficient measurements in C-2. The reactor was subject to long-term losses of reactivity as discussed in Section 4. The losses had been negligible during the week preceding the temperature-coefficient measurement, but a total of 0.3% reactivity was lost during the nine days it took to complete these measurements. No known adjustment fully explains the shallow slope of the curve during cooling while operating in view of the 1.3% reactivity difference between the 60°C data and the room temperature data. The linear data at the higher temperatures may have been influenced by a steady loss of reactivity during this run, although a five-hour run at constant room temperature did not exhibit any remarkable drift in reactivity. Remembering that the reactivity loss is largely due to bubble formation in the fuel region, increased temperatures might have a marked effect on this loss.

Taking into account the 0.3% reactivity lost between the first and last measurements, the "gross" temperature coefficient between 20°C and 62°C is $\sim -0.024\%\ \rho/°C$, which is the same as for C-1 (i.e., dividing the total reactivity change by the temperature change from 20°C $\longrightarrow$ 62°C).

The overall temperature coefficient is negative for both C-1 and C-2 over the temperature ranges investigated, and it does seem to increase markedly with temperature.

12. CONCLUSIONS

The data obtained in the critical experiments described agree reasonably with the design specifications. The peak flux in the ITC for C-1, representing the end-of-cycle core, and for C-2, representing the new core, remains fairly constant at 3×10^7 $n/(cm^2)(sec)(watt)$. Considering that the nature of the fuel available and other factors caused these cores to depart considerably from optimum, the results indicate that somewhat higher peak fluxes might be obtained.

It is evident from Fig. 43 that a 38% "Teflon void" has no significant effect on the peak flux in the ITC. It might therefore be possible to construct a sample for irradiation in such a way as to occupy 40% of the ITC, providing a "safe" condition without losing too much in available flux.

The flux measurements with the aluminum liner in the ITC indicates that the size of the ITC may be decreased with some gain in peak flux. This would, however, also decrease the space available for irradiations.

Measurements made with the C-1 and the C-2 cores immersed in water, without beryllium reflector, indicated that it should be feasible to load and unload the cores as units. Care should be exercised in assembling the cores under water, as an accidental insertion of a fuel cluster into the ITC might approach or exceed a critical configuration in the event that fuel elements should have an unusual amount of fuel or no burnable poison.

ACKNOWLEDGMENTS

In addition to those already mentioned, the following people also contributed to this experiment as indicated. Roland J. Armani provided absolute fission determinations by radiochemical analyses of irradiated uranium samples. Charles E. Cohn conducted the measurements of prompt neutron lifetime, photoneutron effectiveness, and also the ramp reactivity measurements. I. K. Olson assisted with data analysis and curve fitting. H. F. Reed measured the gamma-radiation field in and about the reactor. J. H. Roberts (Northwestern University) measured the fast flux distribution in the reflector region. William R Robinson provided many of the foil-activation measurements. Roger L. Stover aided in measuring corrosion rates. The operating crew of the AHFR critical experiment were: W. C. Redman (Section Head), K. E. Plumlee (Group Leader), Q. L. Baird (Physicist), J. W. Armstrong (Technical Assistant), W. R. Robinson (Sr. Technician), and F. W. Kodrick and R. A. Schultz (Technicians).

REFERENCES

1. L. E. Link et al., Argonne High Flux Research Reactor - AHFR Conceptual Design Study, ANL-5983 (June 1959).
2. W. C. Redman et al., Hazards Summary Report on the Oxide Critical Experiment, ANL-5715 (April 1957).
3. C. N. Kelber, D. H. Lennox, and K. E. Plumlee, Hazards Summary Report on AHFR Critical Experiments, ANL-5715-Addendum 1 (to be published).
4. The Reactor Handbook, Vol. 2 - Engineering, Chapter 1.11, AECD-3646. Technical Information Service, U.S. Atomic Energy Commission (May 1955).
5. C. E. Cohn, Determination of Reactor Kinetic Parameters by Pile Noise Analysis, Nuc. Sci. and Eng. 5, 331 (1959).
6. A. S. Brunson et al., Measuring the Prompt Period of a Reactor, Nucleonics 15, 132 (Nov 1957).
7. Reactor Physics Constants, ANL-5800, p. 239.
8. G. G. Bilodeau et al., PDQ - An IBM-704 Code to Solve Two-dimensional Few-group Neutron Diffusion Equations, WAPD-TM-70 (1959).
9. C. E. Cohn, private communication (Jan 1959).
10. Reactor Physics Constants, ANL-5800, p. 25.
11. S. Bernstein et al., Yield of Photoneutrons from U^{235} Fission Products in Heavy Water, Phys. Rev. 71, 573 (1947).
12. C. E. Cohn, Errors in Reactivity Measurements Due to Photoneutron Effects, Nuc. Sci. and Eng. 6, 284 (1959).
13. Reactor Physics Constants, ANL-5800, p. 238.
14. C. E. Cohn, private communication.
15. C. E. Cohn, private communication.
16. D. P. Gamble, The Effect of Reflector-moderated Neutrons on the Kinetics of the Kinetic Experiment Water Boiler Reactor, Trans. Am. Nuc. Soc. 3, 122 (1960).
17. Atomics International Annual Technical Progress Report No. NAA-SR-5350, p. V-19 (1960).
18. G. R. Keepin and T. F. Wimett, Reactor Kinetic Functions: A New Evaluation, Nucleonics 16, 86 (Oct 1958).
19. J. J. Kaganove, Argonne National Laboratory, Private Communication.

20. K. E. Plumlee and M. T. Wiggins, Foil Activation Data Handling with Automatic Counters and a High Speed Computer, Trans. Am. Nuc. Soc. 4, No. 1 (June 1961).

21. J. C. P. Miller, Numerical Quadrature Over a Rectangular Domain in Two or More Dimensions, Part 1. Quadrature Over a Square, Using Up to Sixteen Equally Spaced Points, Mathematics of Computation 14, 16 (1960).

22. H. Amster and R. Suarez, The Calculation of Thermal Constants Averaged Over a Wigner-Wilkins Flux Spectrum: Description of the Sofocate Code, WAPD-TM-39 (Jan 1957).

23. C. H. Westcott et al., Effective Cross Section Values for Well-moderated Thermal Reactor Spectra, CRRP-787 (AECL No. 670) (1958).

24. C. H. Westcott et al., Effective Cross Sections and Cadmium Ratios for the Neutron Spectra of Thermal Reactors, Proc. of Second Geneva Conference on the Peaceful Uses of Atomic Energy, Vol. 16, 70 (1958).

25. Reactor Physics Constants, ANL-5800, p. 338-340.

26. Ibid., pp. 485-487.

27. J. H. Roberts, Absolute Flux Measurements of Anisotropic Neutron Spectra with Proton Recoil Tracks in Nuclear Emulsions, RSI-28, 677-680 (1957).

28. J. O. Juliano et al., Critical Experiments for the Preliminary Design of the Argonne High Flux Reactor - Part B. Neutron Spectra, Trans. Am. Nuc. Soc. 4, No. 1 (June 1961).

29. M. Ehrlich and S. H. Fitch, Photographic X- and Gamma-ray Dosimetry, Nucleonics 9(3), pp. 5-17 (1951)

30. J. R. Stehn and E. F. Clancy, Fission-product Radioactivity and Heat Generation, Proc. of the Second Geneva Conference on the Peaceful Uses of Atomic Energy, Vol. 3, 726-746 (1958).

31. J. F. Perkins and R. W. King, Energy Release from the Decay of Fission Products, Nuc. Sci. and Eng. 3, 726-746 (1958).

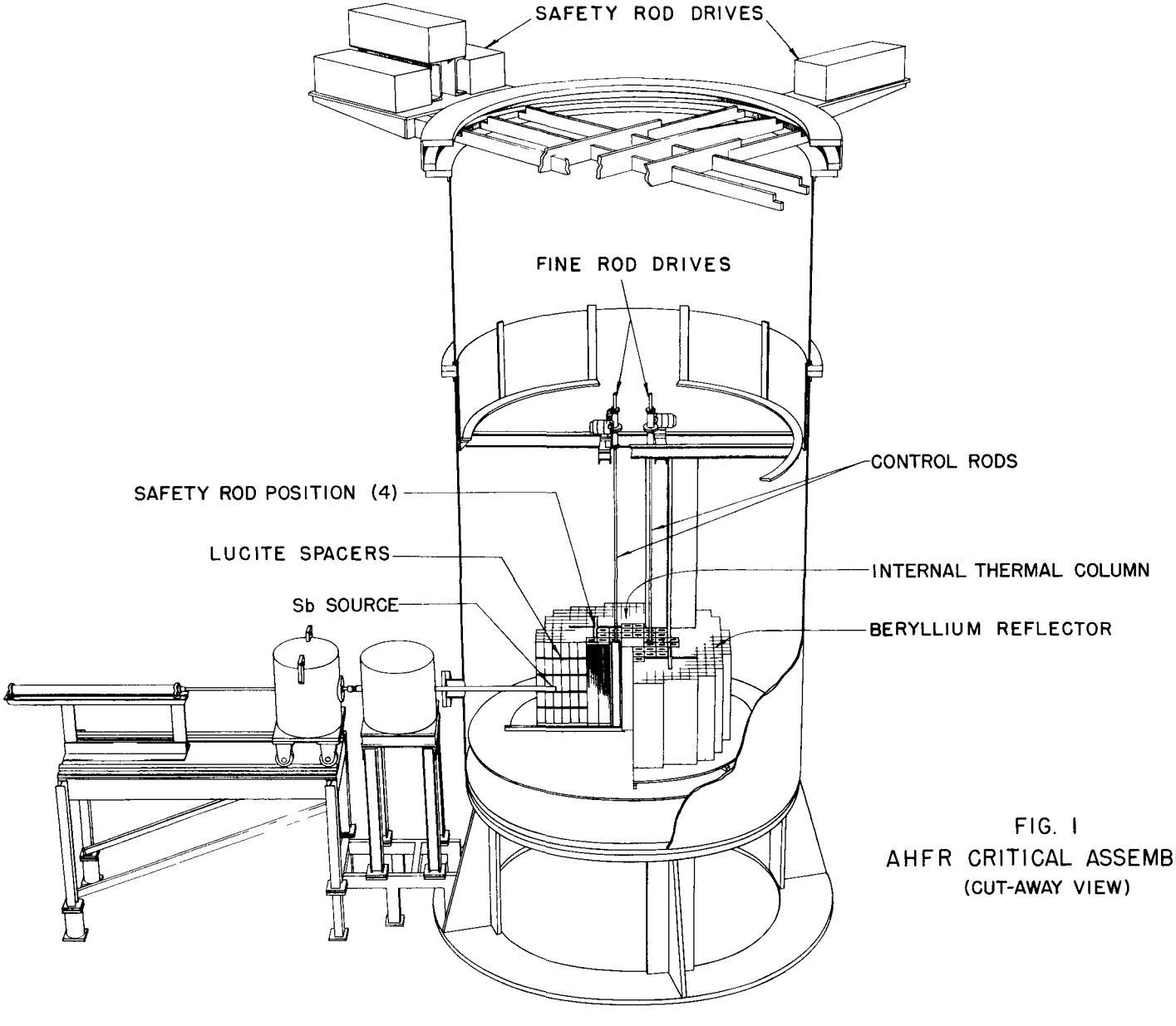

FIG. 1
AHFR CRITICAL ASSEMBLY
(CUT-AWAY VIEW)

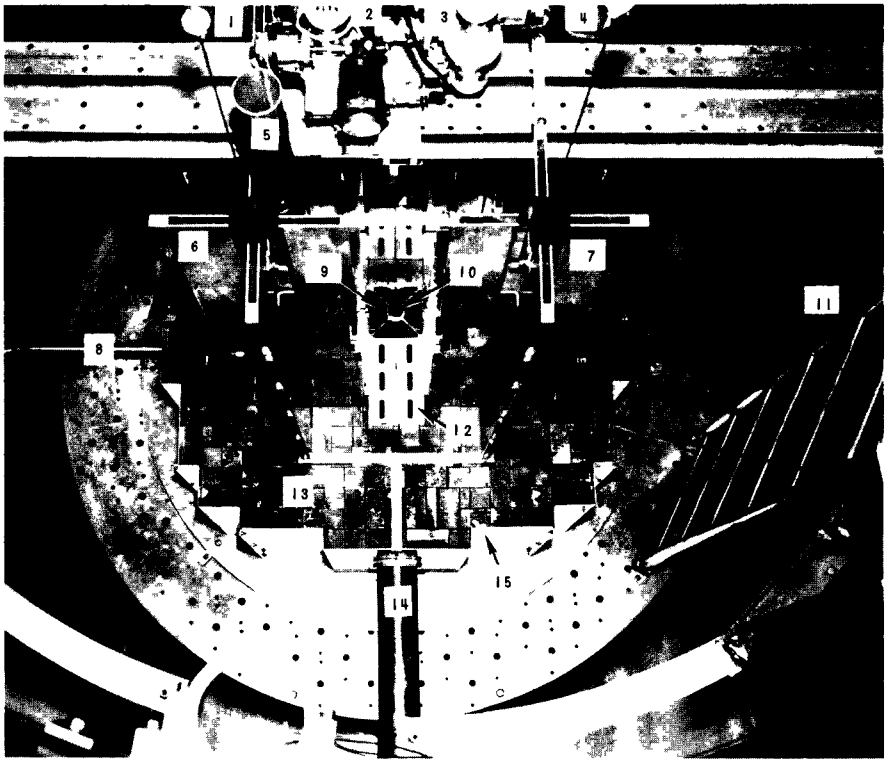

LEGEND

1. SAFETY ROD NO. 1 GUIDE
2. FINE ROD DRIVE NO. 1
3. FINE ROD DRIVE NO. 2
4. SAFETY ROD NO. 3 GUIDE
5. INSTRUMENT THIMBLE
6. SAFETY ROD NO. 7 GUIDE
7. SAFETY ROD NO. 5 GUIDE
8. SOURCE TUBE
9. INTERNAL THERMAL COLUMN
10. CENTRAL THIMBLE
11. SOUTH BEAM TUBE
12. CORE
13. BERYLLIUM REFLECTOR
14. WEST BEAM TUBE
15. REFLECTOR SHROUD

FIG. 2
AHFR COMPONENTS

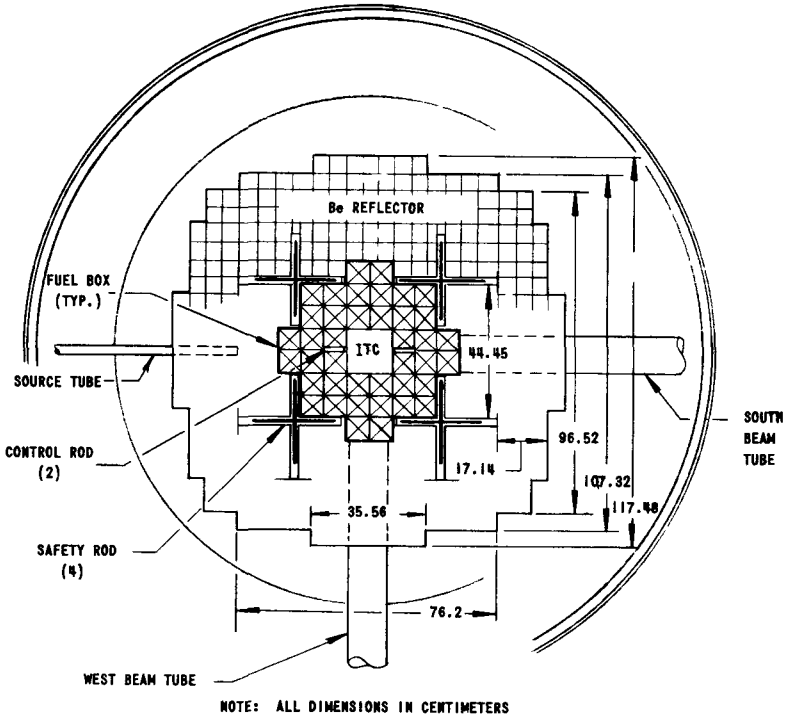

NOTE: ALL DIMENSIONS IN CENTIMETERS

FIG.3
PLAN VIEW OF AHFR CRITICAL ASSEMBLY

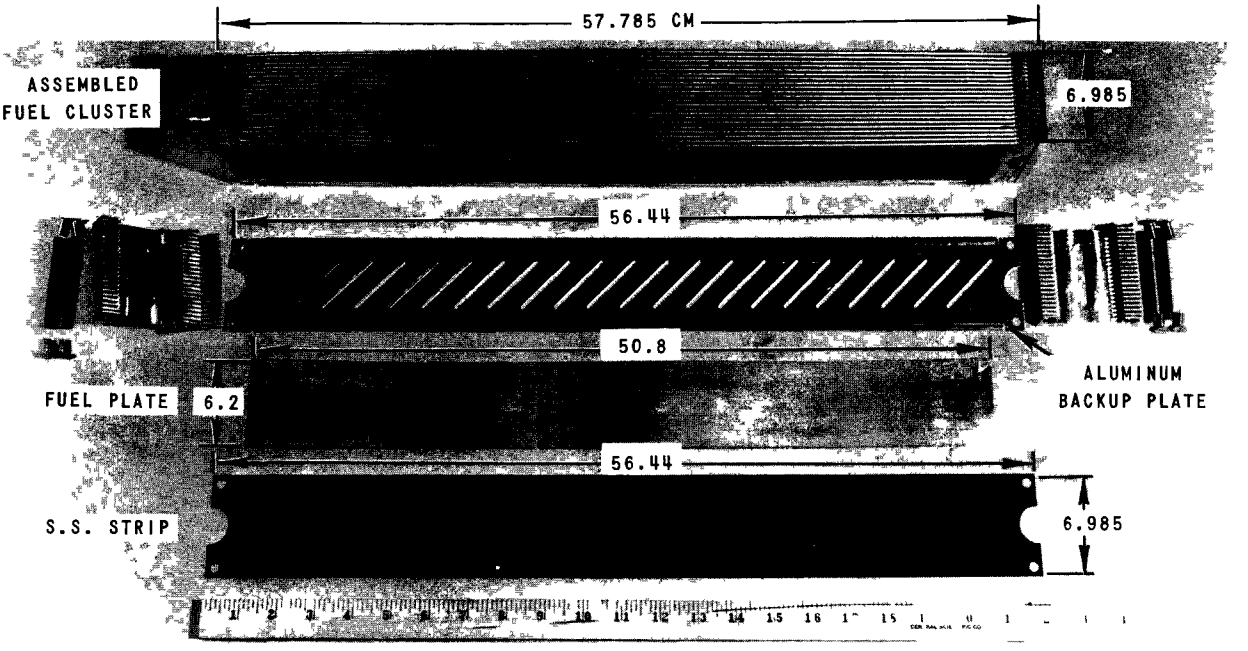

FIG. 4
FUEL CLUSTER

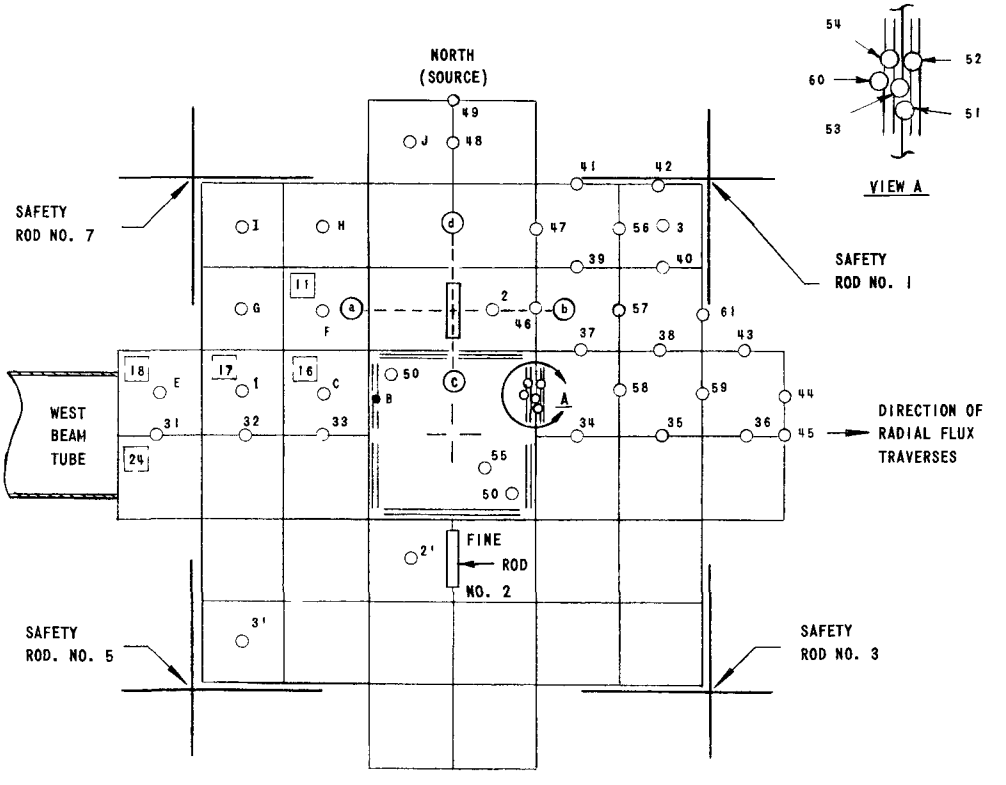

FIG. 5
CORE CONFIGURATION AND POSITIONS WHERE MEASUREMENTS WERE MADE SECTION THROUGH HORIZONTAL MIDPLANE

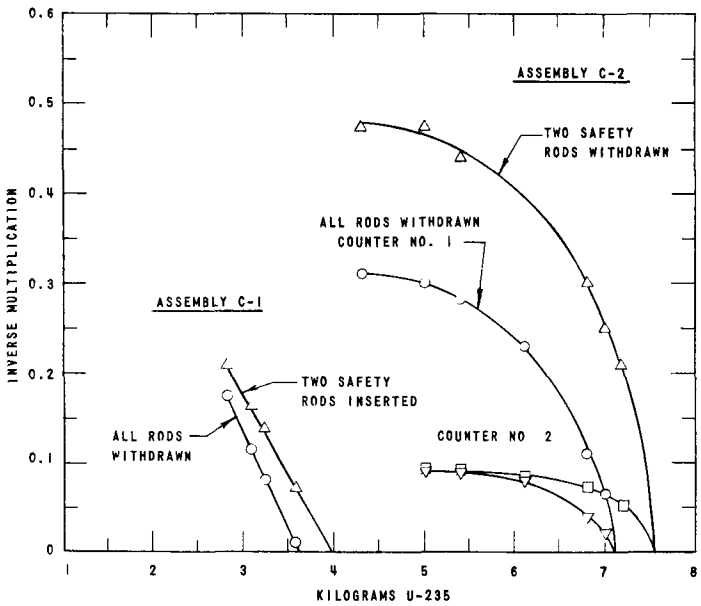

FIG. 6
APPROACH TO CRITICAL-INVERSE MULTIPLICATION MEASUREMENTS, C-1 AND C-2

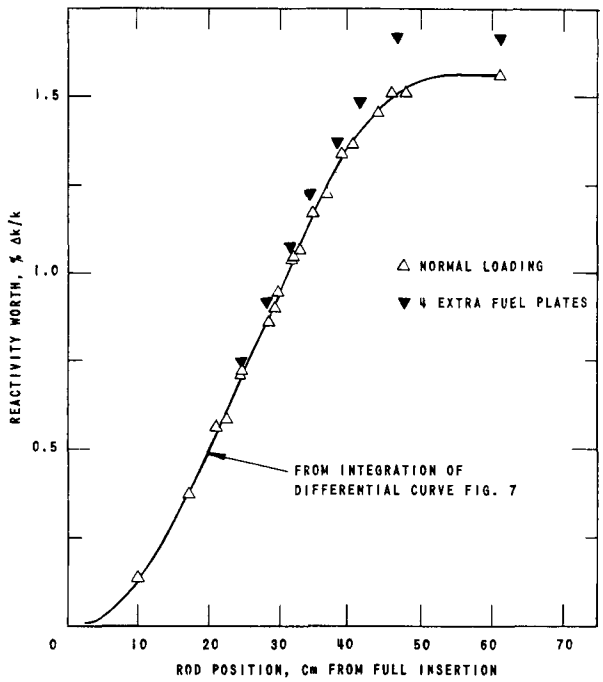

FIG. 8
INTEGRAL WORTH OF SAFETY ROD NO. 5, C-1

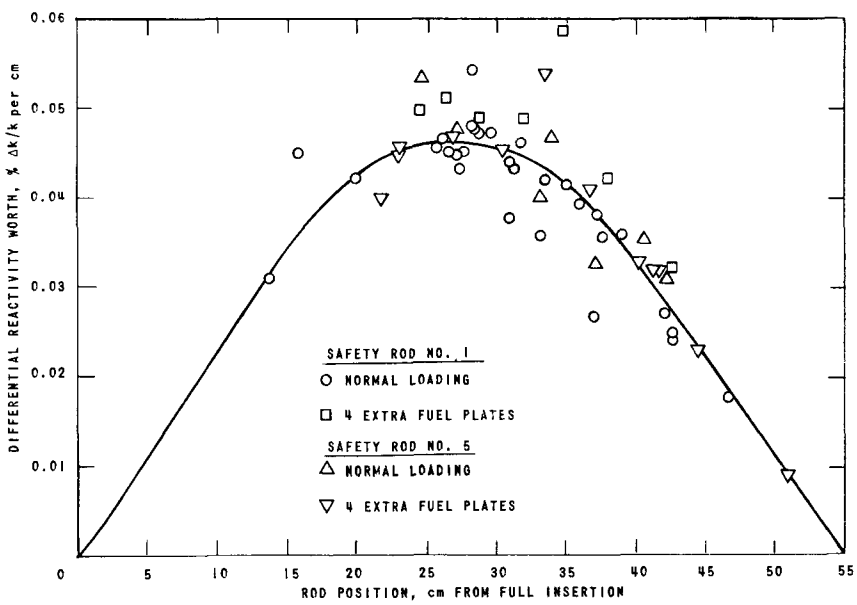

FIG. 7
DIFFERENTIAL WORTH OF SAFETY RODS NO. 1 AND NO. 5, C-1

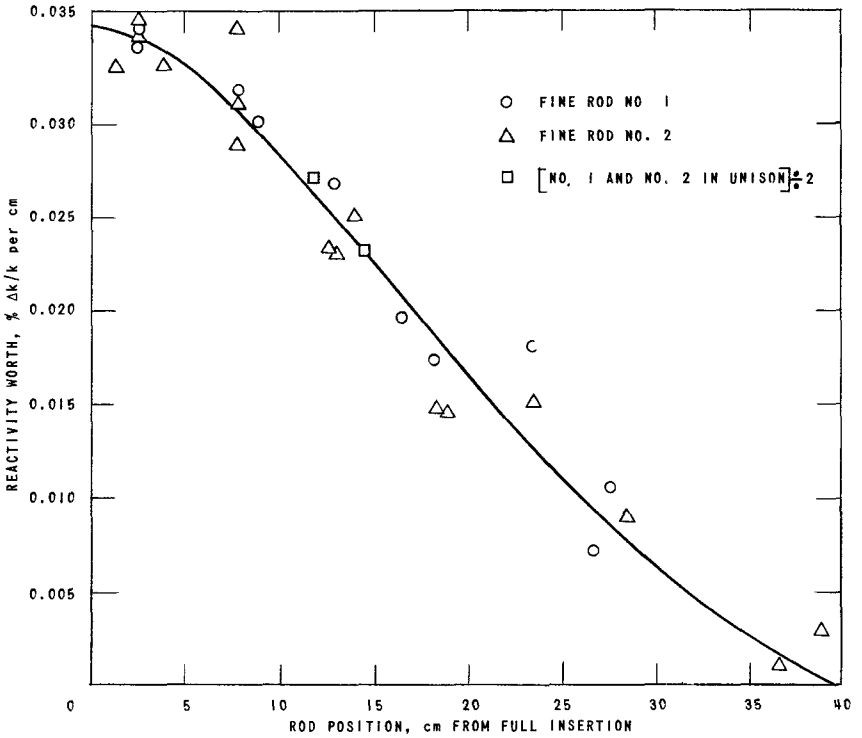

FIG. 9
DIFFERENTIAL WORTH OF FINE CONTROL RODS NO. 1 AND NO. 2, C-1

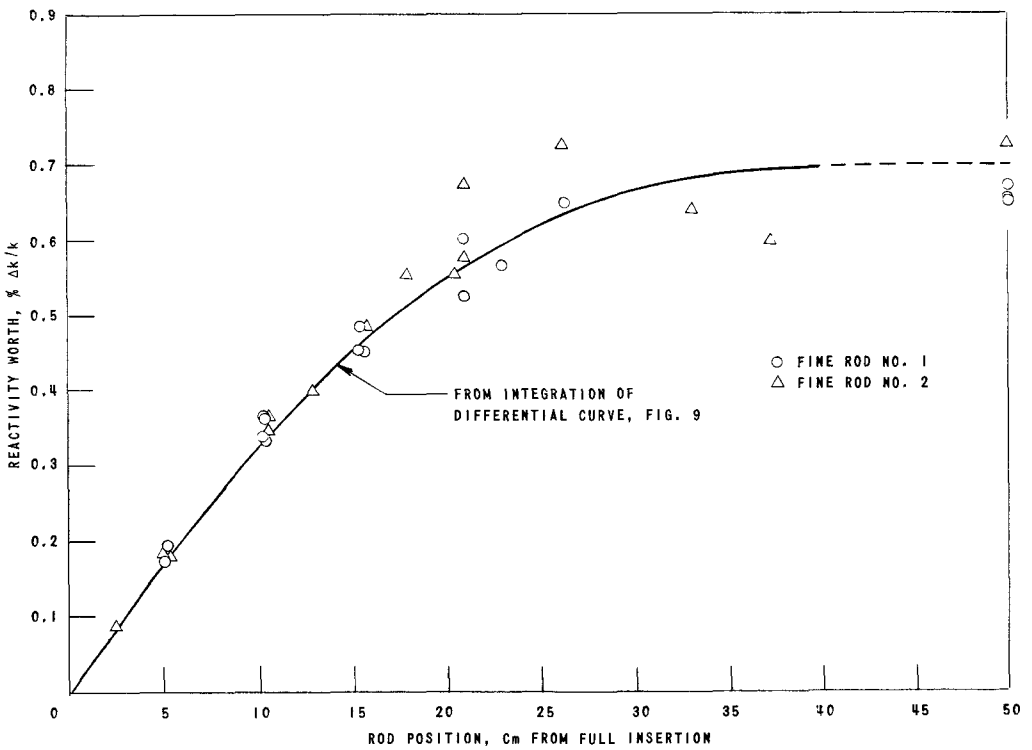

FIG. 10
INTEGRAL WORTH OF FINE CONTROL RODS NO. 1 AND NO. 2, C-1

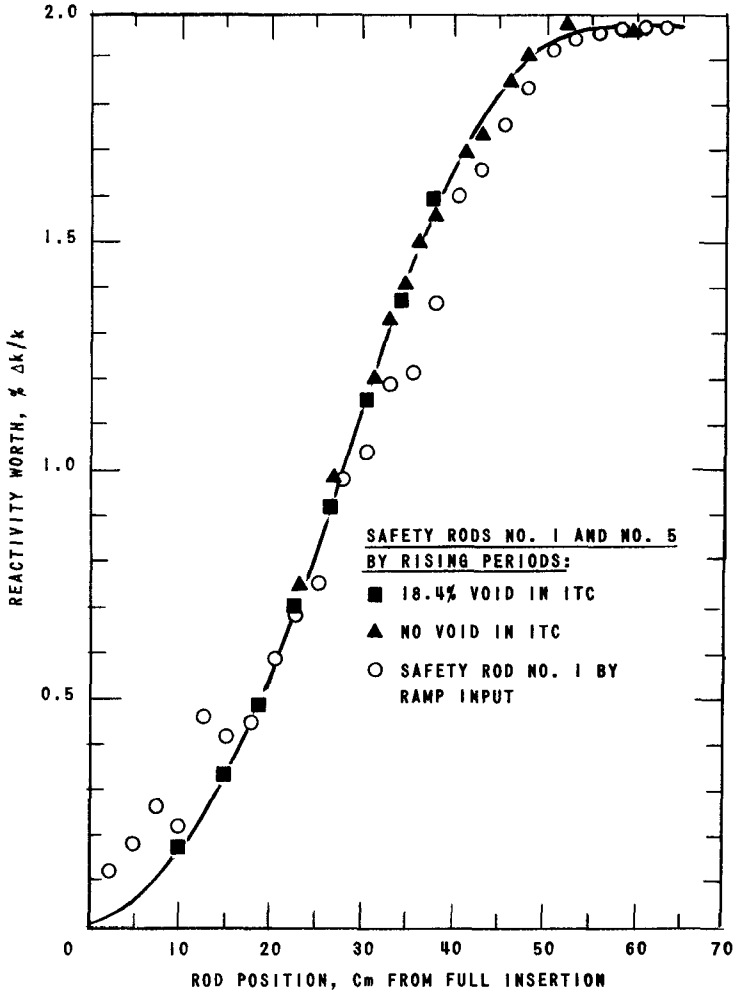

FIG. 11
SAFETY RODS NO. 1 AND NO. 5 INTEGRAL WORTHS FOR FULLY LOADED CORE, C-2

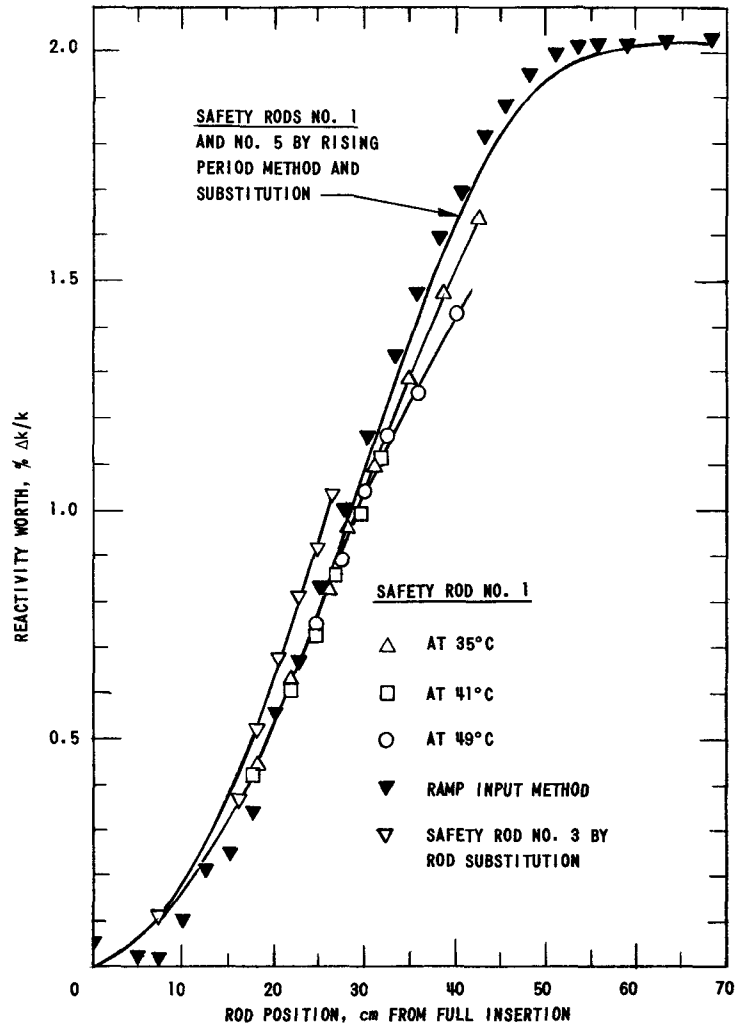

FIG. 12
SAFETY RODS NO. 1, NO. 3 AND NO. 5 INTEGRAL WORTHS FOR REDUCED POISON CORE, C-2'

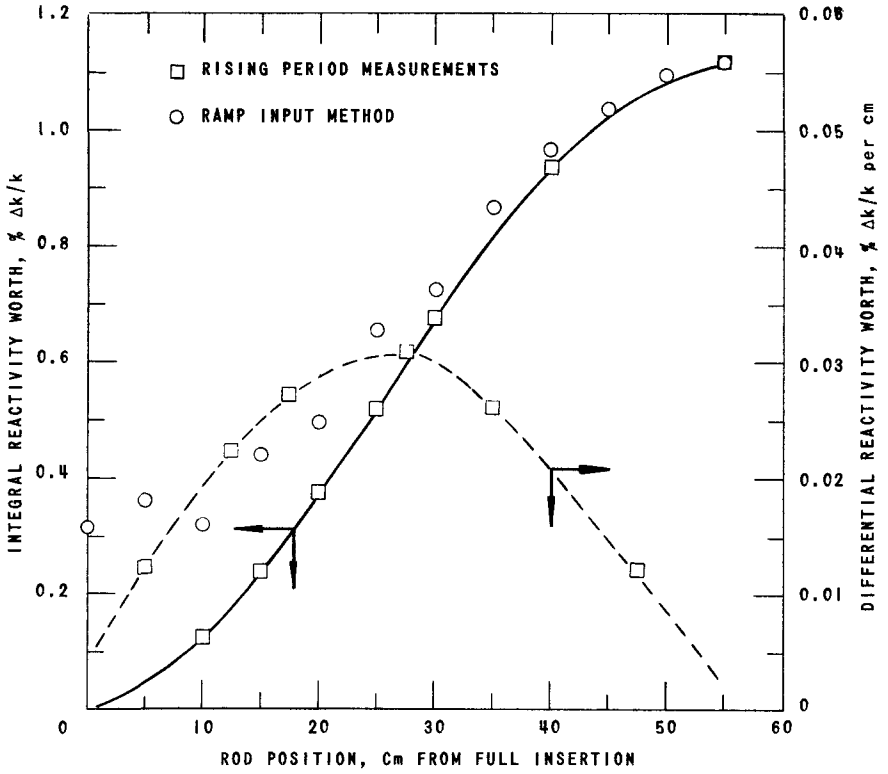

FIG. 13
FINE ROD CALIBRATION FOR REDUCED POISON CORE, C-2'

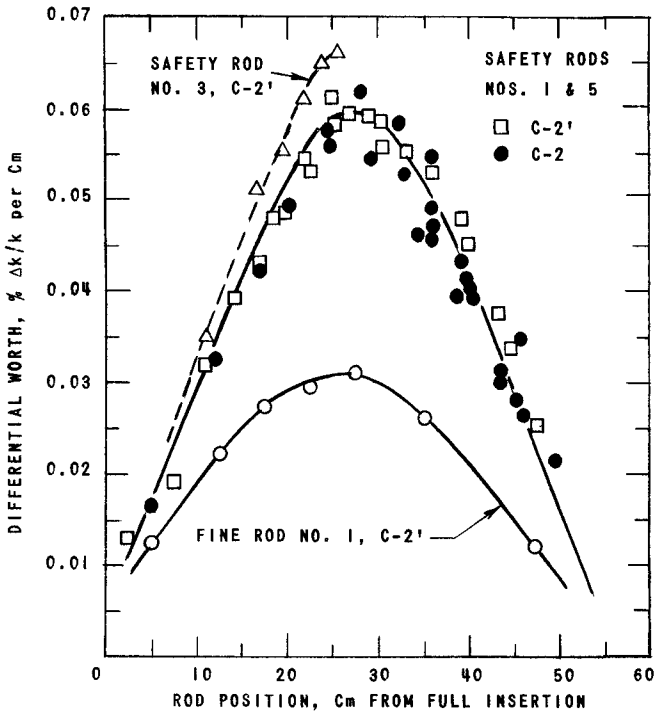

FIG. 14
DIFFERENTIAL ROD WORTHS, C-2 AND C-2'

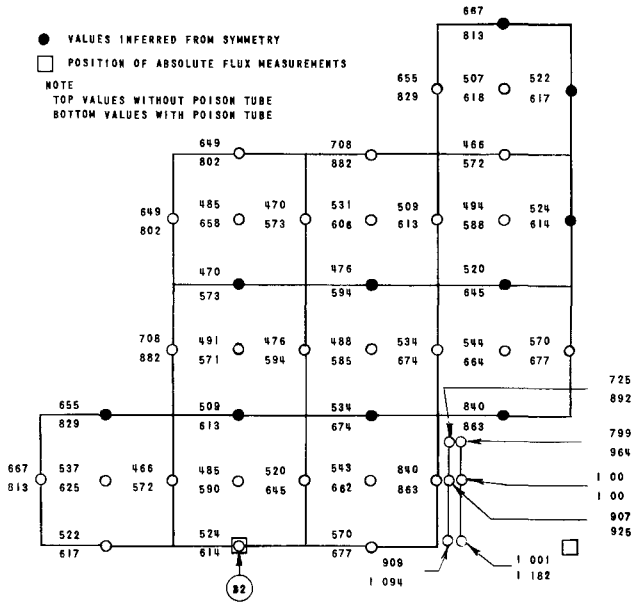

FIG 15
U AL DISTRIBUTED FLUX MAP C 1

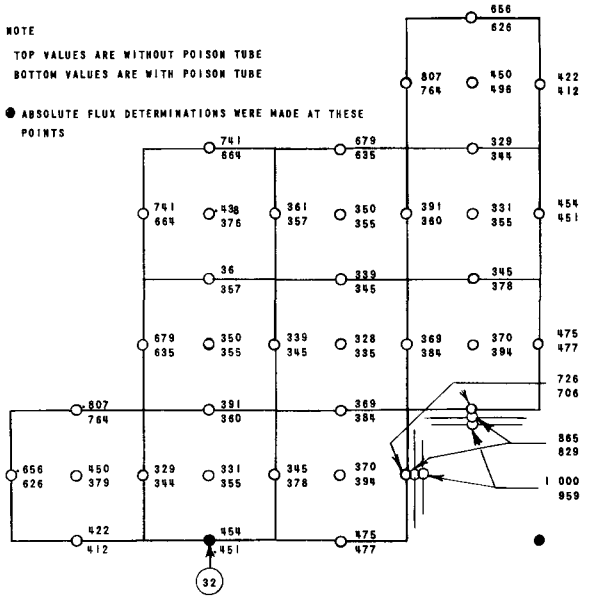

FIG 16
U Al DISTRIBUTED FOIL FLUX MAPs BARE C-2

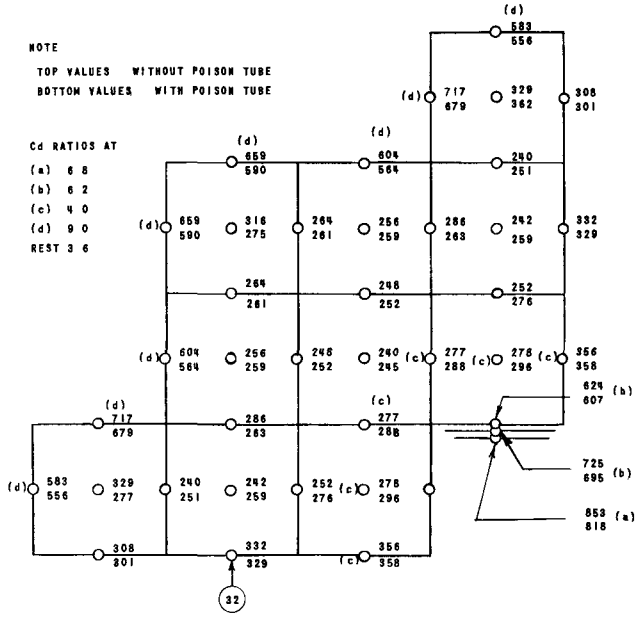

FIG 17
SUB CADMIUM ACTIVATION OF U-Al FOILS OVER QUADRANT OF CORE C-2

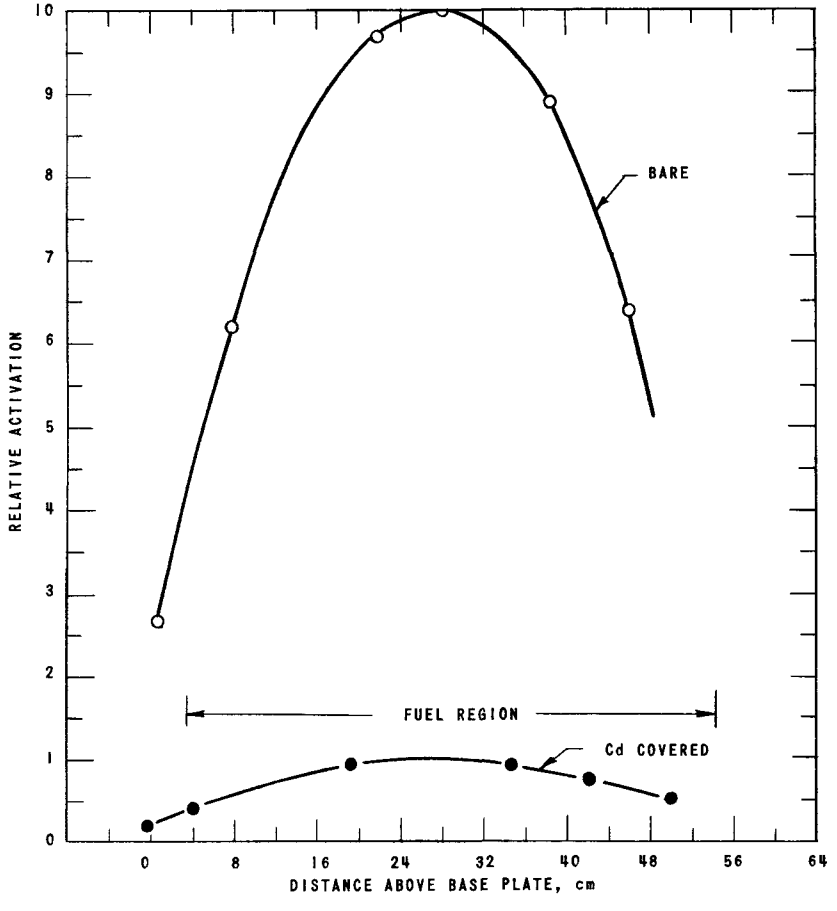

FIG. 18
AXIAL FLUX PLOT USING GOLD FOILS, C-1

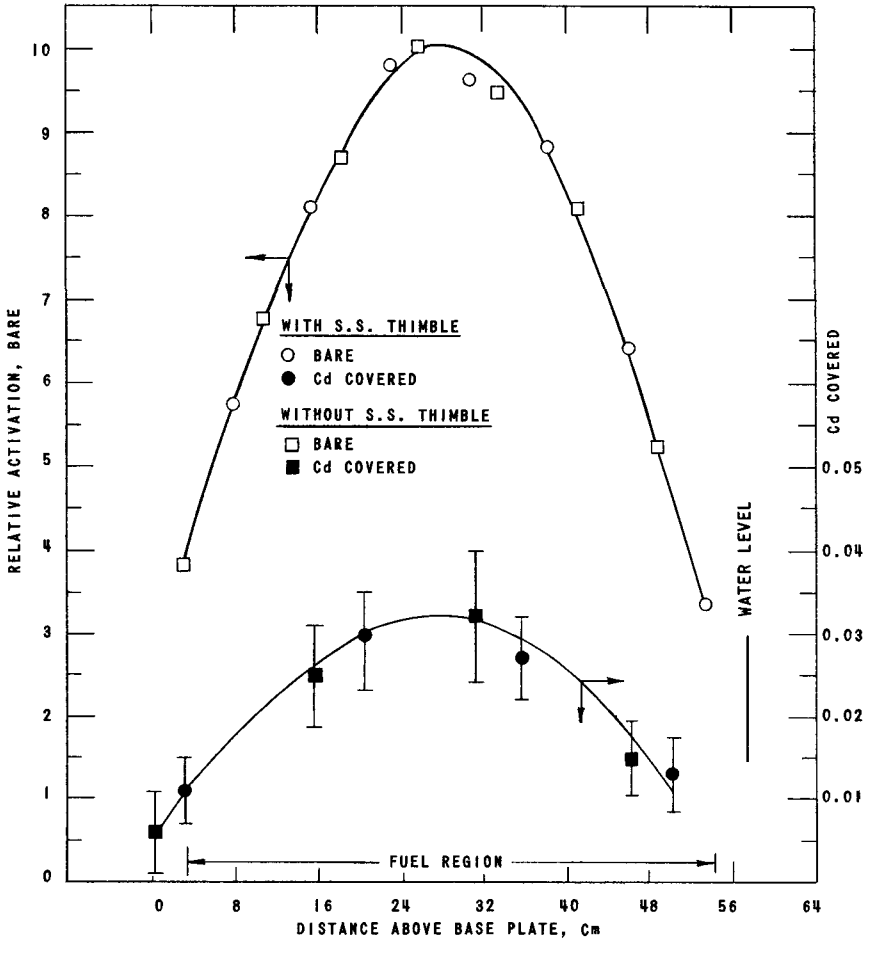

FIG. 19
AXIAL FLUX PLOT USING DYSPROSIUM FOILS, C-1

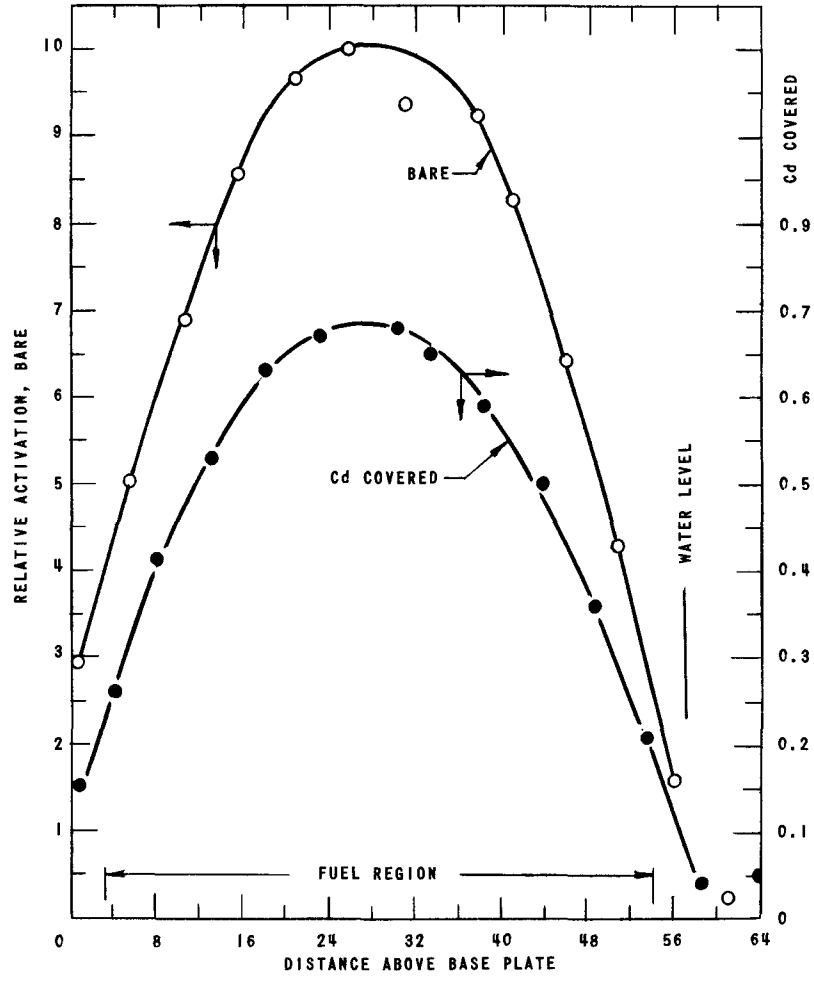

FIG. 20
AXIAL FLUX PLOT USING INDIUM FOILS, C-1

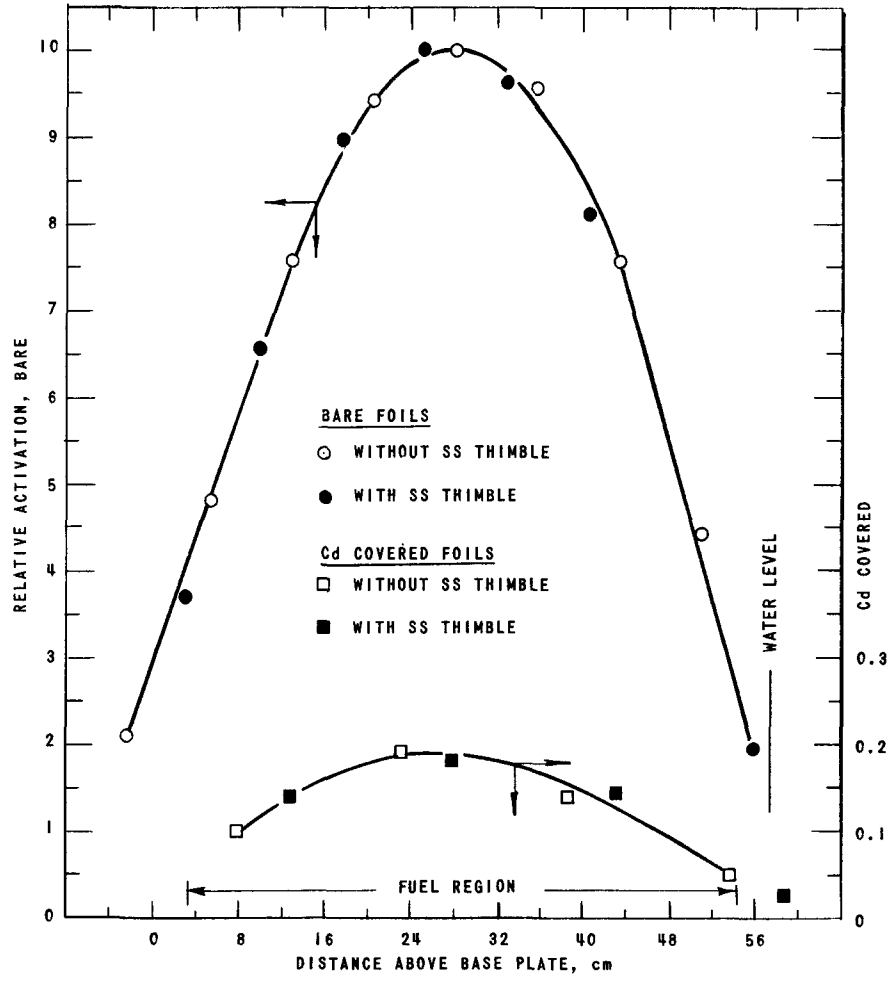

FIG. 21
AXIAL FLUX PLOT USING MANGANESE FOILS, C-1

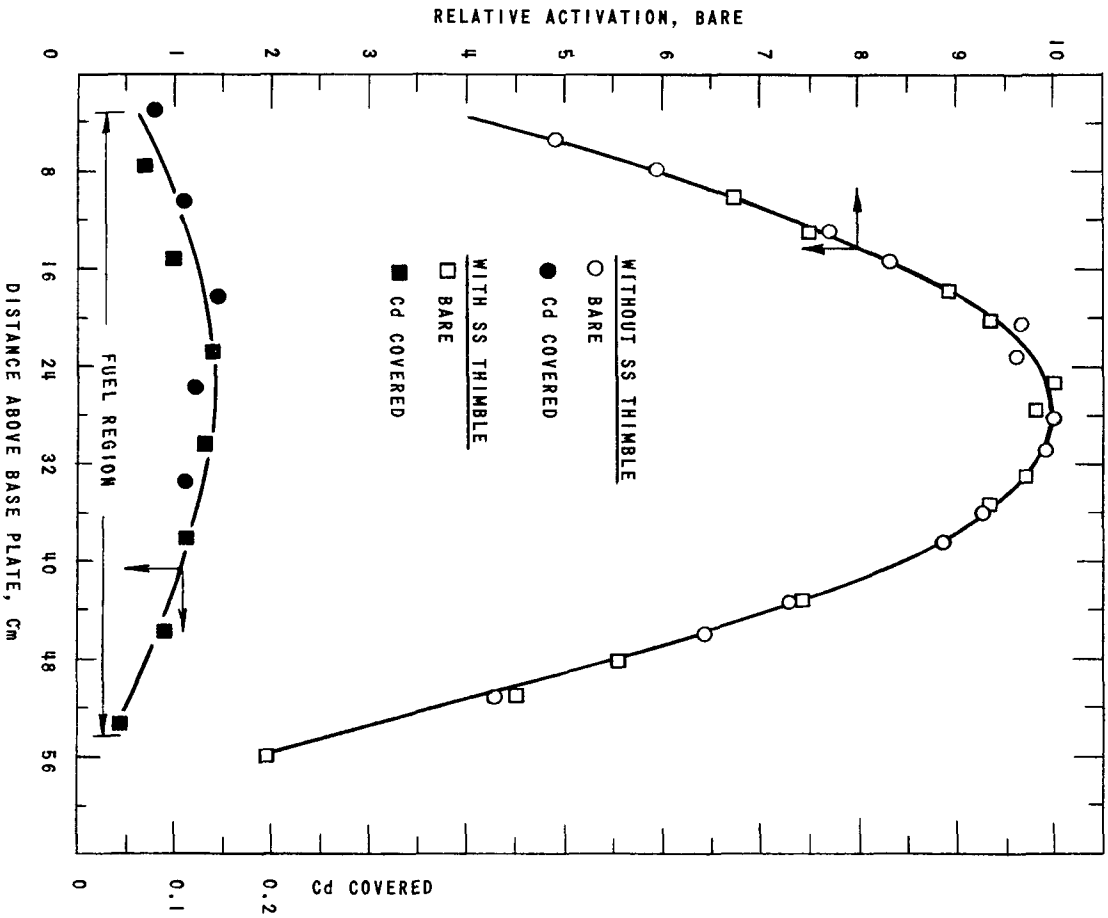

FIG. 22
AXIAL POWER DISTRIBUTION USING U235-Al FOILS, C-1

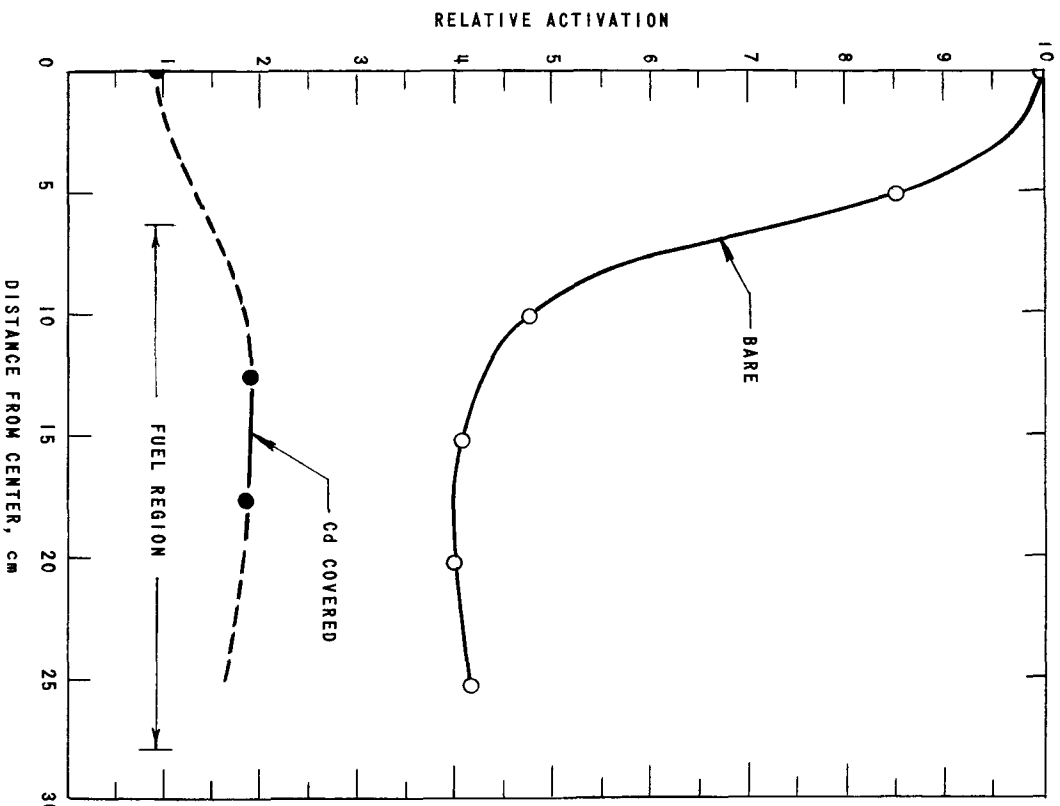

FIG. 23
RADIAL FLUX PLOT USING GOLD FOILS, C-1

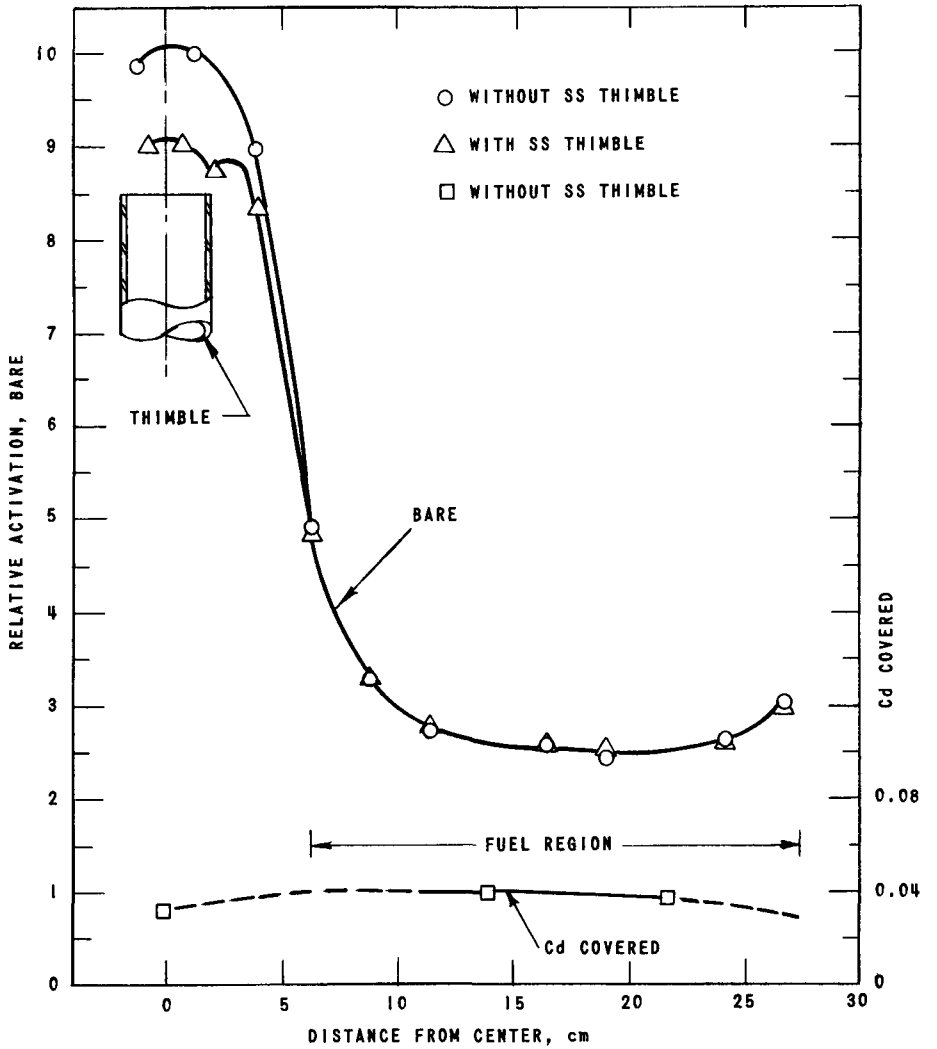

FIG. 24
RADIAL FLUX PLOT USING DYSPROSIUM FOILS, C-1

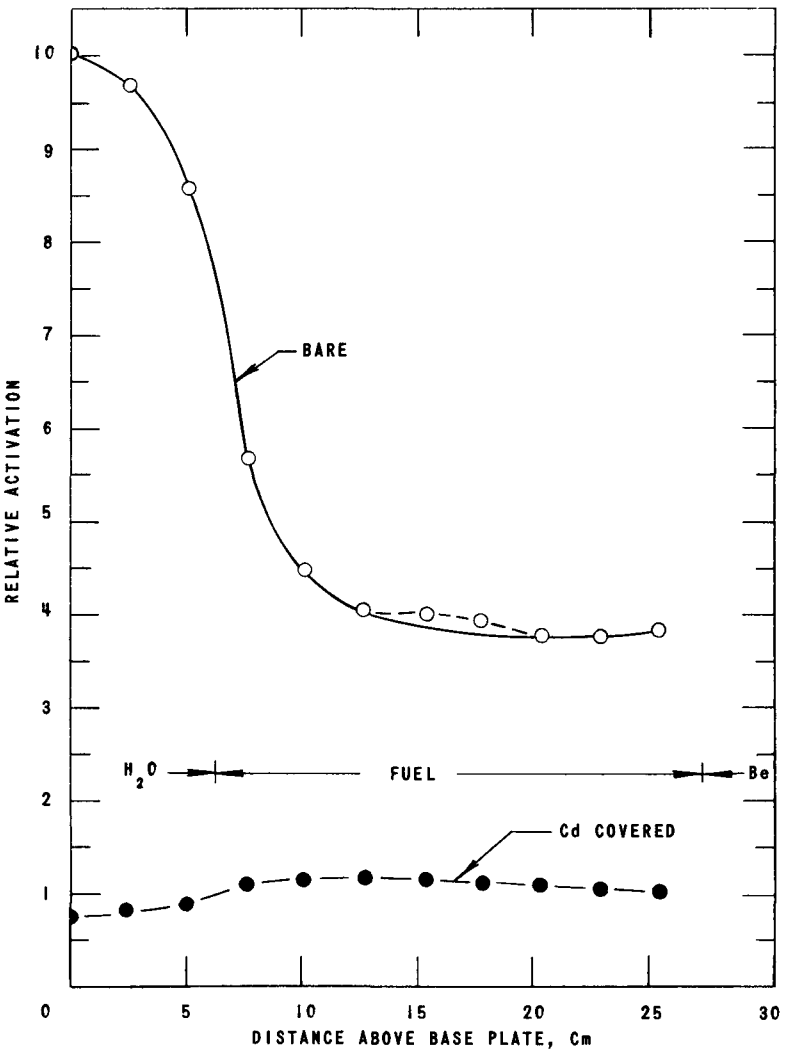

FIG. 25
RADIAL FLUX PLOT USING INDIUM FOILS, C-1

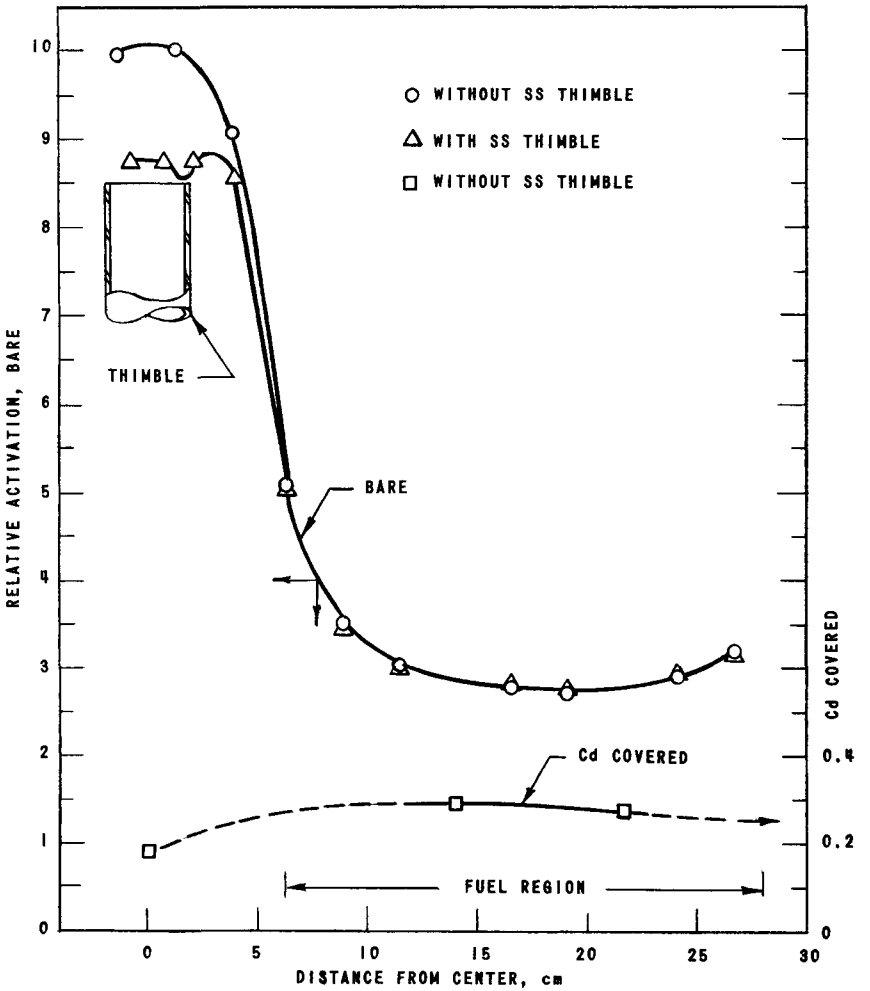

FIG. 26
RADIAL FLUX PLOT USING MANGANESE FOILS, C-I

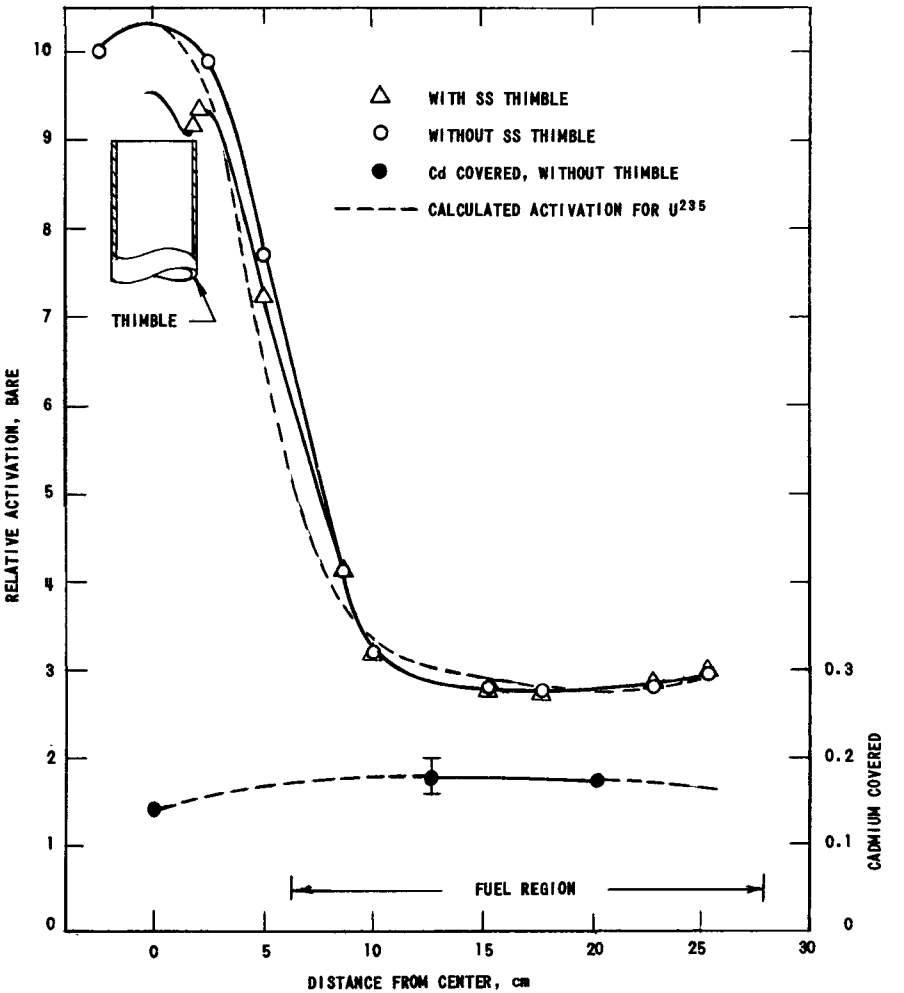

FIG. 27
EFFECT OF CENTRAL STAINLESS STEEL THIMBLE ON RADIAL FLUX DISTRIBUTION AND COMPARISON WITH CALCULATED DISTRIBUTION, C-I

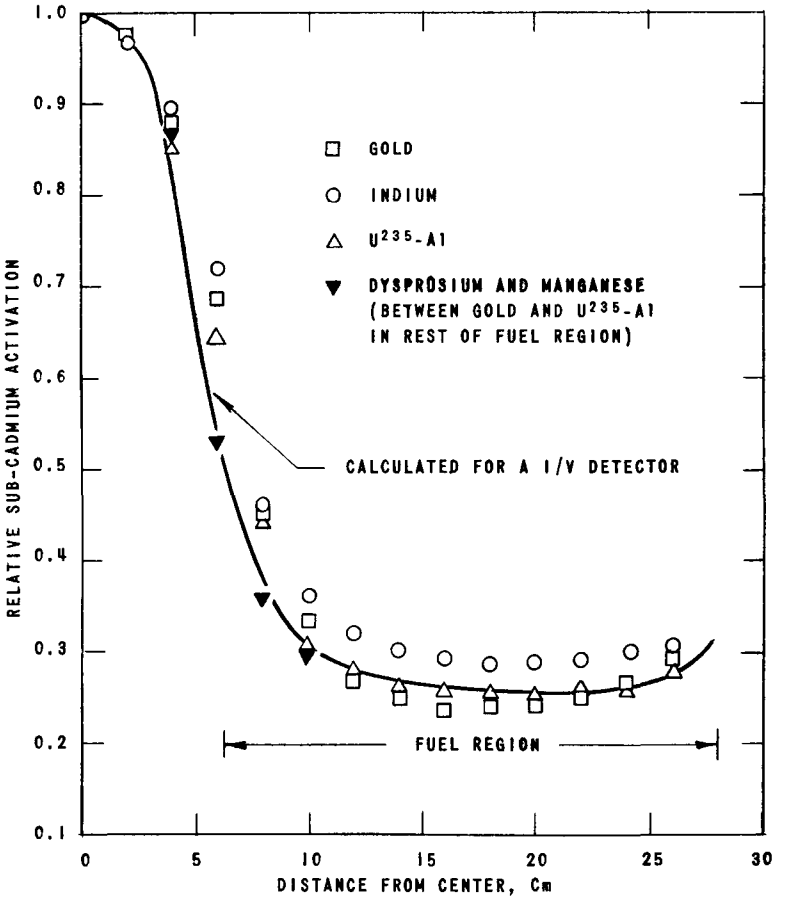

FIG. 28
RADIAL SUB-CADMIUM FOIL ACTIVATIONS, C-1 COMPARISON WITH CALCULATED VALUES FOR A I/V DETECTOR

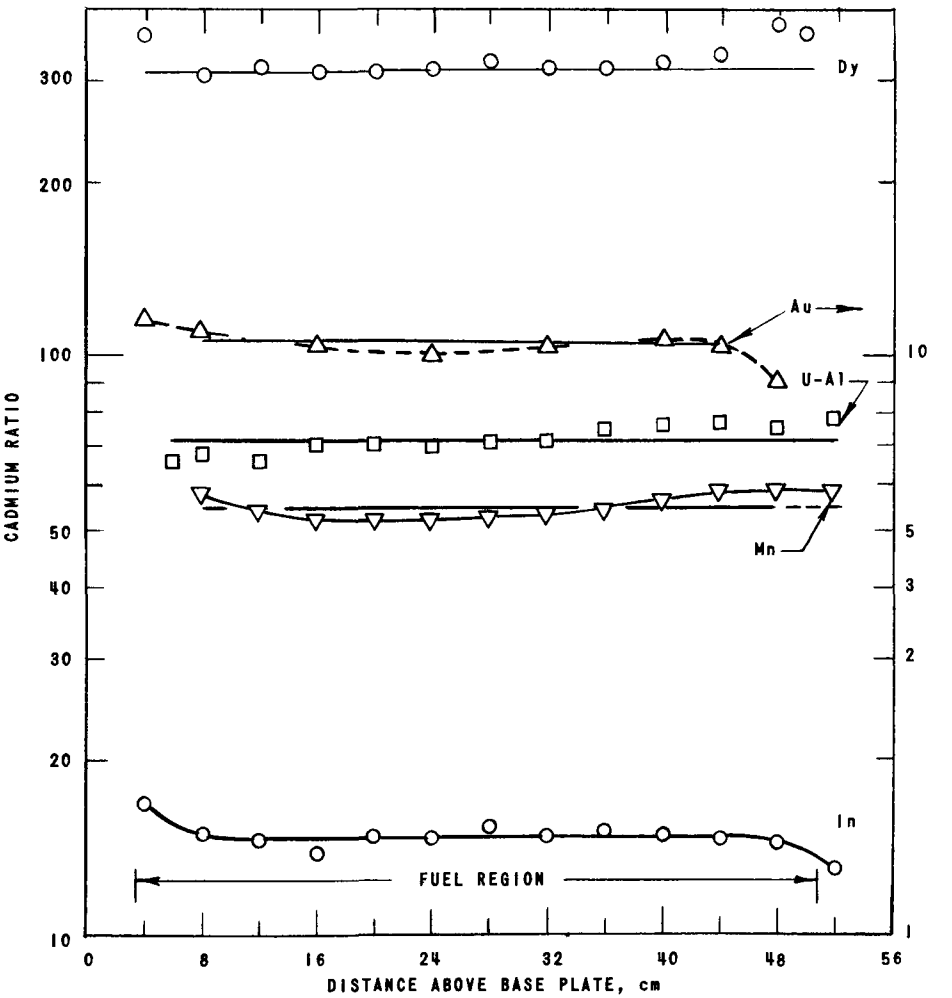

FIG. 29
AXIAL CADMIUM RATIOS, C-1

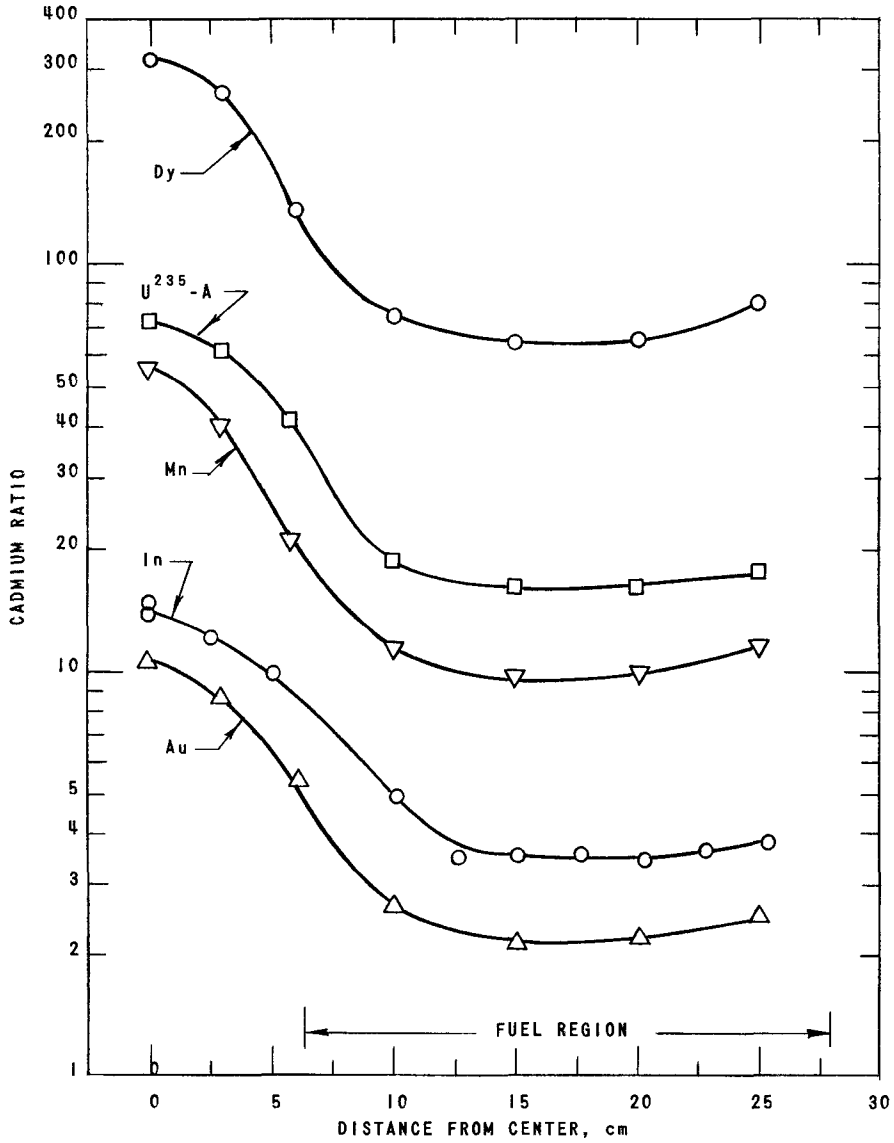

FIG. 30
RADIAL CADMIUM RATIOS, C-1

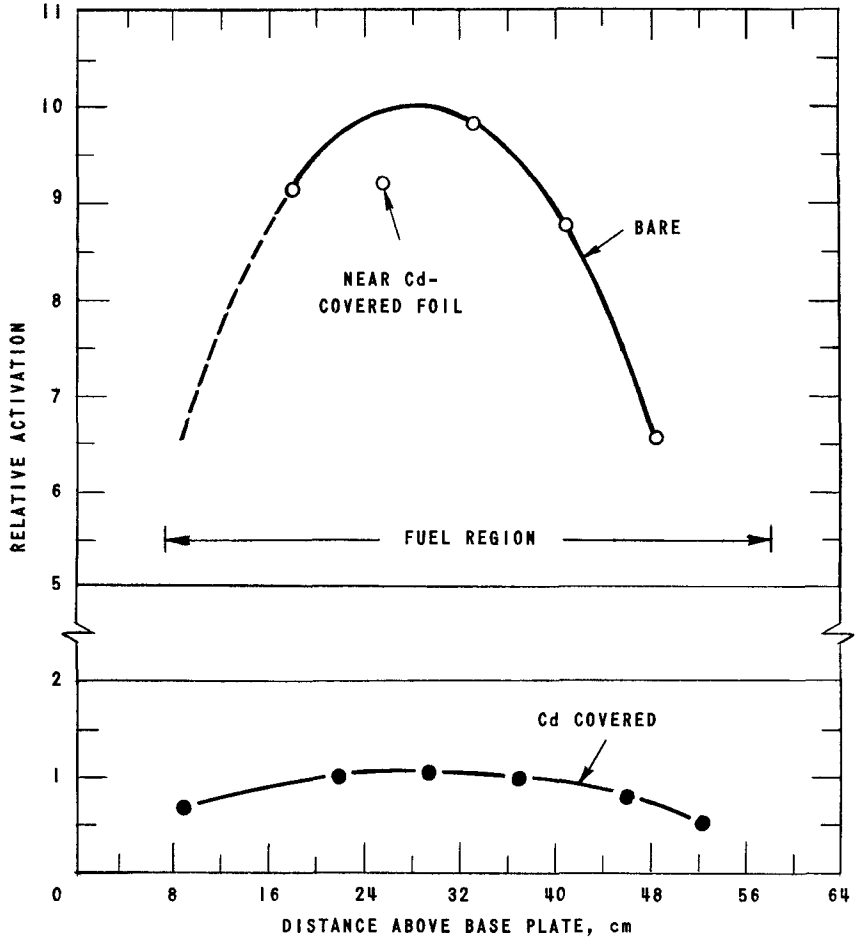

FIG. 31
AXIAL FLUX PLOT USING GOLD FOILS, C-2

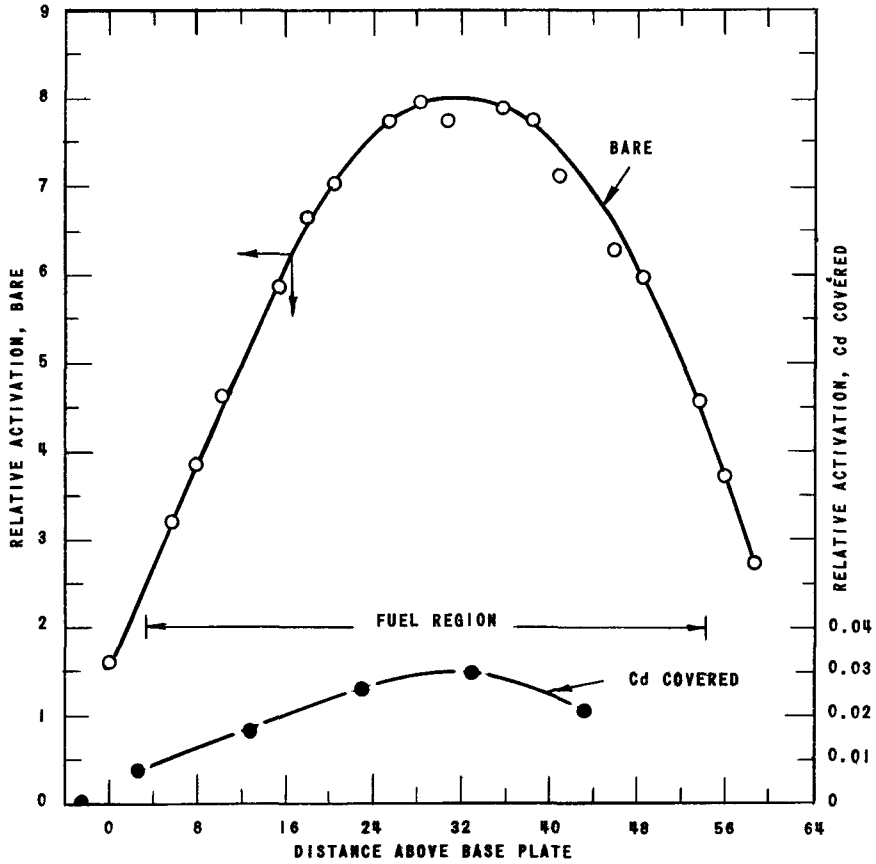

FIG. 32
AXIAL FLUX PLOT USING DYSPROSIUM FOILS, C-2

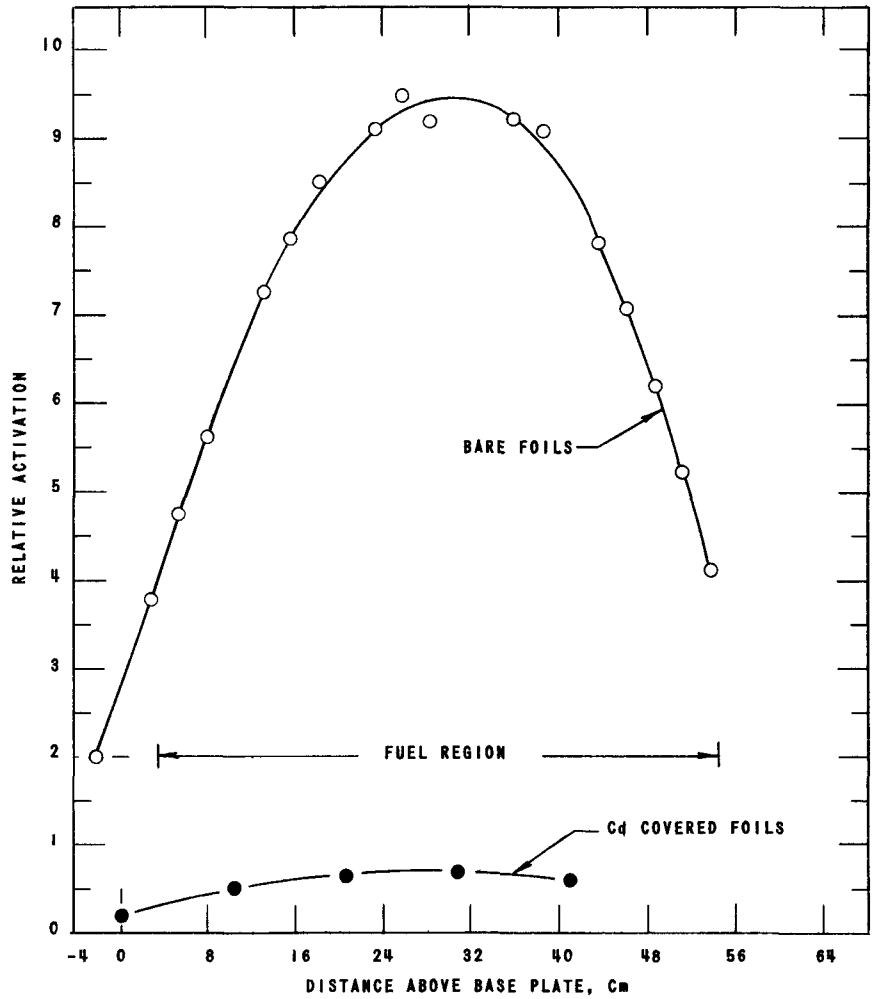

FIG. 33
AXIAL FLUX PLOT USING INDIUM FOILS, C-2

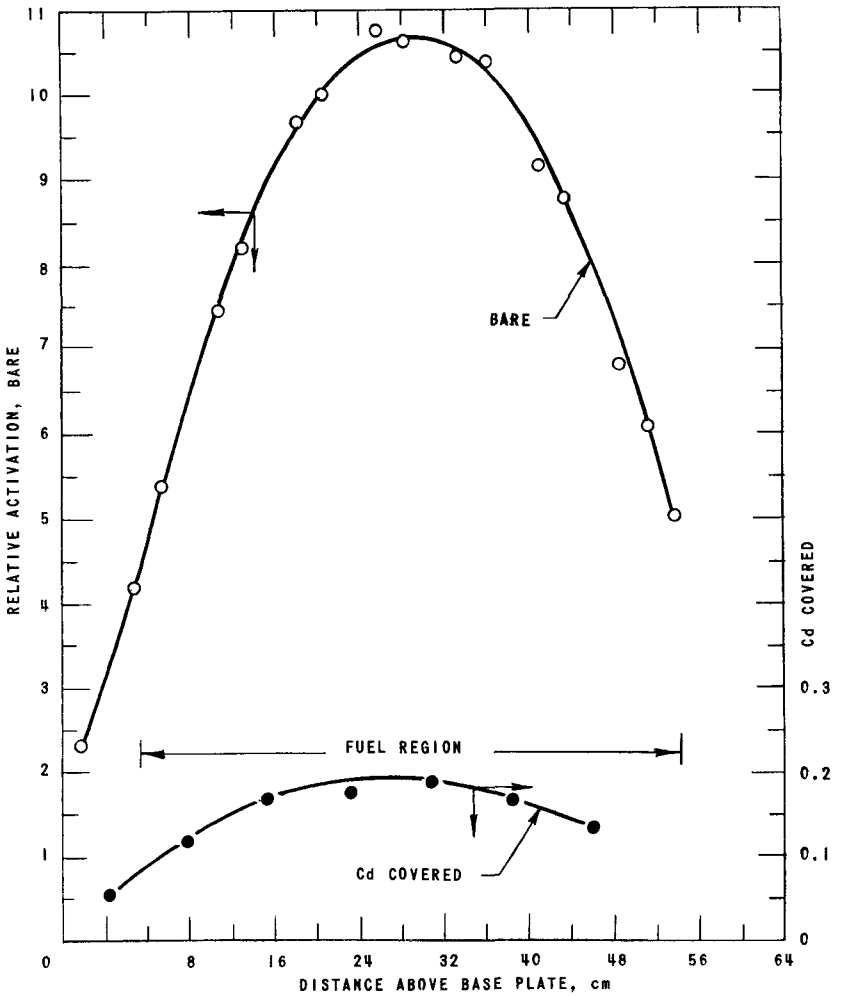

FIG. 34
AXIAL FLUX PLOT USING MANGANESE FOILS, C-2

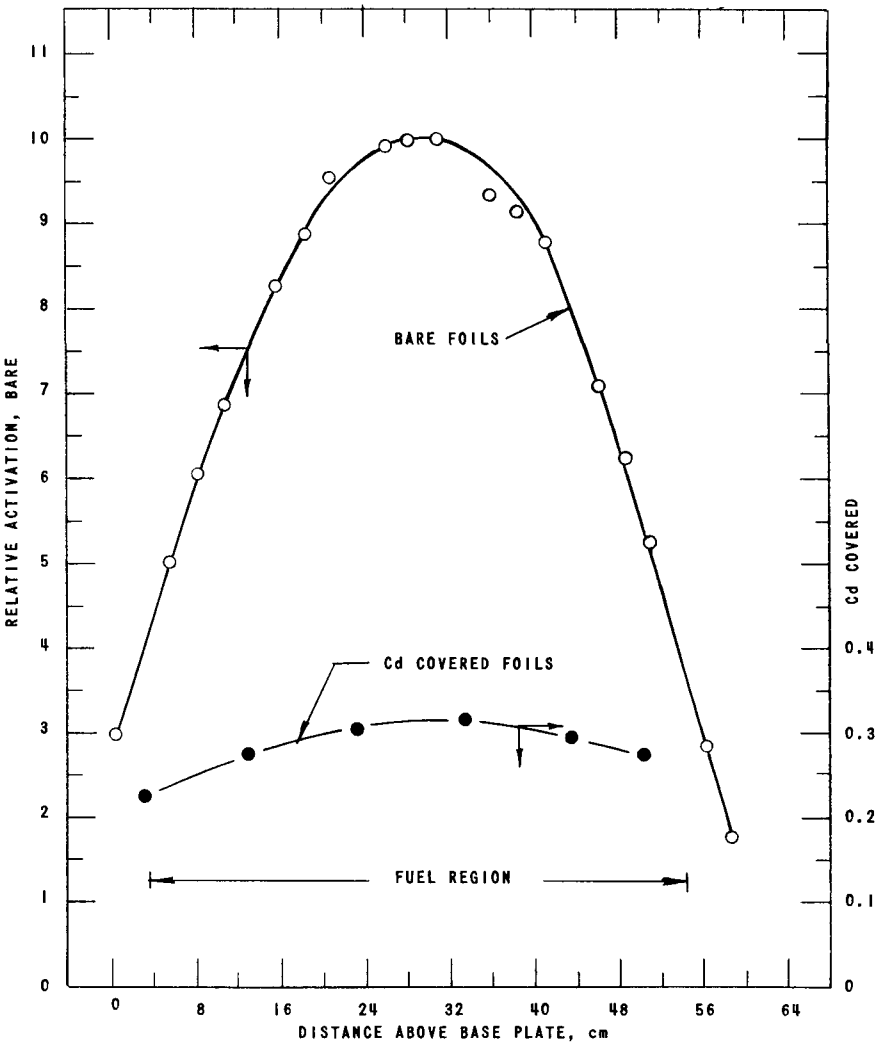

FIG. 35
AXIAL FLUX PLOT USING U^{235}-Al FOILS, C-2

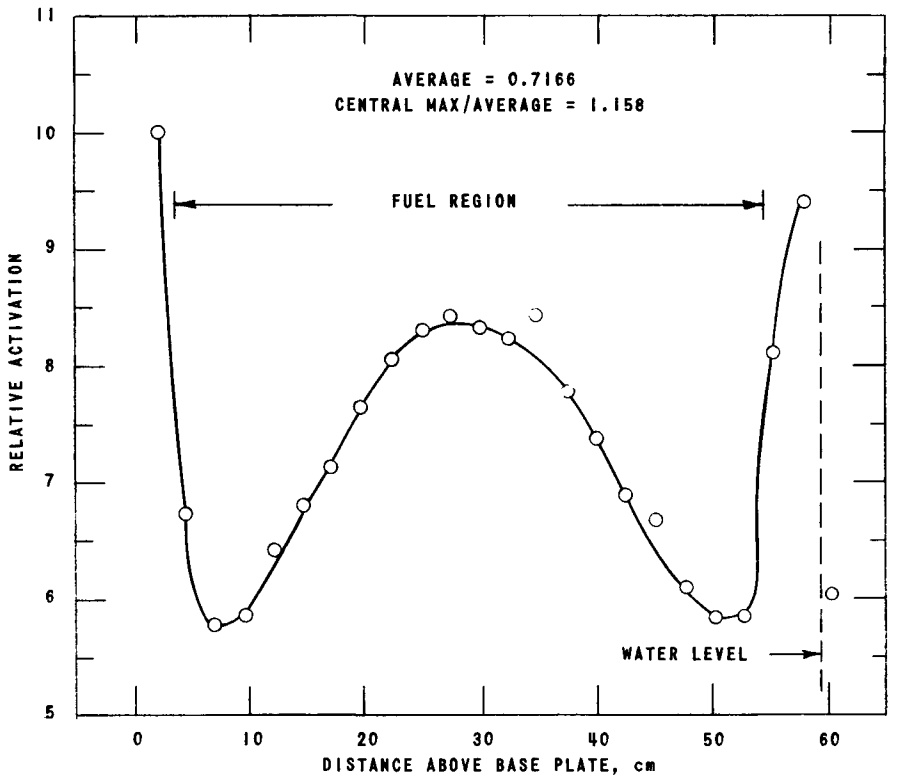

FIG. 36
AXIAL POWER DISTRIBUTION AT POINT 32 IN FUEL REGION (FIG. 5) AS MEASURED WITH U^{235}-Al FOILS, C-2

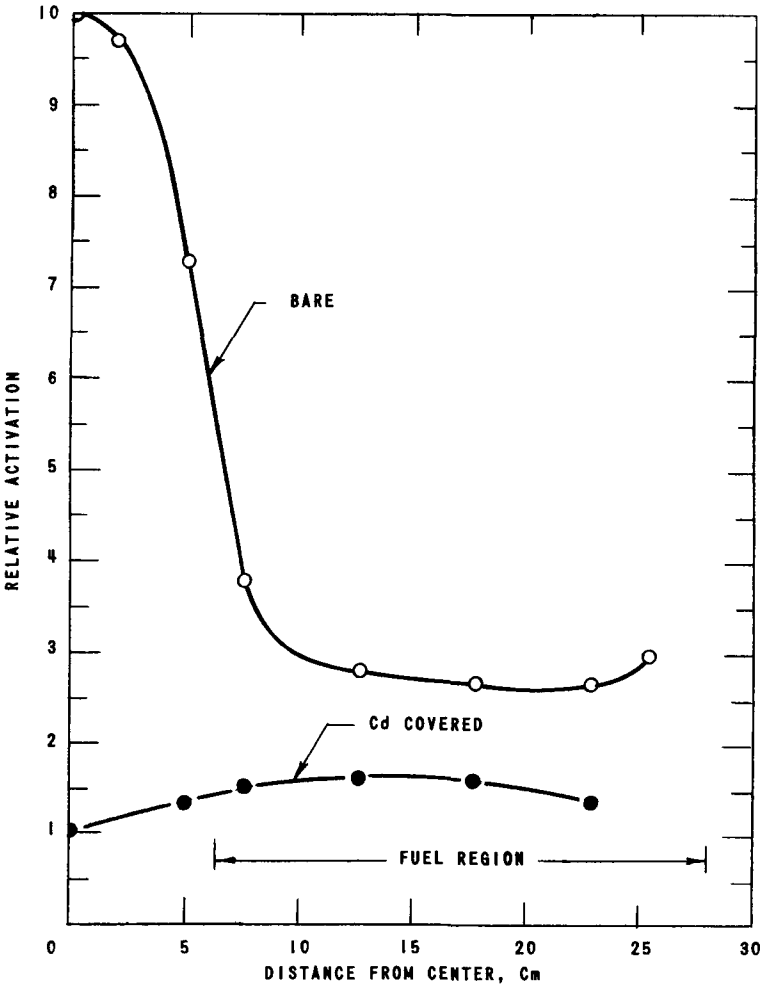

FIG. 37
RADIAL FLUX PLOT USING GOLD FOILS, C-2

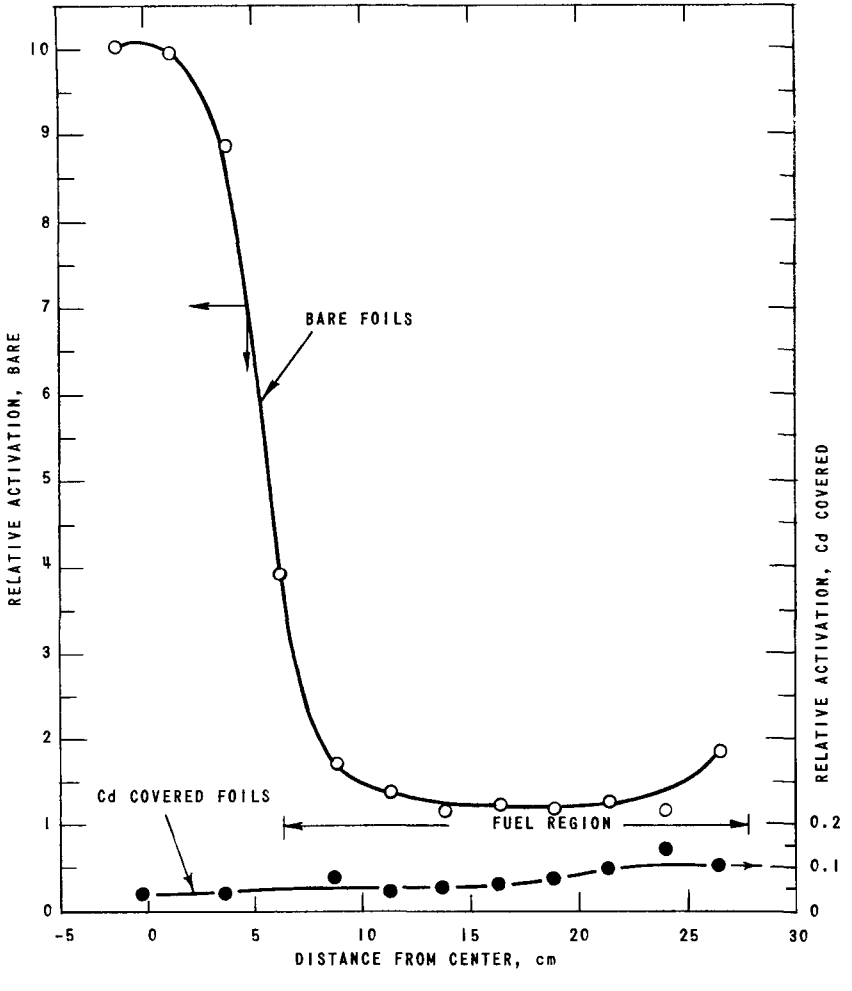

FIG. 38
RADIAL FLUX PLOT USING DYSPROSIUM FOILS, C-2

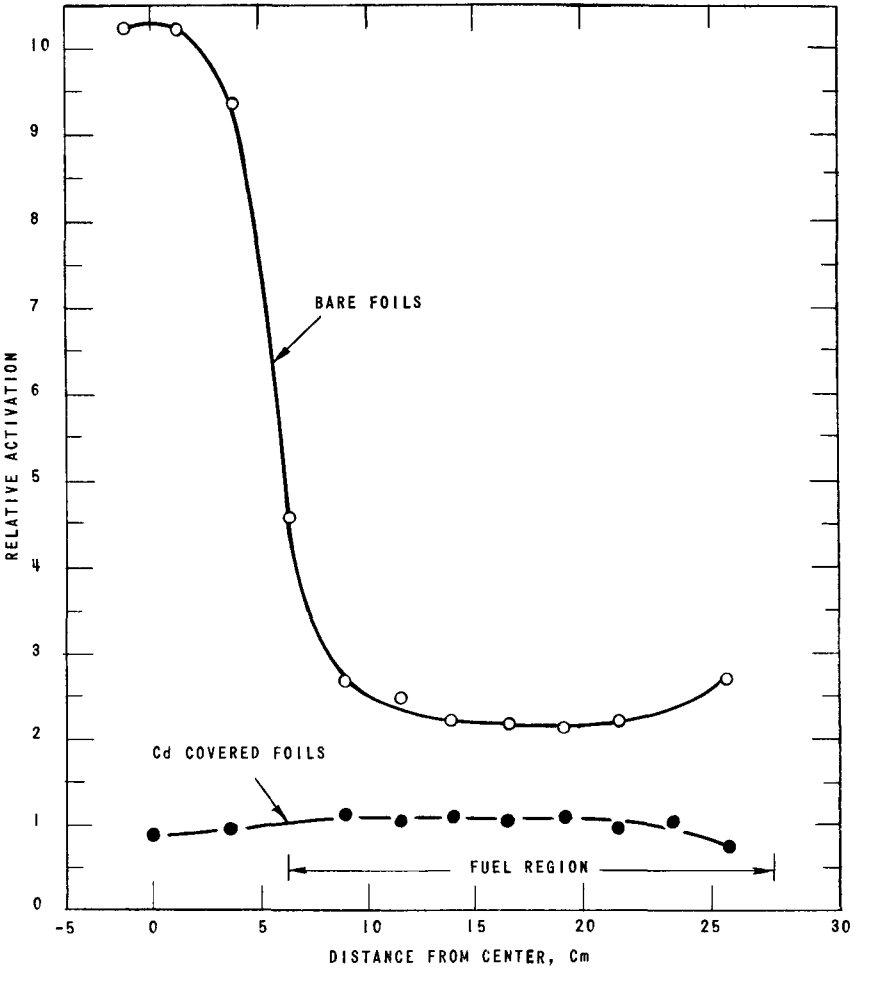

FIG. 39
RADIAL FLUX PLOT USING INDIUM FOILS, C-2

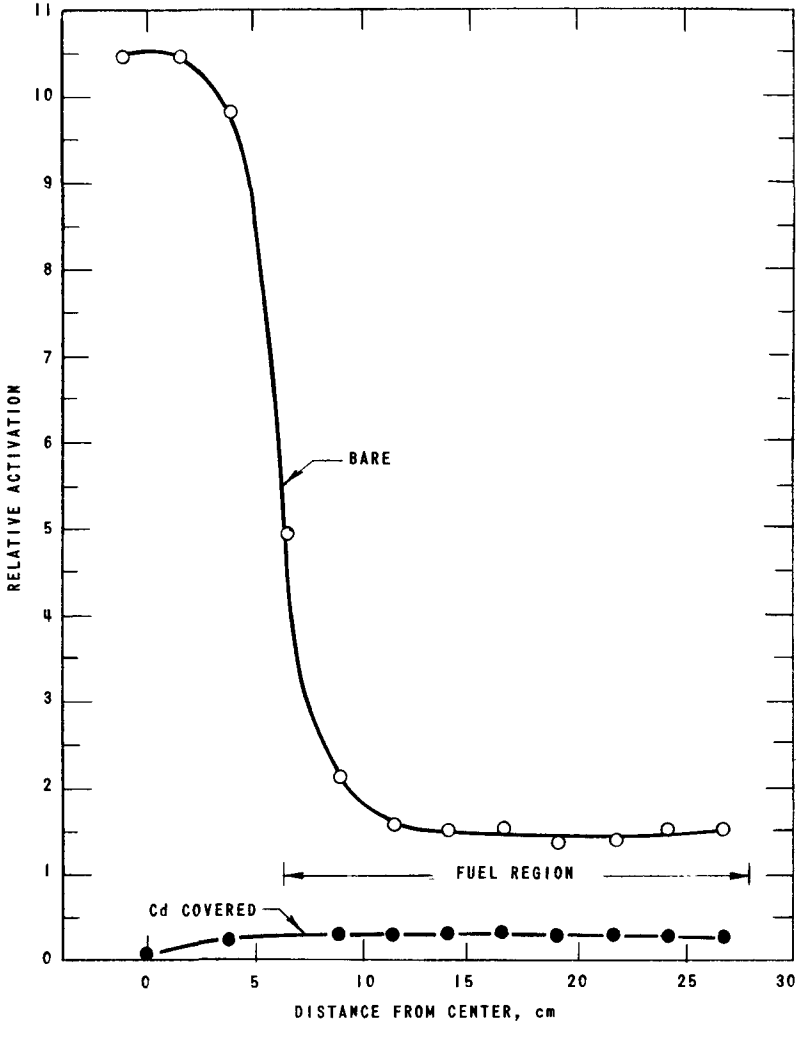

FIG. 40
RADIAL FLUX PLOT USING MANGANESE FOILS, C-2

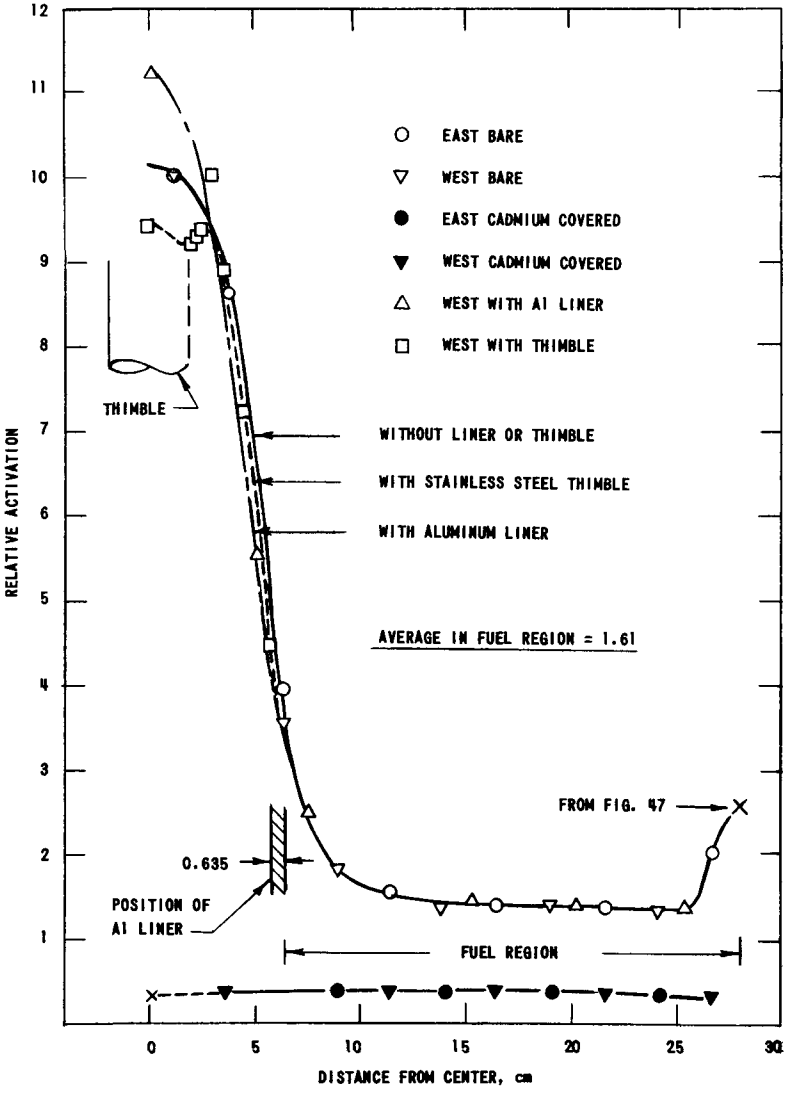

FIG. 41
EFFECT OF AN ALUMINUM LINER AND THE CENTRAL STAINLESS STEEL THIMBLE ON THE RADIAL FLUX DISTRIBUTION AS MEASURED WITH U^{235}-Al FOILS, C-2

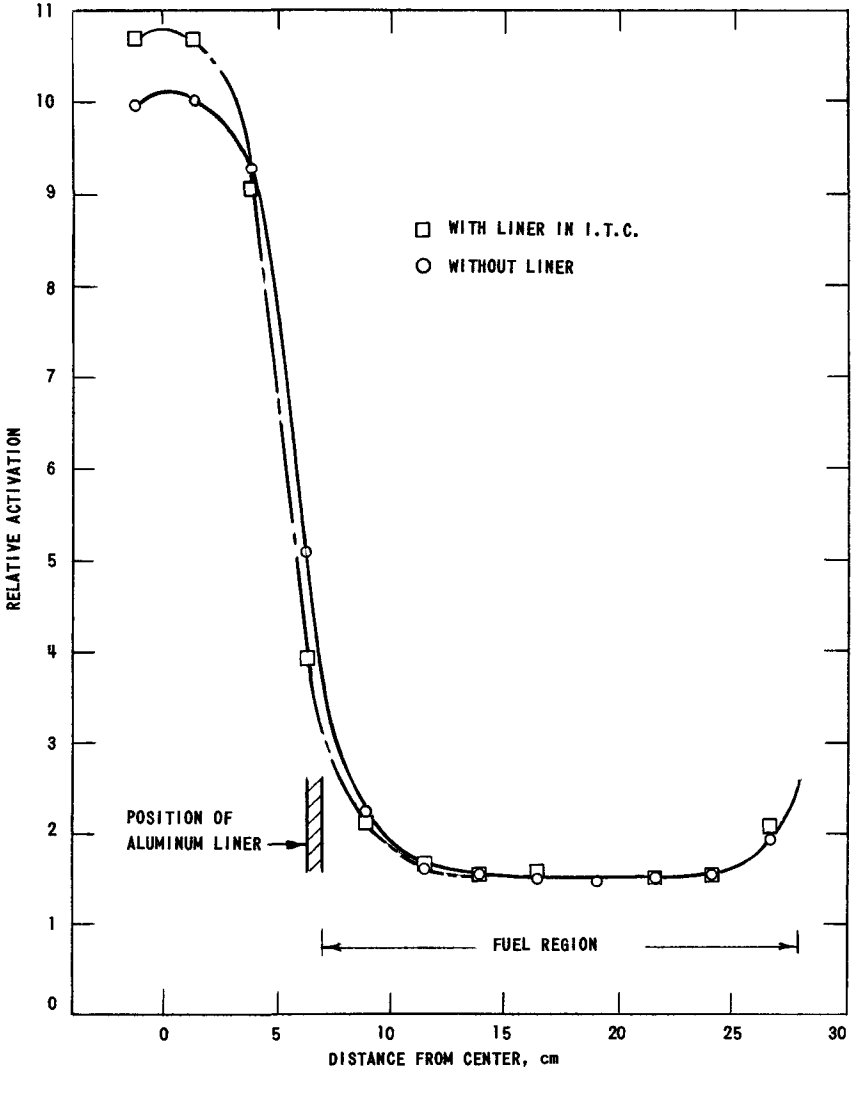

FIG. 42
RADIAL FLUX DISTRIBUTION THROUGH 13.97 cm I.T.C. USING U^{235}-Al FOILS, C-2'

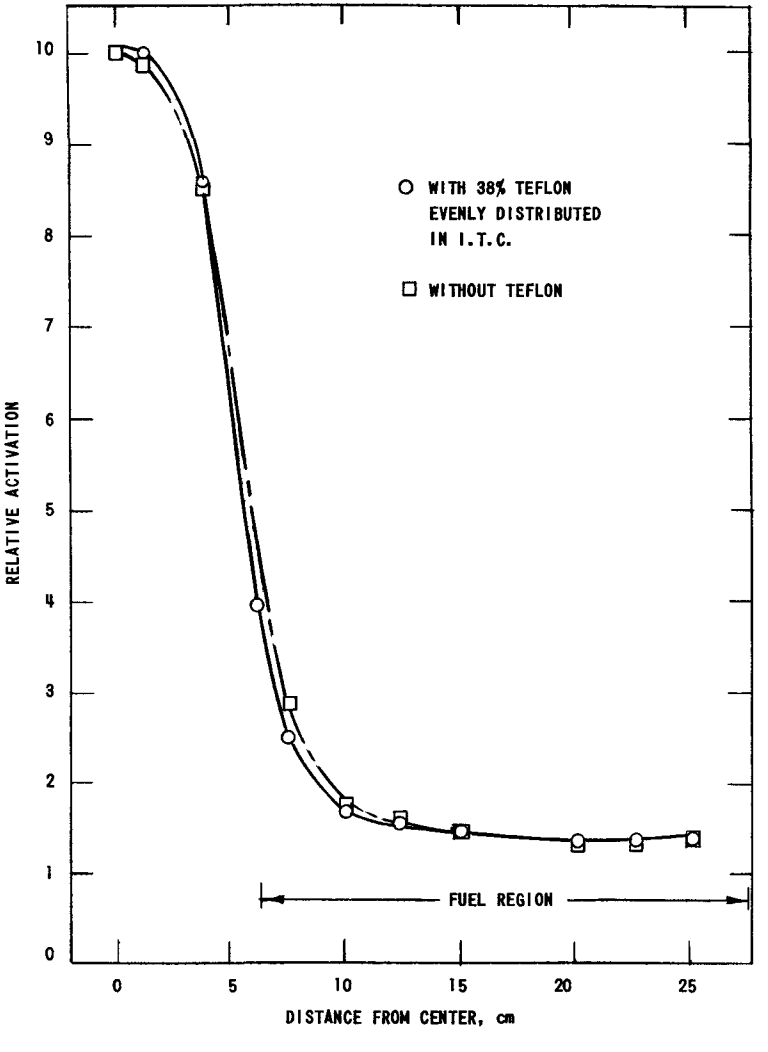

FIG. 43
EFFECT OF VOIDS ON RADIAL FLUX DISTRIBUTION USING U^{235}-Al FOILS, C-2

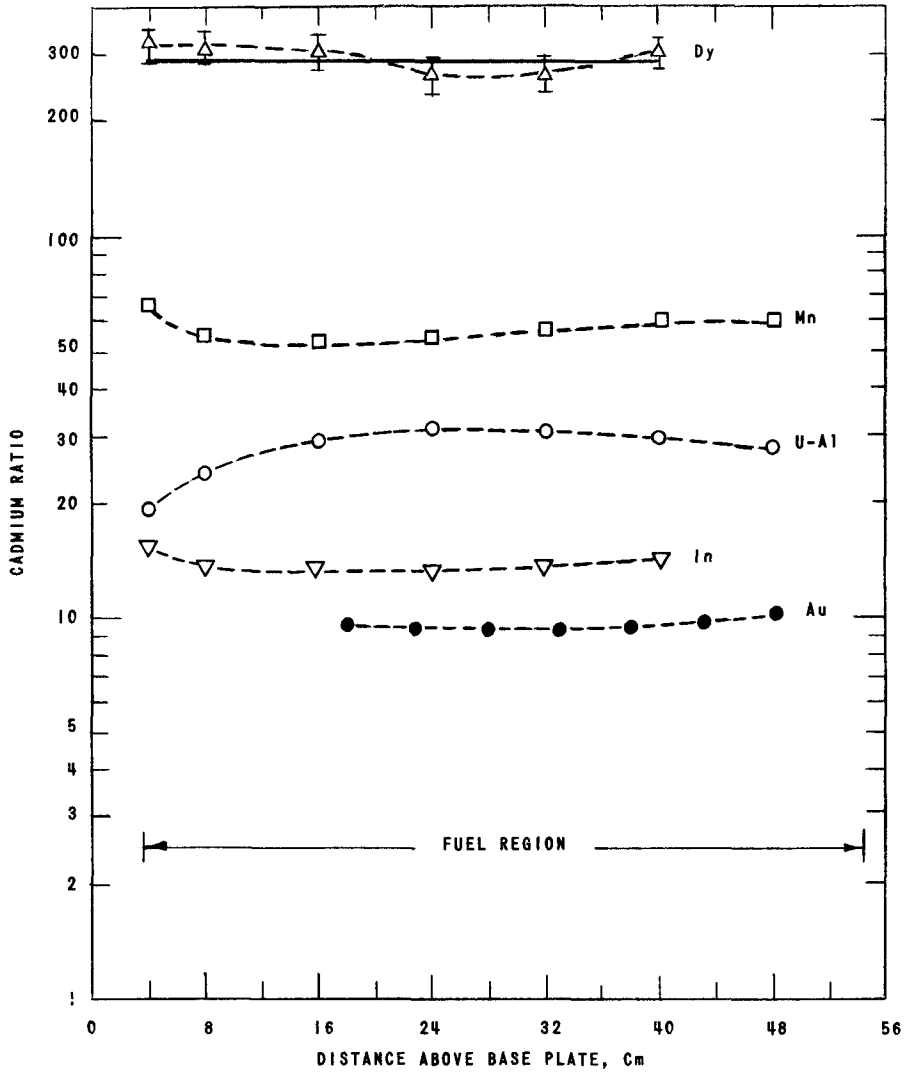

FIG. 44
AXIAL CADMIUM RATIOS, C-2

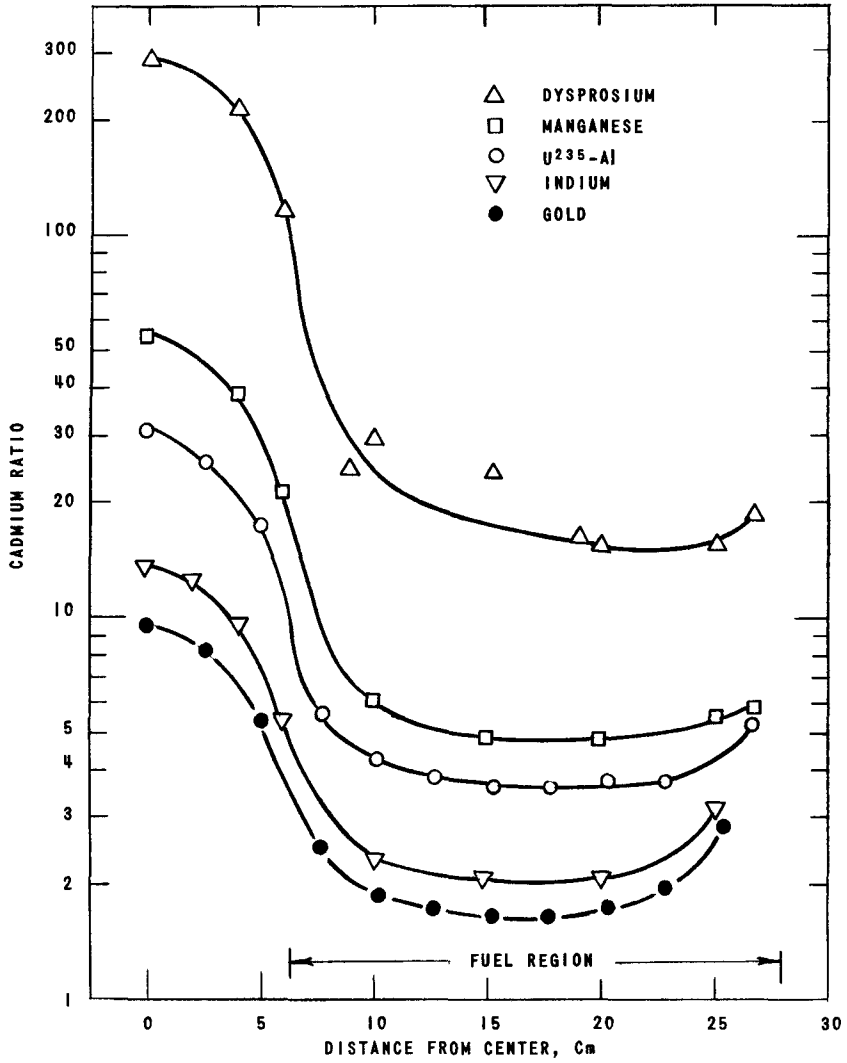

FIG. 45
RADIAL CADMIUM RATIOS, C-2

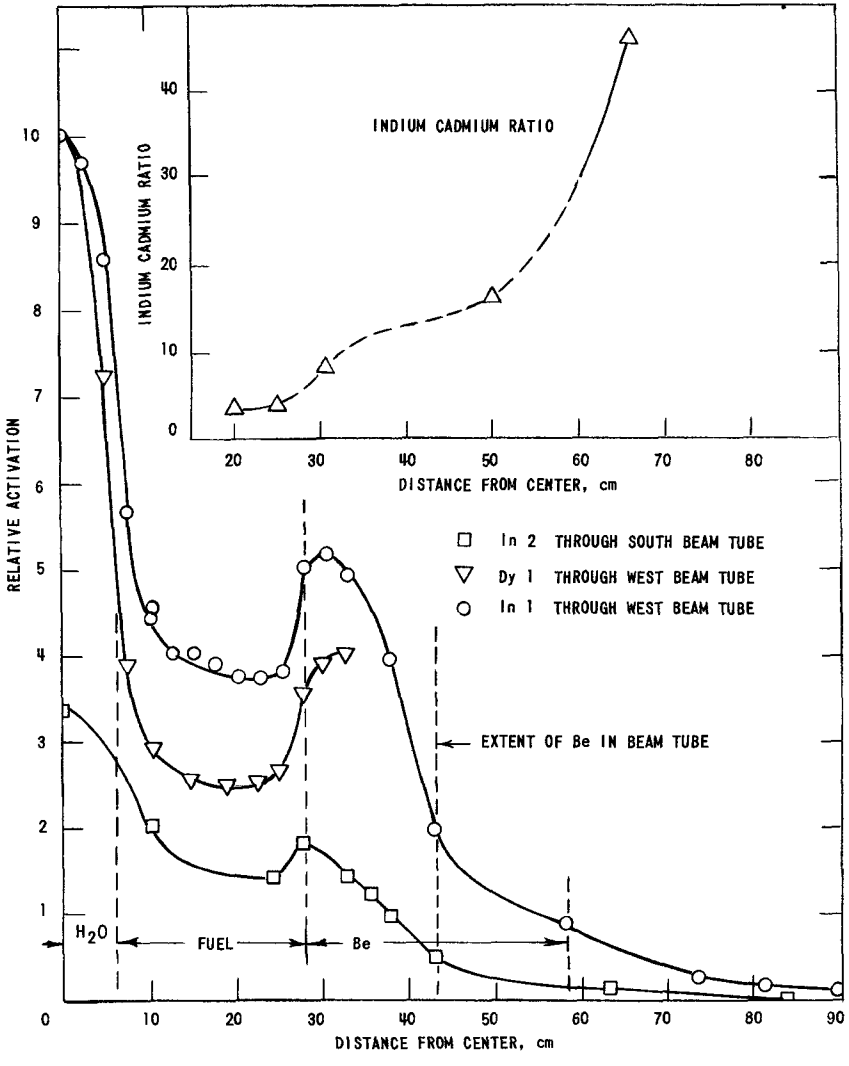

FIG. 46A
RADIAL INDIUM AND DYSPROSIUM FOIL TRAVERSES THROUGH BEAM TUBES, C-1

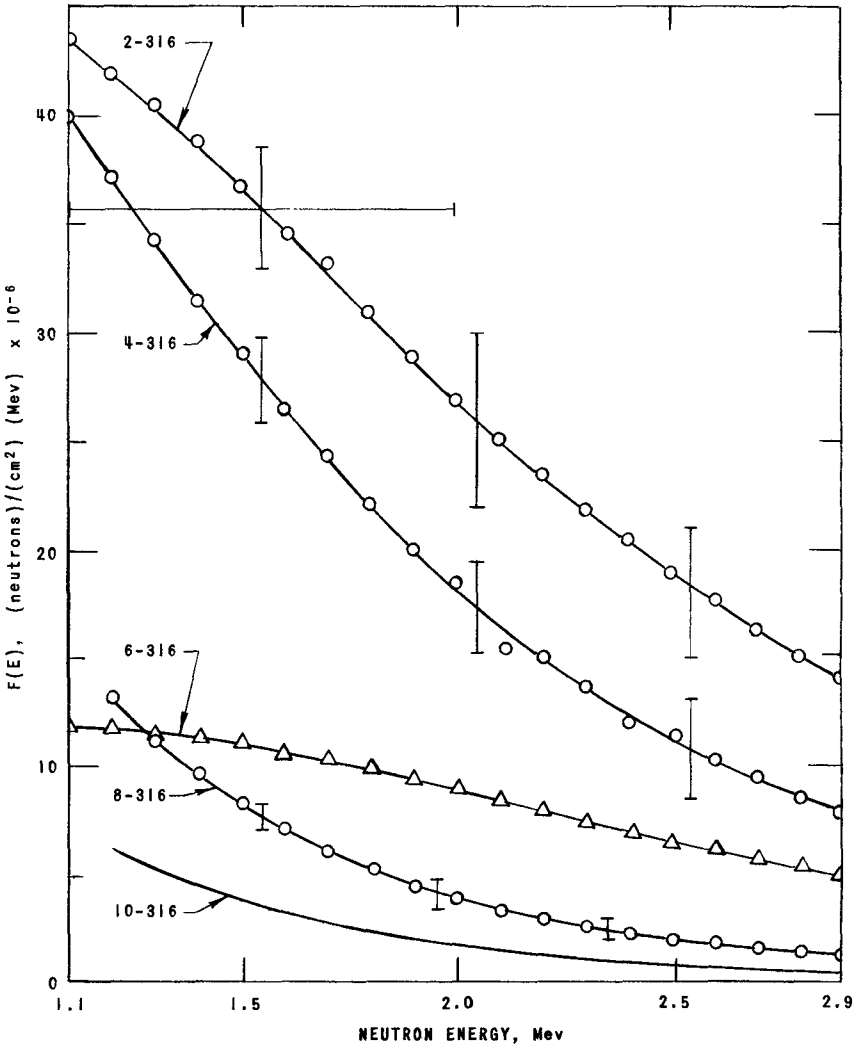

FIG. 46 B
NEUTRON ENERGY SPECTRUM IN WEST BEAM TUBE OF C-1

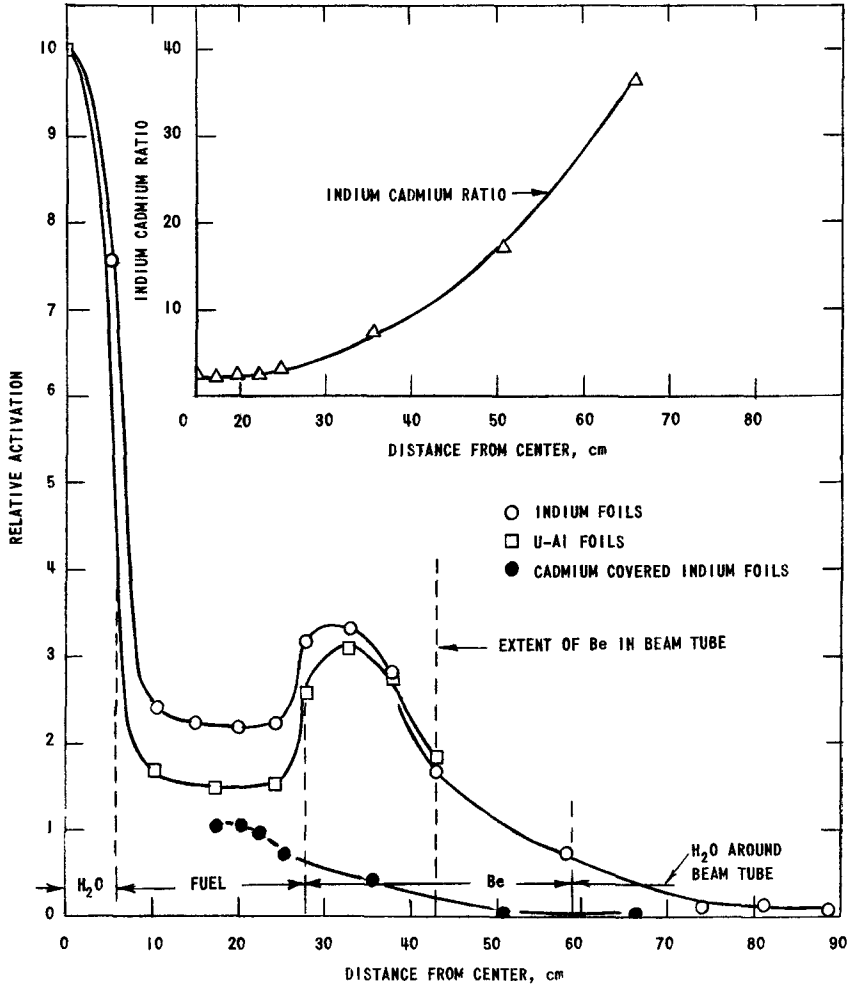

FIG. 47
RADIAL INDIUM AND URANIUM-ALUMINUM FOIL TRAVERSES THROUGH WEST BEAM TUBE, C-2

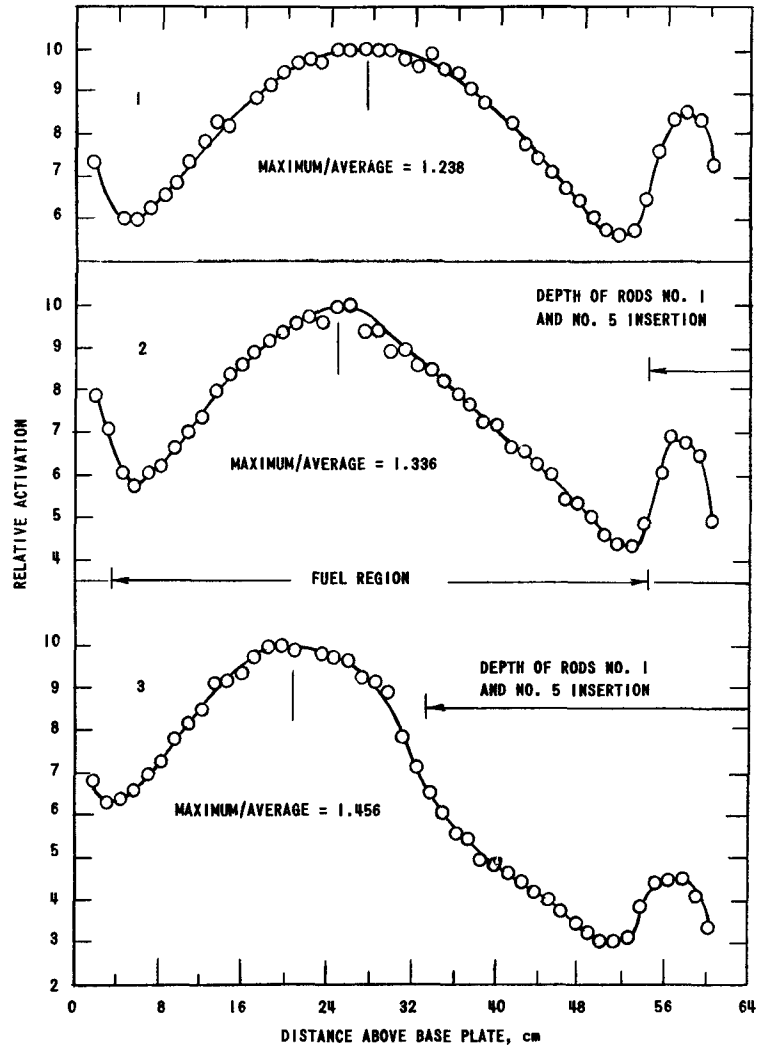

FIG. 48
EFFECT OF CONTROL RODS ON THE AXIAL FLUX DISTRIBUTIONS USING MANGANESE FOILS

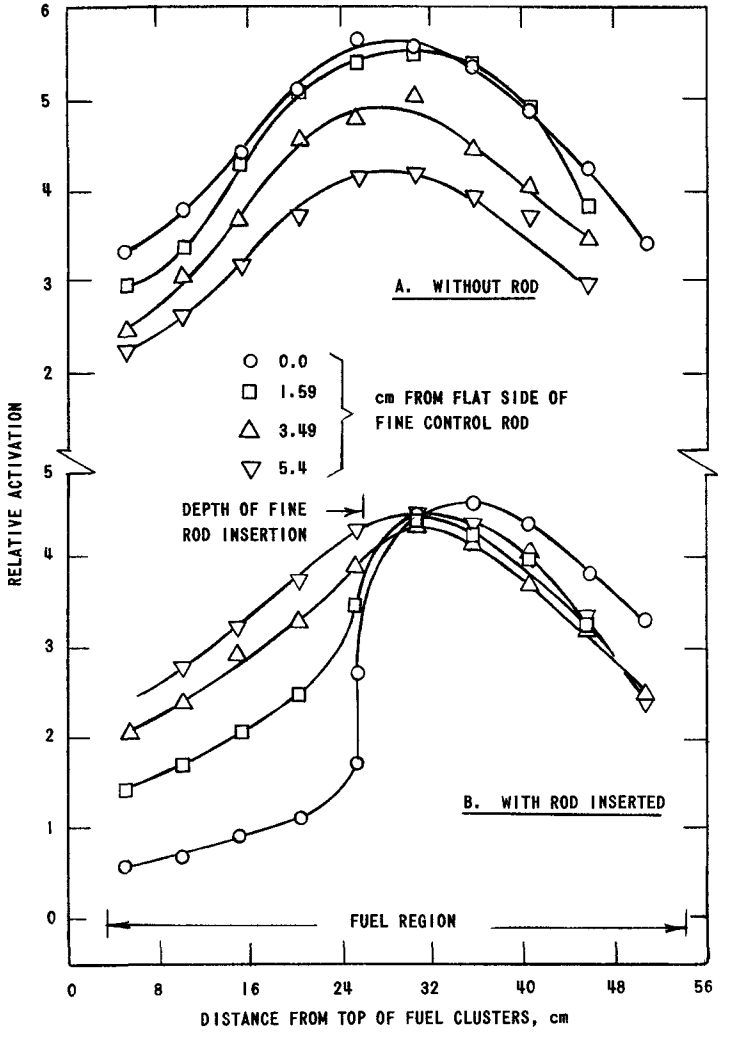

FIG. 49
EFFECT OF FINE CONTROL ROD ON AXIAL POWER DISTRIBUTIONS IN VICINITY OF FINE CONTROL RODS, MEASURED WITH U^{235}-Al FOILS ALONG a-b FIG. 5, C-1

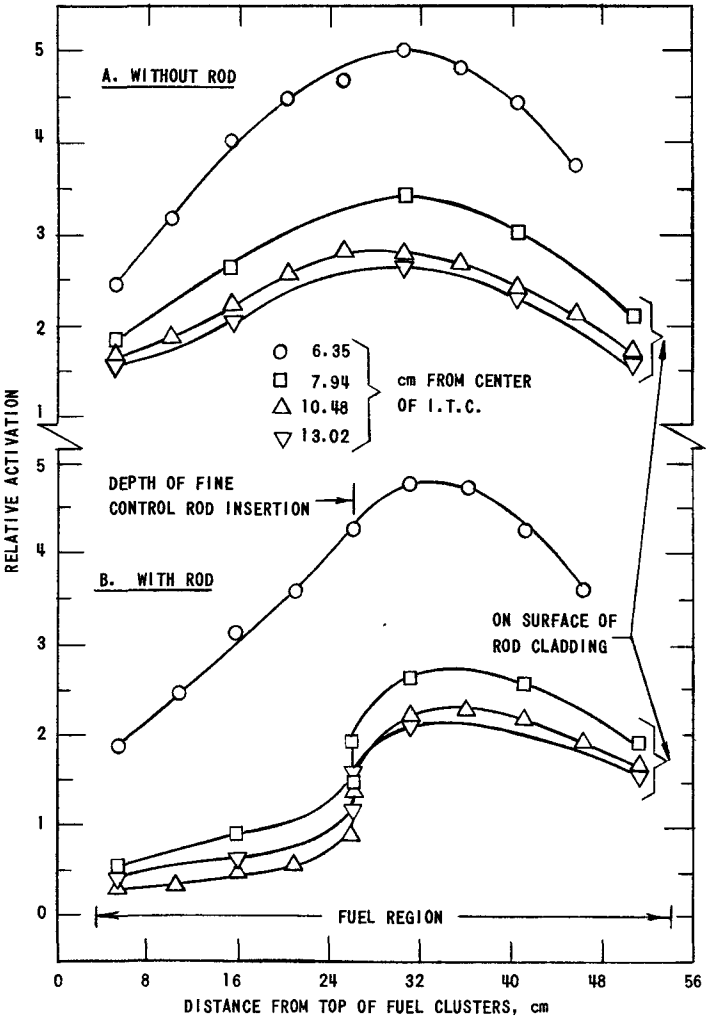

FIG. 50
EFFECT OF FINE CONTROL ROD ON AXIAL POWER DISTRIBUTION AS MEASURED WITH U^{235}-Al FOILS ALONG c-d, FIG. 5, C-1

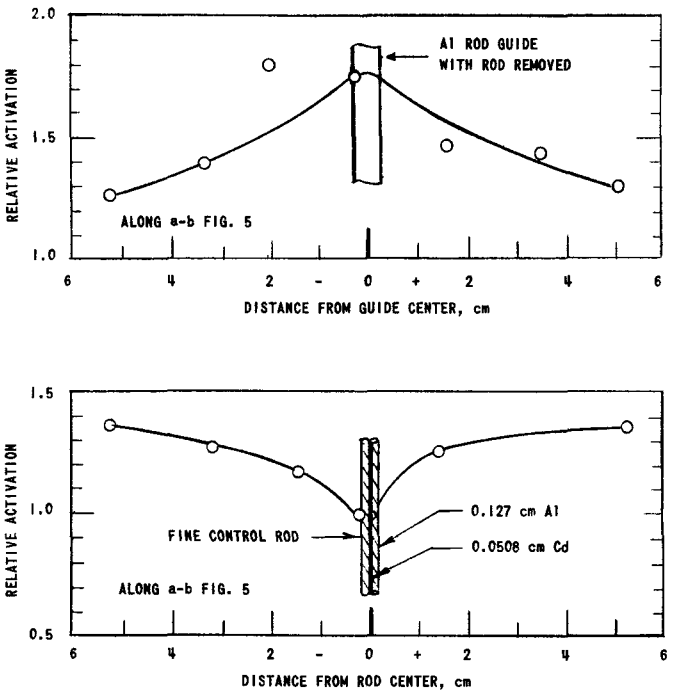

FIG. 51
EFFECT OF FINE CONTROL ROD ON POWER DISTRIBUTION MEASURED WITH U^{235}-Al FOIL AT HORIZONTAL MIDPLANE OF CORE, C-2

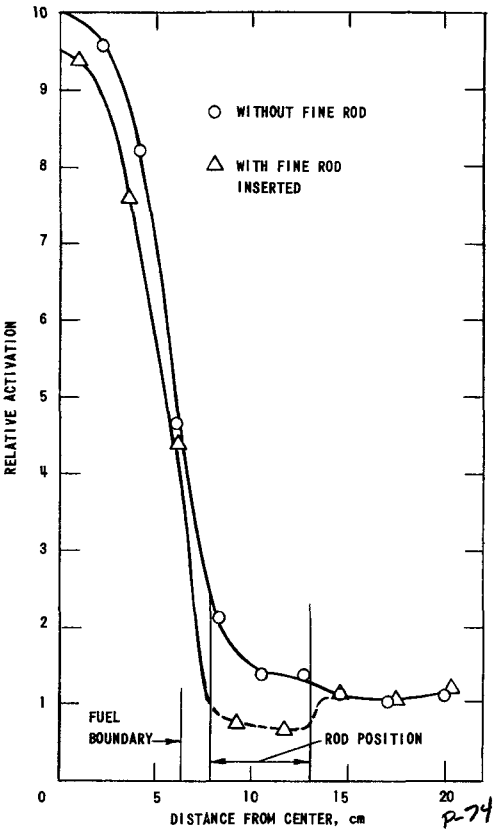

FIG. 52
EFFECT OF FINE CONTROL ROD ON POWER DISTRIBUTION AS MEASURED WITH U^{235}-Al FOILS, C-2

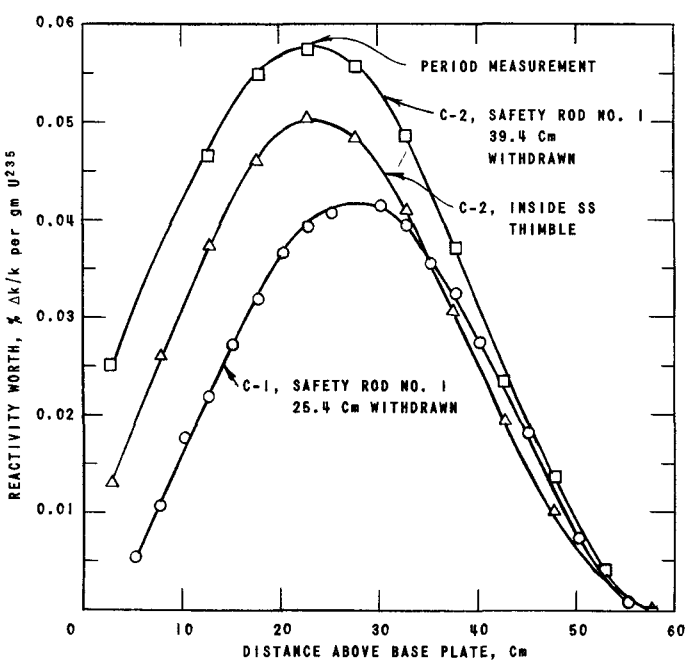

FIG. 53
REACTIVITY WORTH OF U^{235} AS A FUNCTION OF AXIAL POSITION IN THE ITC, C-1 & C-2

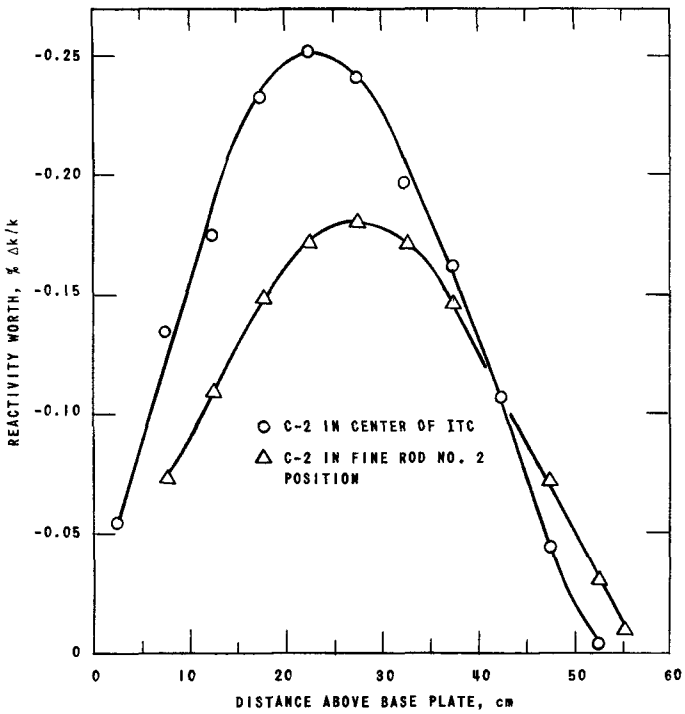

FIG. 54
AXIAL CADMIUM WORTH IN C-1 AND C-2

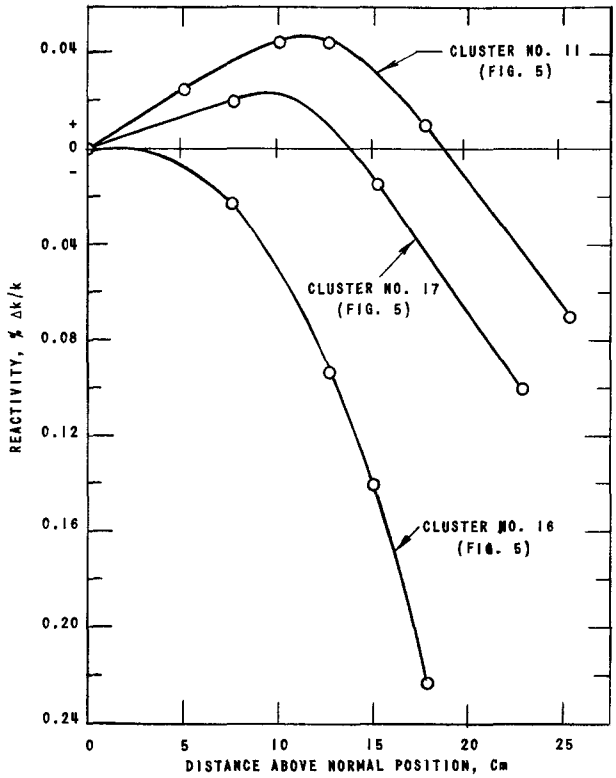

FIG. 55
REACTIVITY EFFECT OF PULLING A CLUSTER VERTICALLY OUT OF THE CORE, C-2

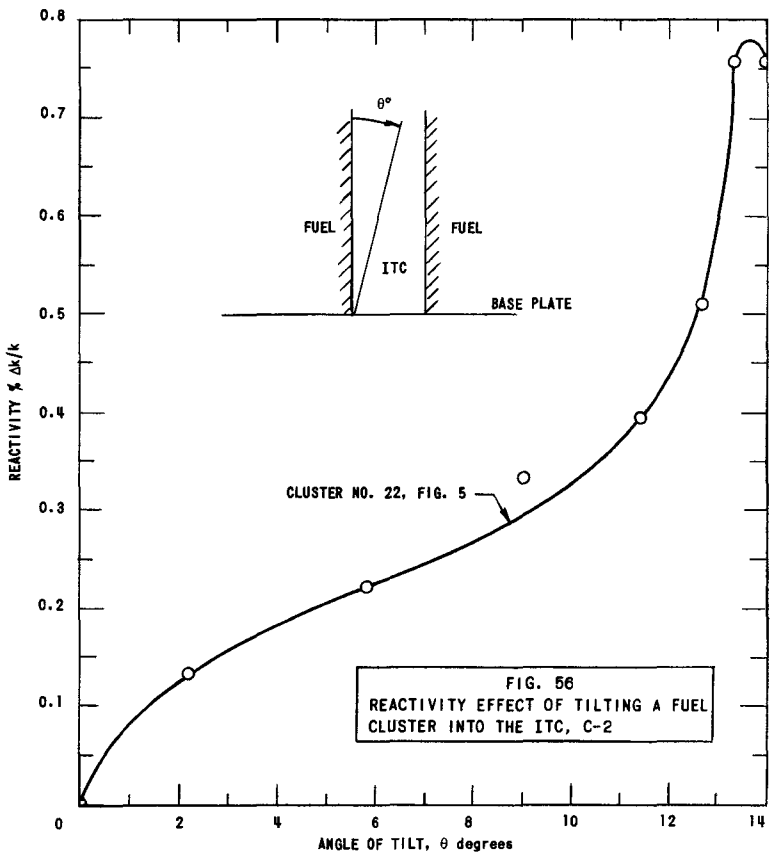

FIG. 56
REACTIVITY EFFECT OF TILTING A FUEL CLUSTER INTO THE ITC, C-2

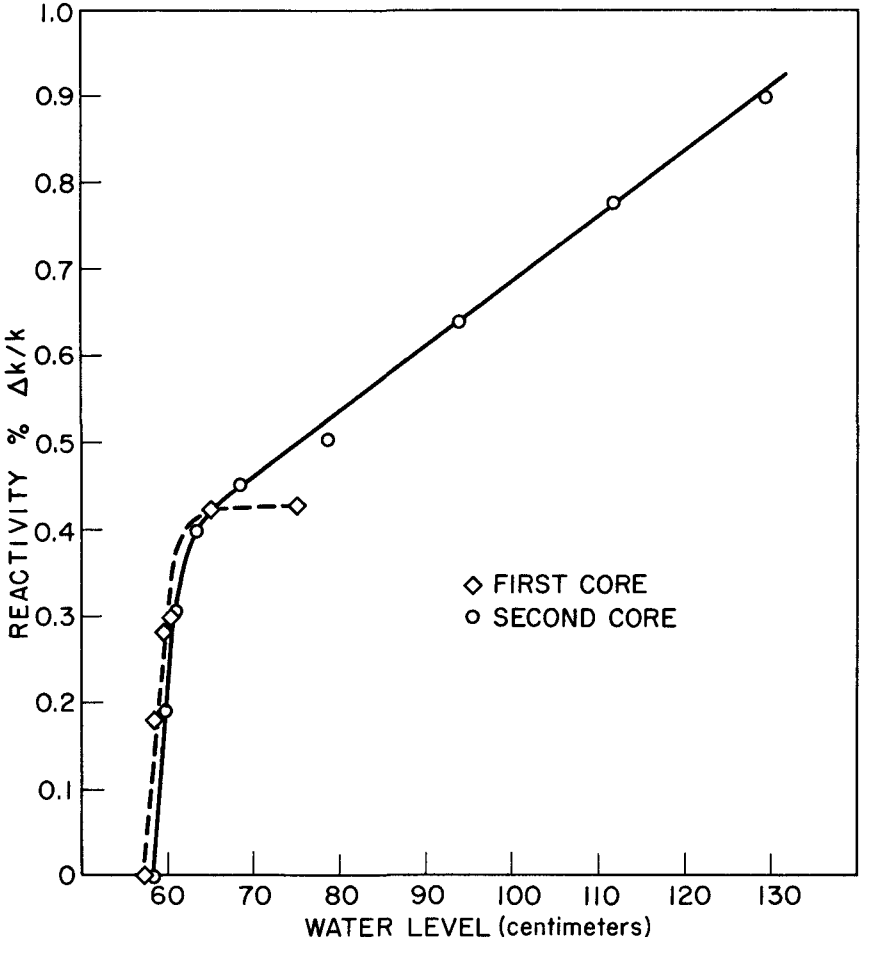

FIG. 57
TOP REFLECTOR WORTH (ROD SUBSTITUTION)

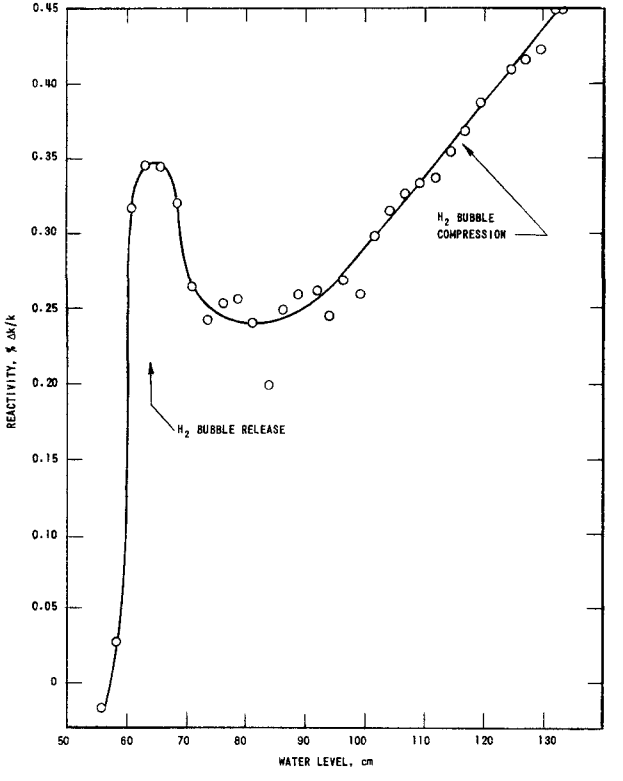

FIG. 58
TOP WATER REFLECTOR WORTH
BY THE RAMP INPUT METHOD, C-2

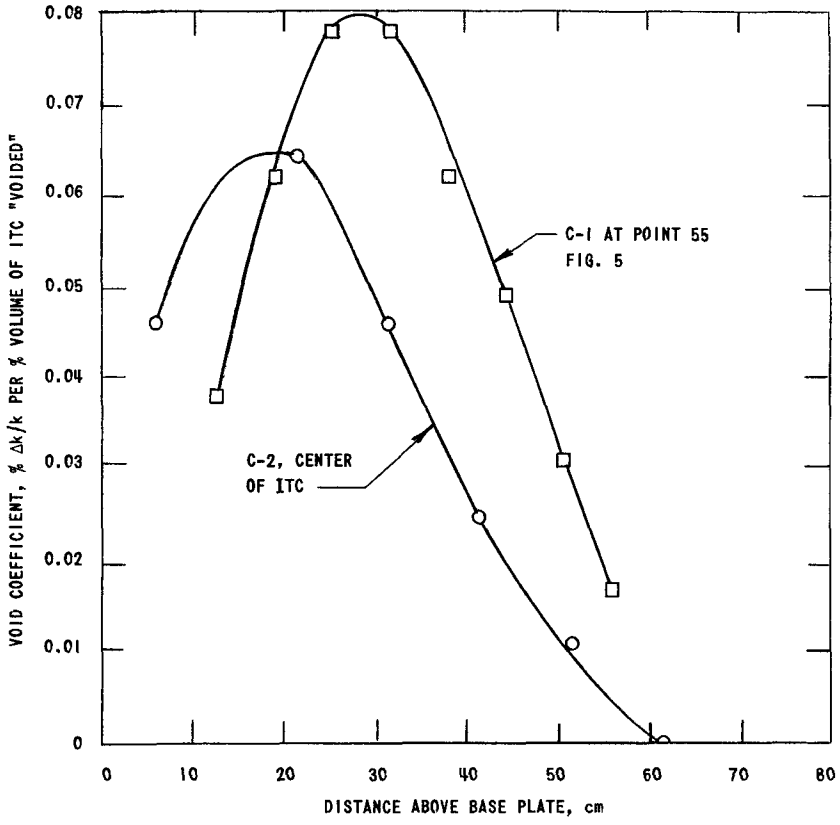

FIG. 59
AXIAL "VOID" REACTIVITY WORTHS AS MEASURED WITH 23.5 cc TEFLON, C-1 AND C-2

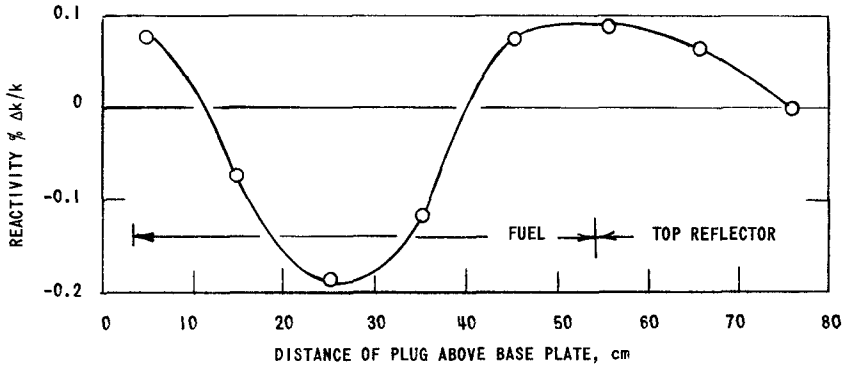

FIG. 60
COMPARISON OF TEFLON AND AIR REACTIVITY WORTH AS MEASURED WITH A 804 cc TEFLON PLUG INSIDE A 10.2 cm DIA. ALUMINUM TUBE CENTERED IN ITC, C-2

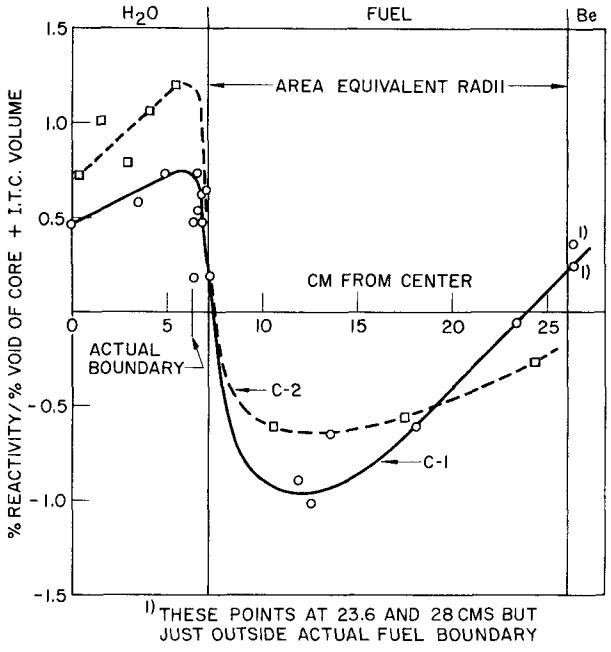

FIG 61
RADIAL VOID COEFFICIENT C-1 AND C-2

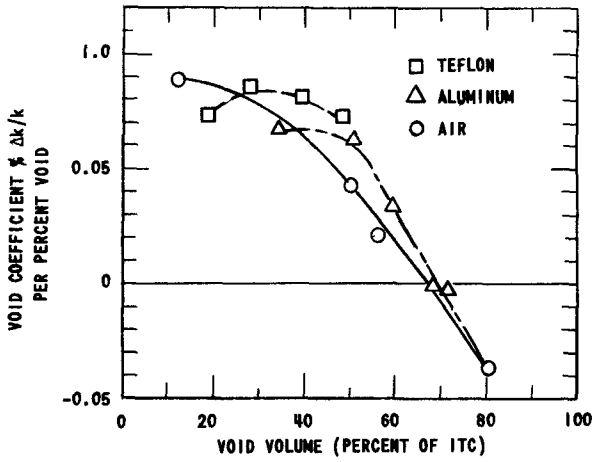

FIG. 62
DIFFERENTIAL VOID COEFFICIENT IN THE ITC, C-2

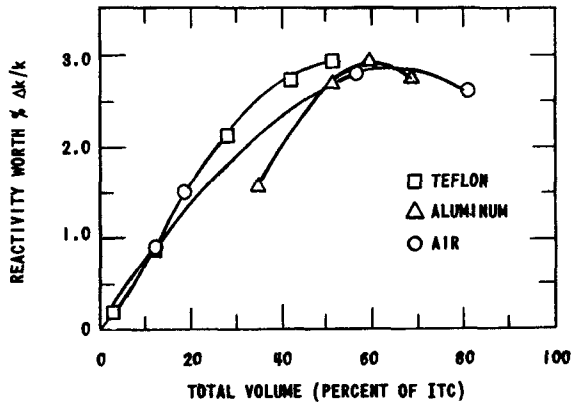

FIG. 63
INTEGRAL VOID, ALUMINUM AND TEFLON WORTH IN THE ITC, C-2

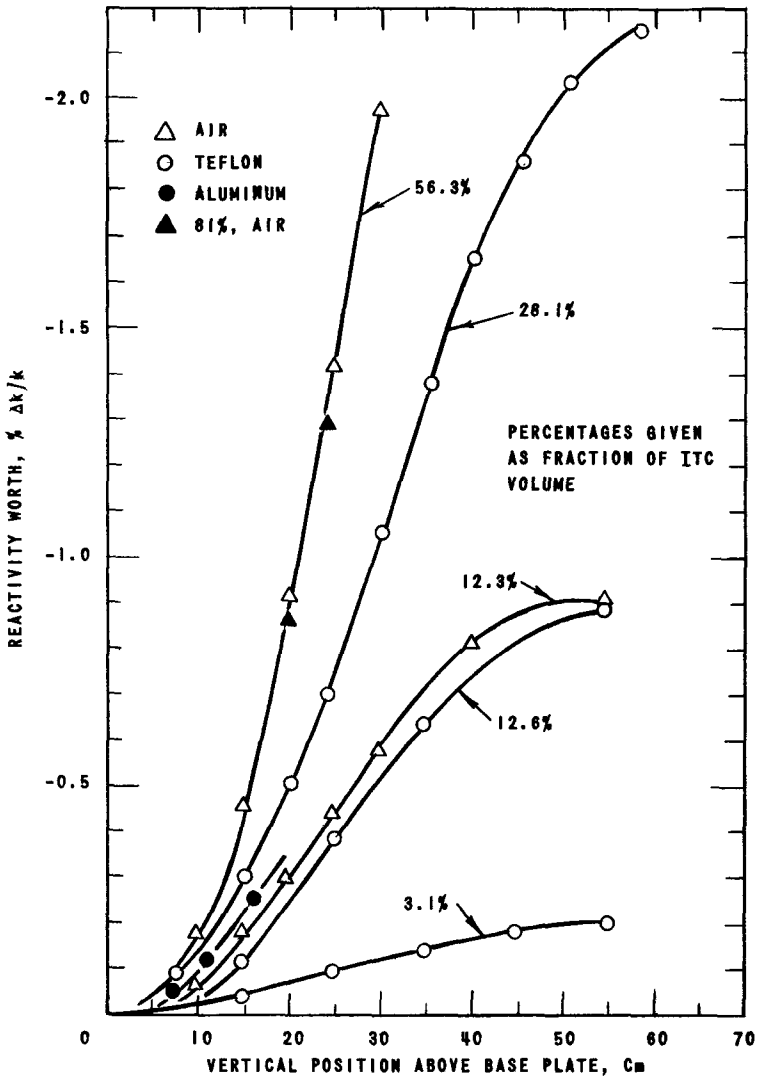

FIG. 64
VOID WORTH ESTIMATION BY REMOVAL OF FIXED VOLUMES OF "VOID MATERIALS" FROM THE ITC, C-2

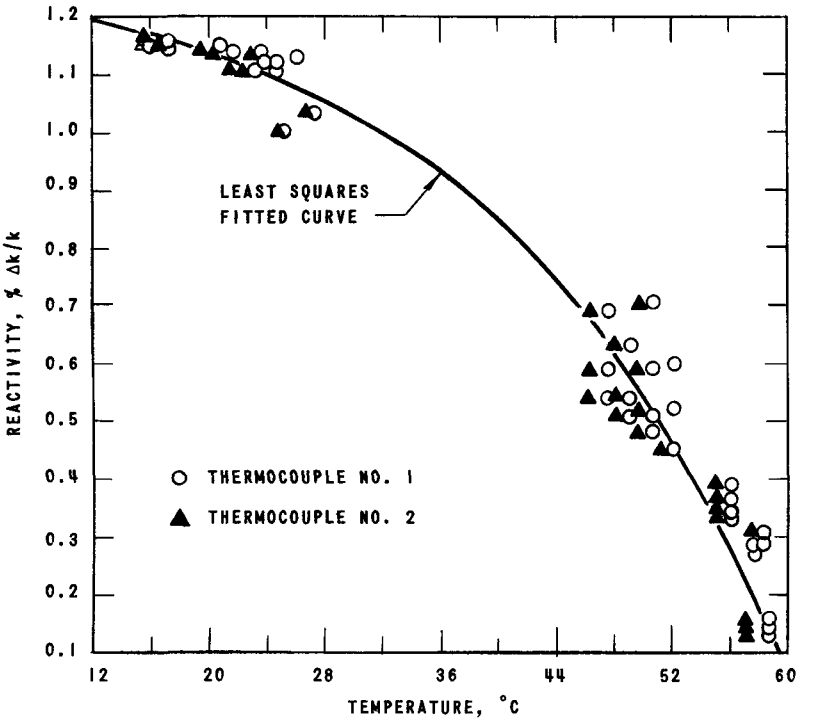

FIG. 65
VARIATION OF REACTIVITY WITH TEMPERATURE, C-1

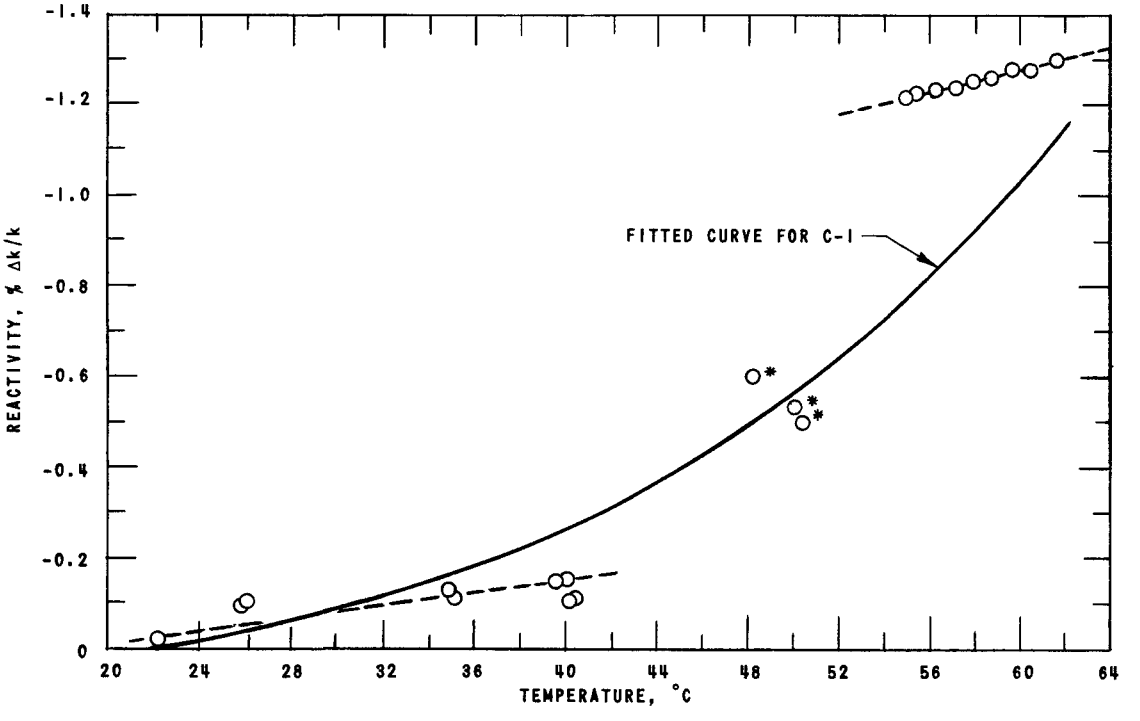

FIG. 66
VARIATION OF REACTIVITY WITH TEMPERATURE, C-2